ARCHITECTURE OF HYBRID TWO-FINGERED MICRO HAND: ANALYSIS, OPTIMIZATION, AND DESIGN

AHMED RAMADAN

MARCH 2009

ARCHITECTURE OF HYBRID TWO-FINGERED MICRO HAND: ANALYSIS, OPTIMIZATION, AND DESIGN

A dissertation submitted to
THE GRADUATE SCHOOL OF ENGINEERING SCIENCE
OSAKA UNIVERSITY
In partial fulfillment of the requirements for the degree of
DOCTOR OF PHILOSOPHY IN ENGINEERING

BY
AHMED RAMADAN
MARCH 2009

Summary

In last few years, the demand for micro motion devices increases in many industrial applications; especially fields of assembling micro machines, manipulating biological cells, and micro-surgical operation. As a consequence, there is an urgent need to develop dexterous micro-manipulators. However, the field of manipulating microscopic objects places hard requirements on the design process such as knowing the dynamics of microscopic objects, actuation mechanisms, and joint types that can be easily realized on a miniature scale. Therefore a successful design of micro-manipulator mechanism has to fulfill the above mentioned design requirements.

This thesis addresses the development process of a compact and yet economical chopstick-like two-fingered micro-manipulator hand based on hybrid structure actuation mechanism. The proposed micro-manipulator hand consists of two modules connected serially back to back; upper and lower modules. Each of them consists of a parallel kinematics chain with a glass pipette, of 1mm diameter and 3 to 10cm length, tapered to a very sharp end as an end effector. The micro-manipulator hand motion mechanism is driven by three piezo-electric actuated prismatic joints in each of the three legs of the parallel kinematics chain. Each leg of the kinematics chain has the structure of Prismatic-Revolute-Spherical (PRS) joint structure. As the length of the glass pipette end effector is decreased, the resolution and accuracy of the micro-manipulator hand is increased but the effective workspace is decreased. Therefore, the proposed two-fingered micro-manipulator hand consists of two 3-DOF PRS parallel mechanism modules connected in series in a mirror image style for enlarging the effective workspace of end effector and ease of fabrication process.

In this thesis, the development process is divided into three main phases; the analysis and mathematical modeling phase, the optimization and design phase, and the realization and implementation phase.

- In analysis and mathematical modeling phase, a novel solution of the inverse kinematics problem (IKP) for a given mobile plate center position of a 3-DOF RPS

parallel mechanism is derived and applied with proper modification to the case of 3-DOF PRS structure of the proposed mechanism. The solution is given in closed form simple equations. The new solution proves that there are eight mathematically accepted solutions with only four solutions that are physically accepted. The IKP for a given end effector position and the forward kinematics problem (FKP) of 3-DOF PRS parallel mechanism are also solved numerically based on the new IKP solution. Then, this solution is extended to the two-fingered hybrid mechanism of the micro-manipulator hand. The workspace volume of each of the two fingers is examined relative to mobile and base reference frames.

- In optimization and design phase, the optimization of the chosen design parameters of a theoretical 3-DOF PRS parallel finger module is carried out using two approaches: discrete search method and genetic and evolutionary algorithms (GEAs). The GEAs are superior in finding the best design parameters than the other method but it needs high accuracy measures that are difficult in practical implementation. Based on the decided optimal design parameters, a CAD model for the 3-DOF PRS finger module is built and a complementary optimization process – using ANSYS Workbench program - is carried out to determine the best characteristics of the pin flexure hinge – revolute joint - used in the CAD structure. Finally, the total CAD model of the hybrid two-fingered micro-manipulator hand is built.
- In realization and implementation phase, the setup description of the hardware system of the first prototype of two-fingered micro-manipulator hand is presented. The program description, calibration method, practical jacobian matrices, end effectors practical workspace, and error analysis of the prototype are discussed.

As a target application, the experiment setup description of how to use the proposed micro-manipulator hand in tissue micro-injection is presented. We plan to use two micro-manipulator hands for micro-injection of high-density cell suspension of Epithelium and Mesenchyme tissues in a collagen gel environment with precise positioning of cytokines inside this gel environment.

Table of Contents

List of Figures

List of Tables

Acknowledgements

First of all, I would like to express my sincere gratitude to my supervisor Prof. *Tatsuo ARAI* for his patience, wise advices, ideas and suggestions and for his strong insistence and high pressure to achieve better work. He has helped me to the utmost of his ability and been patient and understanding at all times. I am proud of working under his capable supervision. I would like to express my gratitude to and thank Prof. *Fumio MIYAZAKI* and Prof. *Toshiyuki OHTSUKA* for their inspiring discussion.

Also, I want to express my gratitude to the laboratory members of Prof. ARAI Lab. for their support and encouragement. I can not forget to express my sincere gratitude to my country *Egypt* for supporting me through an Egyptian governmental scholarship to study Ph. D. in Japan. To all of those who helped in a way or another, I express my gratitude.

This work was supported by MEXT under Grant-in-Aid for Scientific Research on Priority Areas (Project No. 17076010).

Dedication

I would like to dedicate this dissertation to my parents, my wife and all my family members who have supported and encouraged me throughout my academic career. Thanks for showing infinite patience and the will to always listen to me in the most troublesome moments during my work in this thesis. The words are too little to describe my thanks to my wife and family for their patience and endless support to withstand the challenges of life and work.

Ahmed A. Ramadan

CHAPTER 1

Introduction

Micro-manipulation has enabled numerous technological breakthroughs in recent years, from advances in biotechnology to micro-component assembly. Effective manipulation of micro-objects is required for a wide range of industrial applications, such as the assembly of small parts to obtain micro machines or miniature systems, computer micro-electronics, micro-surgical operation like neurosurgery and ophthalmology, and research in biology and biotechnology. The main applications of micro-manipulators are in the area of biotechnology, where urgent needs for automatic operations are going to further increase day by day in the future.

1.1 Brief Introduction to Robots and Parallel Mechanisms

Today, robots can be found in virtually every field, from medical to transport, industrial to recreation. They are slowly becoming part of the background furniture of modern society without most people realizing it. Development of robots started with the need of automation in manufacturing industries. The wide spread use of industrial robots in manufacturing is due to the necessity of increasing the flexibility of manufacturing, improving the product quality, and reducing the overall production costs. Moreover, robots could free a large number of people from hazardous situations. Due to the programming features of robot motion, these devices are playing an important role in the industrial automation processes; they are giving possibilities for a fast and flexible response to required changes in technological equipment and processes.

The most common robot architecture is undoubtedly the serial manipulator, in which the actuators and various links are connected in series from a base to an end-effector, as

depicted in Fig. 1.1. This design offers numerous advantages, including a large workspace. The popularity of this architecture in industry is a clear indication of its ability to fulfill a broad variety of needs. However, serial manipulators also have their drawbacks. Thus, several alternative architectures have been proposed and used in robotics. One well-known example is parallel manipulators. As the name indicates, in this case the actuators and links are mounted in parallel from a base to a common platform, as shown in Fig. 1.2.

Fig. 1.1: Example of serial manipulator.

Fig. 1.2: Example of parallel manipulator

Several types of parallel architectures are possible and the most common is that of the Gough-Stewart platform as indicated in Fig. 1.3. This 6-DOF manipulator has a platform which is moved by the action of six linear actuators. This platform is most commonly used for flight simulator applications to train pilots on the ground, since it can support the very large mass of the cabin which is being subjected to various movements, as in Fig. 1.4.

Fig. 1.3: Gough-Stewart platform.

Fig. 1.4: Flight simulator

The conceptual design of parallel kinematics mechanisms can be dated back to 1947, when Gough first developed the basic principles of a 6-DOF parallel mechanism with a closed–loop kinematics structure for the purpose of testing tires, although the work was not published until 1962 [1]. Stewart introduced a parallel actuated manipulator with 6-DOF that allows the position and orientation of a moving platform for use as a flight simulator for pilot training in 1965 [2]. A lot of work has been focused on the dynamics of the 6-DOF Stewart platform, as it attracted more researchers' attention in the context of industrial applications, especially, the parallel kinematics machine [3-12].

As in the case of conventional serial manipulators, kinematics analysis of parallel manipulators is also performed in two phases. In forward or direct kinematics the position and orientation of the moving platform is determined given the actuators displacements. This is done with respect to the base reference frame. While in the inverse kinematics we use position and orientation of the moving platform to determine the actuators displacements. It is well known that unlike serial manipulators, inverse position kinematics problem for parallel manipulators is usually much simpler than forward position kinematics problem. In inverse kinematics problem, the actuators displacements may be computed independently using the given pose of the moving platform and the solution is in most cases uniquely determined. But the forward kinematics problem is generally very complicated and its solution usually involves systems of nonlinear equations which are highly coupled and in general have no closed form or unique solution. Different approaches are proposed to solve this problem either generally or for special cases. There are also numerous cases in which the solution to this problem is provided for a special or novel architecture. In general, different solutions to this problem can be found using numerical approaches, analytical approaches, artificial intelligence approaches, and closed form solution for special architectures [8-15].

In recent decades, one of the most ever growing research directions is the design of manipulators with parallel architectures. There have been considerable developments in the field of parallel kinematics manipulators because they possess several advantages over traditional serial manipulators such as high positioning accuracy, high speed, better structure rigidity, high load to weight ratio, low inertia, small errors, and they can work at

different scales. One disadvantage of parallel kinematics manipulators is that the particular architecture of the manipulator results in smaller workspaces than that of their serial counterparts [16]. Parallel kinematics manipulators can also be difficult to design, since the relationship between design parameters and the workspace, and behaviour of the manipulator throughout the workspace, is not intuitive by any means [17]. So, since the performance of parallel manipulators is so dependent on their dimensions, customization of these manipulators for each application is absolutely necessary. Hybrid manipulators that combine parallel mechanisms in series connection are one of the good solutions to overcome small workspace [18, 19]. Parallel manipulators can be used as industrial robots, parallel machine tools, flight simulators, special purpose testing machines, force/torque sensors, and micro-manipulators [19-23]. Table 1.1 gives a brief comparison in between serial and parallel manipulator mechanisms.

TABLE 1.1
COMPARISON IN BETWEEN SERIAL AND PARALLEL MANIPULATOR MECHANISMS

	Serial Manipulator Mechanism	Parallel Manipulator Mechanism
Schematic Diagram	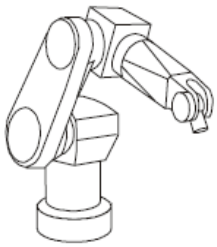	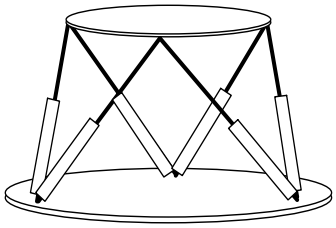
Links Connection	In series	In parallel
Accuracy & Repeatability	Low	High
Load/Mass ratio	Poor	Good
Scalability	Poor	Good
Forward/Inverse Kinematics problem Solution	Simple/Difficult	Difficult/Simple
Working Workspace	Large	Small

1.2 Survey of Micro-Manipulation and Micro-manipulators

As the demand for micro-motion devices increases in many industrial applications - such as chip assembly in the semiconductor industry, cell manipulation in biotechnology, and surgery automation in medicine, – there is an urgent need to develop micro-motion manipulators capable of performing very small motion with high resolution and perhaps high speed [22-25]. So, micro-manipulation technology is one of the most important key issues nowadays. The field of micro-manipulation that deals with objects having dimensions with a magnitude in the thousands of millimeters – few micrometers – places hard requirements on the design of the manipulator. First, the dynamics of microscopic objects are different from that of conventional macro objects. As gravitational forces are proportional to object volume whereas adhesion forces are proportional to object surface, so the later become dominant and larger than the former in the micro world. The literature refers to adhesion forces as: van der Waals forces, electrostatic forces, and surface tension forces [26]. Second, the mechanism should be designed so that small actuators displacements can generate as large workspace as possible. Furthermore, joint types and actuation methods that can be easily realized on a miniature scale are required [20-27].

Micro-manipulators commonly use piezoelectric (PZT) actuators together with compliant mechanisms to provide fine motions with position resolution in the micro/nano-meter range. The most evident difference between the micro and the macro worlds is the increasing importance of adhesion forces, which become much stronger than inertial forces as size decreases. Thus for example, releasing objects is more difficult than grasping them. So, the influence of adhesion phenomena caused by surface forces becomes prominent compared to volumic forces at the micro scale [26, 27]. These forces act when two objects are in contact - contact between one manipulated object and an effector, the work plane or another objet - but also at a distance [28]. Thus they cause lots of troubles for the picking or release of micro-objects. For this reason lots of research teams are working to model and control adhesion forces [26-30]. Additional problems for micro-manipulators drive from the need for achieving dexterity, high accuracy and high speed in a very small workspace, and from the need for operating in different working environments, such as air, liquids or vacuum room.

Several parallel manipulators employing compliant mechanisms have been designed to perform the manipulation in micro/nano-meter scale [31-40]. However, most of the current micro-manipulators can provide only a planar 3- DOF motion, or spatial combined motions of translation and rotation. Since the micro- and nano-scale manipulation is usually performed via a microscope, which provides a quite limited field of vision and even a slight rotation of the end effector will result in the manipulation easily sweeping out of the visual field, the most important motion used in such applications is translational rather than rotary motion. So, in almost all cases, only 3-DOF motion is enough for micro or nano manipulation.

Kallio et al. [41] designed a three-DOF piezo-hydraulic micro-manipulator. The actuation system consists of a piezoelectric actuator, a small tank and a bellows. The bellows is a spring type of passive component, i.e., force required to deform the bellows is directly proportional to the displacement. It can get a displacement about ± 250μm. The manipulator consists of three identical piezo-hydraulic actuation systems. They are connected by a mobile platform forming a parallel tripod-like configuration. It is reported that the planar workspace of the manipulator is 1.5 mm and 0.6 mm and its maximum vertical displacement along z axis is about 0.25 mm, and the displacement resolution of the manipulator is better than 1 μm.

T. Fukuda and F. Arai [42] proposed a prototyping design of a contact type and a non-contact type micro/nano manipulation system. They introduced a micro tri-axial force sensor to be used in micro-manipulation systems.

Chonan et al. [43] studied the hybrid position/force control of a two-fingered miniature gripper. The fingers are flexible cantilevers actuated by piezoelectric bimorph strips at the base and are supported by linear ball bushings which ride on a steel shaft. The cantilever is driven by the bending deformation of the ceramic actuator. The maximum displacement of the actuator is approximately 300 μm and the resolution is 5 μm.

David J. Cappelleri et al. [44] proposed a design of a variable thickness piezoelectric bimorph actuator for application to minimally invasive surgery. The actuator is discretized

into five segments along its length, where the thicknesses of the segments are used as design variables in the problem of optimizing both the force and deflection at the tip.

Angeles et al. [45] studied the design of the mechanical structure of an 11-axis robot to accomplish accurate positioning and velocity-controlled tasks in the presence of a flexible substructure. The manipulator is designed as a cascade of three modules, the proximal one being termed the macro-manipulator which is responsible for a long reach and a high flexibility. The other two modules, comprising the seven-axis micro-manipulator, are responsible for the accurate positioning and orientation of the tool attached to the end-effector.

J.P. Merlet [31] devoloped a micro robot with a parallel mechanical architecture having 3-DOF (one translation and two orientations) MIPS that allows fine positioning of a surgical tool. The purpose of MIPS is to act as an active wrist at the tip of an endoscope and to provide to the surgeon an accurate tool that may furthermore offers a partial force-feedback.

Dezhong Liu, Yihua Xu, and Renyuan Fei [32] developed a micro-manipulator based on 3-PRS in-parallel mechanism for the purpose of handling micro-objects. The micro-manipulator consists of a left finger and a right finger, in a Chinese chopstick like, driven separately by three driving units.

D. Sinan et al. [33] described a dynamical strategy for releasing micro objects picked-up by means of adhesion forces. later they [34] described the micro-manipulation system developed in Laboratoire de Robotique de Paris (LRP) which is based on the use of adhesion forces and inertial effects for handling of objects which range from 1 to 100μm through enhanced user interaction 6-DOF haptic interface for force feedback remote handling. The system is capable of capturing micro-objects smaller than a few micrometers, based on the superiority of adhesion forces for this class of object. The release is accomplished either by adhesion, on a higher energy target substrate, or by amplification of inertial force by way of an instantaneous acceleration applied to the gripper.

Qingsong Xu and Yangmin Li [35] proposed a 2-DOF compliant parallel micromanipulator for 2D nano-manipulation and proposed 3-PUU spatial compliant parallel micro manipulator (CPM) utilizing flexure joints [36]. Then the authors [37] presented the design issues of a compliant parallel micro-manipulator (CPM) for nano-manipulation from the mechanical design point of view. Its applications as a two fingers manipulator are presented for nano scale manipulation. Their CPM is an integration of parallel and compliant mechanisms.

T. Tanikawa and T. Arai [38] developed a dexterous micro manipulation system having a two-fingered micro-hand to manipulate micro objects by simulating chopsticks motion. The micro-hand is based on 6-DOF Stewart platform and uses two long glass pipettes as its end effector. The two-fingered micro manipulator hand uses a wire – as a ball joint - to connect the sides of piezo electric actuators to the lower and upper plates, as shown in Fig. 1.5. Later, T. Tanikawa et al. [39] designed a two-fingered micro manipulator based on thin plate flexure joints technique, as depicted in Fig. 1.6. In which, the piezo electric actuators push the thin plate flexure joints to produce the motion. The thin plate flexure joints can be produced using press-machining through punching holes and bending the plate to take a certain shape. Finally, the design is modified to be Magnetic Resonance Imaging (MRI) compatible [40].

Fig. 1.5: Two-fingered micro manipulator, old prototype 1996.

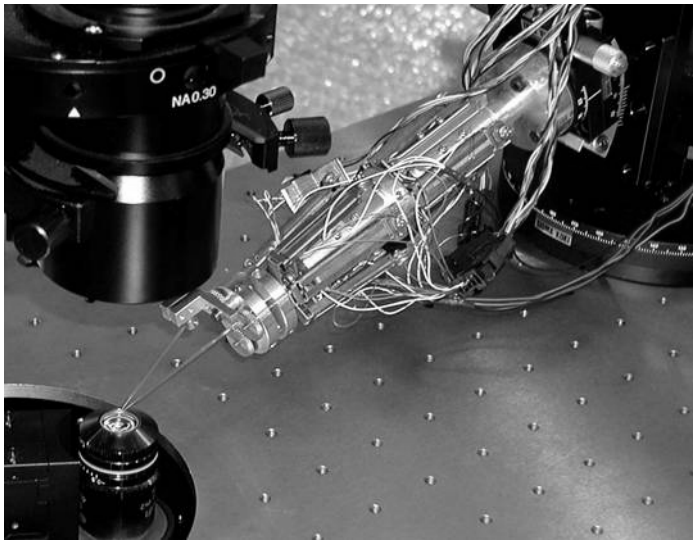

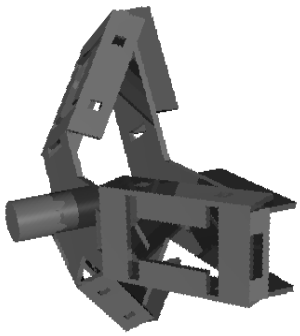

(a) Two fingered micro manipulator hand (b) Thin plate mechanism

Fig. 1.6: Two-fingered micro manipulator hand with thin plate flexure joints, 2002

In our research work, we designed a new architecture for a two-fingered hybrid micro-manipulator hand Based on deep mathematical analysis and optimization. The development process consists of three main phases; analysis and mathematical modeling phase, optimization and design phase, and realization and implementation phase [52-65].

1.3 Research Objectives

Any piece of research has a number of objectives, but these objectives can be generalized to three basic motivations; invention, extension, or explanation. Either a new technique/mechanism is developed which is superior to an existing technique/mechanism on a standard criteria, or an existing technique/mechanism is shown to be applicable to a new problem. In both cases some degree of explanation is desirable.

The main objective of our research is to develop a new architecture micro-manipulator hand that can be used to manipulate effectively microscopic objects. It will be used to manipulate biological cells for the purposes of auto cloning, DNA extraction, cutting …etc. Almost all tasks mentioned above becomes very crucial, which usually depends on precise instruments with micro or sub-micrometer resolution. By effective manipulation

we mean that the operations of grasping, catching, rotating, moving, and releasing should be performed precisely.

This thesis is concerned with the development process of a chopstick-like two-fingered micro-manipulator hand based on hybrid mechanism. The development process includes three phases, which are;

1. First phase: Analysis and Mathematical Modeling, in which we will try to find a simple mathematical methodology to model our proposed micro-manipulator hybrid mechanism.
2. Second phase: Optimization and Design, in which we will use the mathematical model to optimally choose the design parameters of our proposed micro-manipulator mechanism so that it will have a large workspace. Then, these design parameters will be used to build the CAD model of the proposed new architecture of manipulator mechanism.
3. Third phase: Realization and Implementation, in which we will build the prototype of the proposed micro-manipulator hand and implement the whole system for micro-manipulation. Then, the practical workspace of the prototype will be compared with the theoretical workspace to see to what extend they are close to each other.

1.4 Main Contributions

This thesis presents a new structure of two-fingered micro-manipulator hand based on hybrid motion mechanism. The proposed new structure of micro-manipulator hand consists of two 3-DOF PRS (Prismatic – Revolute - Spherical) parallel mechanisms assembled together back to back in series connection in a mirror image style.

The development process of the proposed micro-manipulator has three phases, in which the contributions are as follows;

- In first phase, Analysis and Mathematical Modeling, a novel closed form solution for the inverse kinematics problem (IKP) of 3-DOF PRS and 3-DOF RPS parallel mechanisms is derived. The IKP solution is expressed in a set of

simple equations. This closed form solution is used to solve the forward kinematic problem (FKP) in an easy way of the same structure using Newton-Raphson method. Moreover, this solution is used to solve the IKP of the micro-finger parallel mechanism based on the position of the finger tip, which is more practical than that of normal IKP. Then, the solution is extended to the total hybrid motion mechanism of the micro-manipulator hand.

- In second phase, Optimization and Design, the optimization of the chosen design parameters of the micro-finger parallel mechanism is carried out in two steps. The first step concerns with the optimization of the design parameters of the theoretical model using two approaches – discrete search method and Genetic and Evolutionary algorithms (GEAs) - based on the derived new closed form IKP solution. Then, a CAD model for the 3-DOF PRS micro finger mechanism using these optimal design parameters is built. The second step concerns with the optimization of the mechanical properties of the pin flexure hinge in the micro-finger CAD model using ANSYS Workbench program. Finally, the total CAD model of the hybrid two-fingered micro-manipulator hand is built. The workspace of the optimized CAD model is about 5% only of that of the theoretical model in this stage.
- In third phase, Realization and Implementation, the prototype of our micro-manipulator hand CAD model is assembled. The hardware system of the micro-manipulation system is built, tested, and calibrated. Then, the practical workspace of the real micro-manipulator hand prototype is compared with that of the theoretical model and they are close to each other. The error norms for both the upper and lower fingers are checked. The error norm of the lower finger is found to be about 1.2μm and that of the upper finger is found to be about 1μm. Besides, the opening range of the two fingers is about 300μm.

1.5 Thesis Outline

This chapter presents a brief overview of the main topics that will be discussed in details in the following chapters. First, we begin with a brief introduction about robots and parallel mechanisms. Second, we introduce a brief Survey about Micro-Manipulation and

Micro-manipulators. Then, the main objectives of any piece of work, specially our thesis, are presented. Then, the main contribution of the research work in this thesis is addressed. Finally, the outline of the thesis including brief details about each chapter is presented.

Chapter 2, *Phase One: Analysis and Mathematical Modeling,* starts with literature review of the research background on the solution of the kinematics problem of 3-DOF RPS and PRS parallel mechanisms. Then, we will derive a new closed form solution for the IKP of 3-RPS parallel mechanism and modify it to be applicable for the case of 3-PRS parallel mechanism. The feasible workspace volume will be derived for both mechanisms to decide which one is more appropriate to our application. Next an algorithm will be presented for solving the IKP of 3-DOF PRS parallel structure with a numerical example. The application of the derived solution to solve the FKP of 3-DOF PRS parallel mechanism in an easy way is presented based on the Newton-Raphson method with a numerical example. Moreover, the application of the derived solution to solve the IKP based on the tip position of the end effector is discussed using Newton-Raphson method with a numerical example. Finally, this closed form solution will be extended to the hybrid structure motion mechanism of the micro-manipulator hand.

Chapter 3, *Phase Two: Optimization and Design*, begins with a brief introduction on search/optimization techniques. The optimization process is carried out in two sequential steps. First step carry out the optimization of the design parameters of the 3-DOF PRS parallel mechanism ideal model - based on the solution algorithm derived in chapter 2 - using discrete search method and Genetic and Evolutionary Algorithms (GEAs) for comparison purposes. The optimization goal is to maximize the workspace volume of the end effector. Based on the output of first step, a CAD model for parallel 3-DOF PRS micro finger module is build. Then the optimization of the pin flexure hinge mechanical parameters is carried out as a complementary step to decide the most suitable web thickness for the hinge. Finally, the CAD model for the hybrid two-fingered micro-manipulator hand is build.

Chapter 4, *Phase Three: Realization and Implementation*, presents the prototype realization of the two-fingered micro-manipulator hand CAD model. The description of

the practical hardware system for the two-fingered micro-manipulator hand is discussed. Actually we imitated the same hardware system of the old version of the two-fingered micro-manipulator hand with few differences. The program description, practical calibration method, practical jacobian matrices, practical workspace, and error analysis of the prototype are discussed and presented.

Finally, chapter 5 concludes our thesis with a brief summary of achievements, an outline of possible directions for future research, and some speculations about issues which have not been resolved.

CHAPTER 2

Phase One: Analysis and Mathematical Modeling

In this chapter, a mathematical analysis and modeling of the basic unit of our proposed two-fingered micro-manipulator hand are discussed. First, a literature review of the research background on the solution of the kinematics problem of 3-DOF RPS and PRS parallel mechanisms is presented. Then, a novel closed form solution for the IKP of 3-RPS parallel mechanism is derived and modified to be applicable for the case of 3-PRS parallel mechanism. The feasible workspace volume is derived for both mechanisms to decide which one can be used in our design. A solution algorithm is presented for solving the IKP of 3-DOF PRS parallel structure with a numerical example. The application of the derived solution to solve the FKP of 3-DOF PRS parallel mechanism and to solve the IKP based on the tip position of the end effector is discussed based on the Newton-Raphson method both with a numerical example. Finally, the derived closed form solution will be extended to the hybrid structure motion mechanism of the micro-manipulator hand.

2.1 Literature Review

The motion of 3-DOF PRS parallel mechanism, in both orientation and translation degrees of freedom, is highly coupled and nonlinear which complicates the investigation. This problem does not exist in the manipulators with a different parallel structure [9-13]. The IKP for 3-DOF RPS, which is similar but simpler in analysis to 3-DOF PRS, parallel mechanism was studied by S. M. Song and M. D. Zhang [13]. They showed that in the general case there are eight different IKP solutions for a given position of mobile plate center. L. Tsai [12] mentioned the same conclusion with reference to the results achieved by previous authors. This chapter proves that among those solutions there are only four solutions which satisfy both mathematical and physical conditions. Therefore the number

of solutions for the IKP was not fully investigated by the authors. Besides, the derived equations of their solution are very complex.

K. M. Lee and D. K. Shah [14] investigated the inverse and direct kinematics problem for the case when the manipulator motion is determined by two degrees of orientation and the vertical coordinate. The direct kinematics and physical constraints were also studied in that paper.

Yi Lu et al [18] introduced a solution for the IKP based on first determining three φ-angles (φ1, φ2, φ3) for each 3-DOF RPS module. The equations given for those angles are nonlinear, highly coupled, and there is no clear closed form solution for them. So, the authors concluded that analytic approach is not straightforward and quit complicated for compiling computer program. Therefore, they used a computer aided geometric approach in Solidwork software for constituting the mechanism simulation.

A. Sokolov and P. Xirochakis [46] presented a theoretical analysis for the IKP of 3-DOF RPS parallel mechanism. They derived a solution for the IKP based on using five sign variables (s1, s2, s3, s4, s5) and then they reduced them to only four sign variables. The solution suffers from complexity because of using many sign variables. They concluded that for a given position of mobile plate center, there are only four acceptable solutions for the IKP.

O. Ibrahim and W. Khalil [47] and J. Gallardo-Alvarado et al [48] proposed a solution based on screw theory. Also H. Pendar et al investigated the mechanism through Lagrange method [49]. K. Fan et al studied the sensitivity analysis of the 3-PRS mechanism [50]. Y. Ohya et al [25] presented a solution for IKP of 3-PRS parallel manipulator but also based on the solution of S. M. Song and M. D. Zhang. Y. Li and Q. Xu [51] investigated the kinematics analysis of 3-PRS parallel mechanism of different structure other than the one presented in this thesis based on screw theory.

The main objective of the current phase is to investigate the kinematics problem of both 3-DOF RPS and 3-DOF PRS parallel mechanisms and drive an IKP closed form

solution - in the form of simple equations - for that class of parallel mechanisms, besides the FKP will be solved based on that solution using Newton-Raphson method [52-65].

2.2 Structural Mechanism of Micro-Manipulator Hand

One possible structure of a two-fingered micro-manipulator hand consists of two finger modules arranged in parallel as shown in Fig. 2.1. Two problems arise for this structure. The first one is a small effective workspace volume for the two fingers. The effective workspace for two fingers is the overlapping space of each finger's workspace volume. The other problem is that cooperative control of two fingers for manipulating microscopic objects is rather difficult, because the relative position of the fingers must be tightly controlled. If the manipulator hand mechanism is calibrated accurately, the position of each finger tip can be accurate, but in practice, model errors by temperature changes and long term usage disrupt this approach [39, 52].

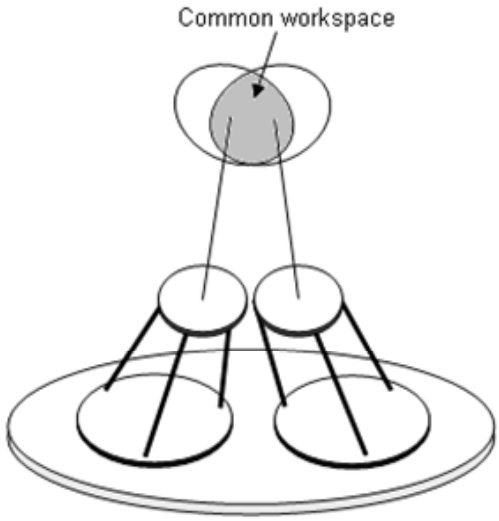

Fig. 2.1: In parallel two-fingered micro-manipulator hand.

The proposed hybrid two-fingered micro-manipulator hand consists of two modules connected in series, upper and lower modules; each of them has 3-DOF architecture. One finger set on upper module is attached to the mobile plate of lower module and another finger set is attached to the mobile plate of upper module as shown in Fig. 2.2. The two fingers are made of long glass pipettes tapered to very sharp end. The lower module is the mirror image, with 60 deg rotation, of the upper module about the middle plate. That is,

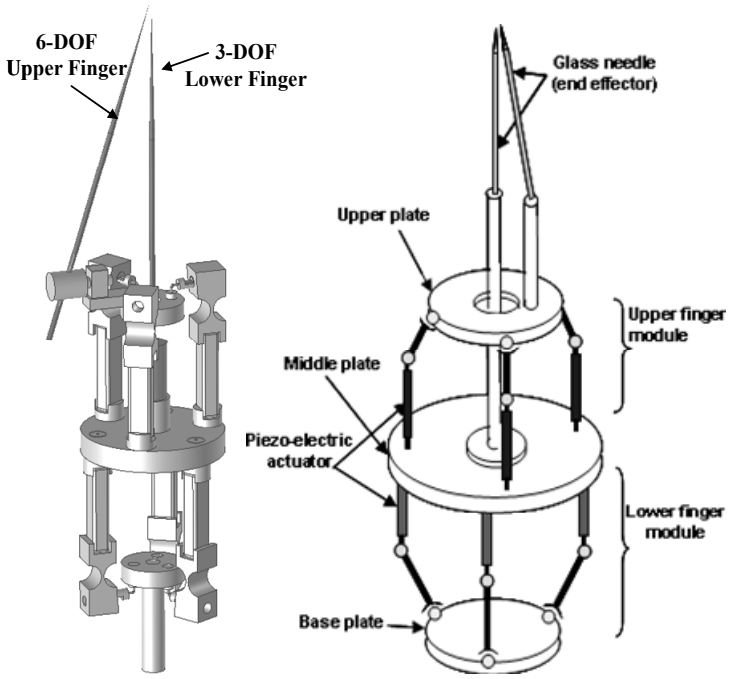

Fig. 2.2: In series two-fingered micro-manipulator hand.

the upper module consists of three identical kinematics chains with PRS joint structure, while the lower module consists of three identical kinematics chains but with SRP joint structure. The mechanism is actuated by three piezo-electric actuators in each module. By this configuration the two fingers can be controlled like chopstick motion, one chopstick for support and the other for fine motion. We adopt a pin flexure hinge to act as a revolute joint and a wire to act as a ball joint. This arrangement has the advantages that the micro-manipulator hand with optimal design parameters has small size, simple, compact, and large workspace volume.

For microscopic objects manipulation, it is found that a 3-DOF finger module is functionally equivalent to a fully 6-DOF finger module in this two-fingered arrangement [25]. Thus a 3-DOF finger has advantages in cost, control complexity, weight and size over a 6-DOF finger.

Due to the serial configuration of the two finger modules in the proposed architecture, the lower finger will have 3-DOF while the upper finger will have 6-DOF. As for the chopstick like mechanism, the lower finger will be used mainly for support only while the

upper finger will be used for generating dexterous motion around the lower finger for effective handling of the microscopic objects [53].

2.3 Novel Closed Form Solution of IKP

To control a robot mechanism motion, it is necessary to establish the location of the end-effector relative to the base. This can be achieved based on the position analysis, which consists in solving the *inverse* and *direct* kinematics problems.

The relation that determine the articular coordinates - or joint variables; in Fig. 2.3 the joint variables are the lengths of the legs *AB* - for a given known pose - the position of point C and the mobile platform orientation - of the end-effector is called *inverse kinematics*. The inverse kinematics deals with calculating the value of the articular coordinates corresponding to the end-effector configuration [11]. On the other hand, for direct kinematics, the joint variables are given and the problem is to find the location and orientation of the end-effector [12].

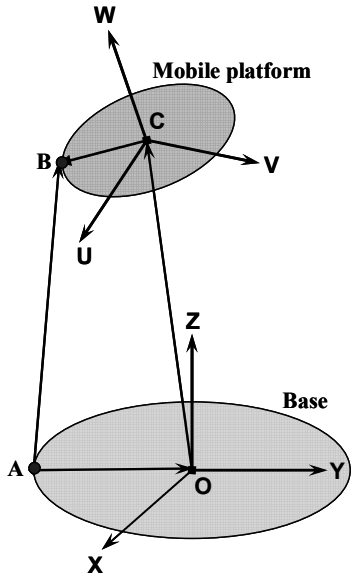

Fig. 2.3: Position vectors of the connecting points of the linking leg.

Consider a general parallel manipulator as in Fig. 2.3. The coordinate system *O-XYZ* is fixed to the base while *C-UVW* is fixed to the mobile platform. Each leg *AB* is linking the

base to the mobile platform. The leg is connected to the base at point *A*, which is fixed to the base. The location of the leg-platform connecting point *B* is determined from the position *OC* and orientation *CB* of the mobile platform. The inverse kinematics problem concerns with the calculation of *AB* given *OC* and *CB* according to (2.1).

$$AB = AO + OC + CB \tag{2.1}$$

For 6-DOF parallel manipulators the inverse kinematics task is straightforward and simple since the position and orientation of the mobile platform is given and consequently the length of the legs can easily be determined using (2.1). However, for 3-DOF manipulators the inverse kinematics task is not so simple since only three of the six coordinates of the mobile platform are given and the rest must be determined by employing the joint kinematic constraints. Therefore, the goal of this section is to present the derivation of the solution equations of the IKP for 3-DOF RPS and 3-DOF PRS parallel mechanisms.

From the literature review of section 2.1, the previous research work in finding the IKP solution for 3-DOF RPS and 3-DOF PRS parallel mechanisms can be categorized into two main groups;

- *Group one*: the IKP has eight "8" solutions like S. M. Song and M. D. Zhang [13] (1995), L. W. Tsai [12] (1999), Y. Ohya et al [25] (1999), and Yi Lu et al [18] (2005). All authors after S. M. Song and M. D. Zhang [13] refer to their solution that is based on very complicated equations.
- *Group two*: the IKP has four "4" solutions as stated by A. Sokolov and P. Xirochakis [46] (2005). But the given solution is very complicated and depends on many sign variables.

In this section we will prove that IKP solutions are not completely investigated. We will define two condition – Mathematical condition and Physical condition – that have to be satisfied by the IKP solution. Based on the two condition defined, we found that there are eight "8" mathematically accepted solutions but only four "4" of them are physically accepted. So, there are only four "4" solutions satisfying both conditions.

The idea behind the solution is to decouple the equations of position and orientation variables of the mobile plate to get the orientation matrix in terms of the position variables. Each position of the mobile plate center will have eight mathematically accepted solutions for orientation matrix; four of them are physically accepted while the other four are rejected due to physical limitation

2.3.1 Solution of 3-DOF RPS Parallel Mechanism IKP

Consider a 3-DOF RPS parallel mechanism represented in Fig. 2.4 with its vector representation of a single kinematics chain. A mobile plate and a base plate are linked by three limbs exhibiting same topology, each limb is connected to the base with R-joint and to the mobile plate with S-joint. Points P_i and B_i (i=1,2,3) are symmetrically arranged on the circumference of circles with radii R and r respectively. A fixed Cartesian frame *O-XYZ* is attached to the center of the base plate with *X*-axis in the direction of OP_1, *Z*-axis is vertical to the plane of the base. A mobile frame *C-UVW*, which has the same pose as the frame *O-XYZ*, is attached to the center of the mobile plate. The P-joint in the connecting rods is the active joint. The end effector can be attached to the center of mobile plate perpendicular to the plate surface in the *W*-direction for symmetrical workspace.

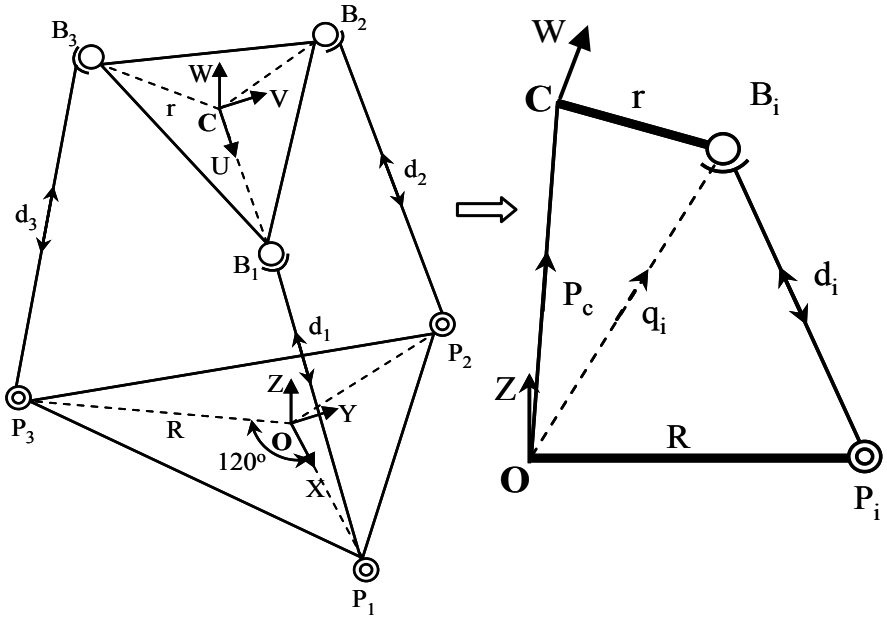

Fig. 2.4: Geometrical structure (left) and vector representation of a single chain (right) of the 3-DOF RPS parallel mechanism.

The considered 3-DOF RPS parallel mechanism has three degrees of freedom, as can be proved by Grübler/Kutzbach criterion [11, 12].

$$\begin{aligned} F &= \lambda(n - j - 1) + \sum_i f_i \\ F &= 6(8 - 9 - 1) + 3(1 + 1 + 3) = 3 \end{aligned} \tag{2.2}$$

where F is the number of DOF, n is the number of links, j is the number of joints, λ is the DOF of the space within which the mechanism operates; $\lambda = 6$, and f_i is the DOF of the i^{th} joint in the kinematics chain.

From Fig. 2.4, the coordinates of the points P_i referred to the base fixed reference frame XYZ are given by (2.3).

$$P_1 = \begin{bmatrix} R \\ 0 \\ 0 \end{bmatrix}, \quad P_2 = \begin{bmatrix} -0.5R \\ 0.5\sqrt{3}\ R \\ 0 \end{bmatrix}, \quad P_3 = \begin{bmatrix} -0.5R \\ -0.5\sqrt{3}\ R \\ 0 \end{bmatrix} \tag{2.3}$$

Similarly, the coordinates of the points B_i referred to the mobile frame UVW are given by (2.4).

$$B_{1m} = \begin{bmatrix} r \\ 0 \\ 0 \end{bmatrix}, \quad B_{2m} = \begin{bmatrix} -0.5r \\ 0.5\sqrt{3}\,r \\ 0 \end{bmatrix}, \quad B_{3m} = \begin{bmatrix} -0.5r \\ -0.5\sqrt{3}\,r \\ 0 \end{bmatrix} \tag{2.4}$$

The transformation from mobile frame to fixed base frame is expressed by a position vector P_c equal to OC and a rotation matrix ${}^bR_m$ described by the direction cosines of unit vectors u, v, and w as specified in (2.5) and satisfy the orthogonal conditions given by (2.6).

$$P_c = \begin{bmatrix} P_{cx} \\ P_{cy} \\ P_{cz} \end{bmatrix}, \quad {}^bR_m = \begin{bmatrix} u_x & v_x & w_x \\ u_y & v_y & w_y \\ u_z & v_z & w_z \end{bmatrix} \tag{2.5}$$

$$\begin{aligned} u \cdot u &= v \cdot v = w \cdot w = 1 \\ u \cdot v &= v \cdot w = w \cdot u = 0 \end{aligned} \tag{2.6}$$

The coordinates of points B_i referred to fixed base frame are:

$$B_i = {}^{b}R_m \cdot B_{im} + P_c \tag{2.7}$$

Substituting by (2.4) and (2.5) into (2.7), we get the ball joints center points referred to the fixed base frame.

$$B_1 = \begin{bmatrix} P_{cx} + ru_x \\ P_{cy} + ru_y \\ P_{cz} + ru_z \end{bmatrix}, \quad B_2 = \begin{bmatrix} P_{cx} - 0.5ru_x + 0.5\sqrt{3}rv_x \\ P_{cy} - 0.5ru_y + 0.5\sqrt{3}rv_y \\ P_{cz} - 0.5ru_z + 0.5\sqrt{3}rv_z \end{bmatrix},$$
$$B_3 = \begin{bmatrix} P_{cx} - 0.5ru_x - 0.5\sqrt{3}rv_x \\ P_{cy} - 0.5ru_y - 0.5\sqrt{3}rv_y \\ P_{cz} - 0.5ru_z - 0.5\sqrt{3}rv_z \end{bmatrix} \tag{2.8}$$

But the revolute joints at P_i constrain the motion of these points in the workspace as given by (2.9).

$$B_{1y} = 0, \quad B_{2y} = -\sqrt{3}B_{2x}, and \quad B_{3y} = \sqrt{3}B_{3x} \tag{2.9}$$

Substituting from (2.8) into (2.9) and simplifying to get the abbreviated form of the constraints equations, we can prove that:

$$P_{cy} + ru_y = 0, \quad v_x = u_y, and \quad P_{cx} = 0.5r\left(u_x - v_y\right) \tag{2.10}$$

Using (2.10) with the orthogonal conditions (2.6) and for a given position of mobile plate center - P_{cx}, P_{cy}, and P_{cz}, - we can infer that the rotation matrix can be expressed as given by (2.11).

$$C_1 = \begin{bmatrix} 2a + v_y \\ -b \\ S_u\sqrt{1-(2a+v_y)^2 - b^2} \end{bmatrix}, \quad C_2 = \begin{bmatrix} -b \\ v_y \\ S_v\sqrt{1-b^2 - v_y^2} \end{bmatrix}, \qquad (2.11)$$

$${}^{b}R_m = \begin{bmatrix} C_1 & C_2 & C_1 \times C_2 \end{bmatrix}$$

where C_1 is the direction cosines of U-axis, C_2 is the direction cosines of V-axis, $C_1 \times C_2$ is the cross product of the first two columns that represents the direction cosines of W-axis, v_y is the solution of the 4th order equation given by (2.12) and S_u and S_v are sign variables that have the value +1or -1.

$$v_y^{\,4} + 4av_y^{\,3} - fv_y^{\,2} - gv_y + k = 0$$

$$where, \quad a = \frac{P_{cx}}{r}, \quad b = \frac{P_{cy}}{r}, and$$

$$f = 2 - 4a^2 + 2b^2$$

$$g = 4a + 4ab^2 \qquad (2.12)$$

$$k = 1 - 4a^2 - 2b^2 + b^4$$

Equation (2.12) has four solutions given by (2.13).

$$v_{y1} = -a + 1 + \sqrt{a^2 + b^2}$$

$$v_{y2} = -a - 1 - \sqrt{a^2 + b^2}$$

$$v_{y3} = -a - 1 + \sqrt{a^2 + b^2} \qquad (2.13)$$

$$v_{y4} = -a + 1 - \sqrt{a^2 + b^2}$$

Two solutions - v_{y1} and v_{y2} - each has an absolute value greater than or equal to unity which are mathematically rejected and the other two each has an absolute value less than or equal to unity that are mathematically accepted. This is because the absolute value of v_y, that is a direction cosine term, must be less than or equal to unity. For mathematically accepted two solutions; one of them - v_{y3} - is physically accepted and the other one - v_{y4} –

is physically rejected due to legs interference or violation of actuators limitation. So, *there are eight mathematically accepted solutions but when we consider the physical constraints they reduced to only four solutions*. These four solutions correspond to minimum actuator displacements without leg interference.

As a result, the same center position of mobile plate is associated with four alternatives of orientation matrix ${}^{b}R_{m}$ which satisfy two conditions [53]:

1- *Mathematical condition*: The absolute values of the directional cosine terms of the mobile plate orientation matrix must be real and less than or equal to unity.
2- *Physical condition*: The *w*-axis of the mobile frame has the same pose as *z*-axis of the base frame with minimum actuator displacement and without leg interference.

In the derived solution, a given position of the mobile plate center P_c has only four - mathematically and physically accepted - solutions for the orientation matrix correspond to v_{y4}. The accepted four orientation matrices ${}^{b}R_{m}$ can be constituted from expression (2.10) using table 2.1.

TABLE 2.1
SOLUTION CASES OF ORIENTATION MATRIX

	${}^{b}R_{m1}$	${}^{b}R_{m2}$	${}^{b}R_{m3}$	${}^{b}R_{m4}$
S_u	+1	-1	-1	+1
S_v	+1	+1	-1	-1

Once we have the orientation matrix ${}^{b}R_{m}$ and know the position vector P_c, using Fig. 2.4, we can proceed to determine the actuator displacements as follows:

$$\vec{P}_c + {}^{b}R_m \cdot \vec{B}_{im} = \overrightarrow{q_i} = \overrightarrow{P_i} + \overrightarrow{P_i B_i} = \overrightarrow{P_i} + \overrightarrow{d_i}$$
$$\therefore \vec{d}_i = \vec{q}_i - \vec{P}_i \qquad (2.14)$$

Dot product (2.14) by itself and simplify, we get (2.15).

$$\left\|P_i B_i\right\|^2 = {d_i}^2 = {q_i}^2 - 2\vec{q}_i \cdot \vec{P}_i + R^2 \tag{2.15}$$

Equation (2.15) is a 2nd order equation in d_i with a completely known right hand side. The general solution of the link length can be expressed as;

$$d_i = \sqrt{{q_i}^2 - 2\vec{q}_i \cdot \vec{P}_i + R^2} \tag{2.16}$$

Only the positive value of square root is accepted, because link length d_i can not be negative. If the initial length of the link is L_0, the actuator displacement required can be calculated as;

$$disp_i = d_i - L_0 \tag{2.17}$$

To prove the dependency of three parameters of the position and orientation variables, we will use Euler *ZYZ* angles (α, β, γ) as the rotation matrix ${}^{b}R_m$ [13, 53]. From (2.10), we can prove that;

$$\gamma = -\alpha \tag{2.18}$$

Substituting in Euler angles *ZYZ* rotation matrix ${}^{b}R_m$ and then substitute in (2.10) again, we get (2.19).

$$\begin{aligned} P_{cx} &= -0.5r(1 - \cos\beta)\cos 2\alpha \\ P_{cy} &= 0.5r(1 - \cos\beta)\sin 2\alpha \end{aligned} \tag{2.19}$$

From (2.16), (2.18), and (2.19), we conclude that P_{cz}, α, and β are the independent variables while P_{cx}, P_{cy}, and γ are the dependent variables. So, this mechanism has 3-DOF that are one translational P_{cz} and two rotational α and β.

2.3.2 Solution of 3-DOF PRS Parallel Mechanism IKP

The geometrical structure of a 3-DOF PRS parallel motion mechanism and its vector representation is shown in Fig. 2.5. A mobile plate and a fixed base plate are linked by three legs exhibiting same topology, each leg is connected to the base with P-joint and to the mobile plate with S-joint. Links $P_{0i}P_i$ and P_iB_i (i=1,2,3) are joined by R-joint. Points P_{0i} and B_i are respectively arranged symmetrically on the circumference of circles with radii R and r. Lengths of links $P_{0i}P_i$ and P_iB_i are respectively denoted as d_i and L_i. A fixed Cartesian frame XYZ is attached to the center of the base plate with X-axis along direction of OP_{01} and Z-axis vertical to the plane of the base. A mobile frame UVW, which has same pose with the frame XYZ, is attached to the center of the mobile plate. Links P_iB_i are of fixed length L while links $P_{0i}P_i$ are of variable length in the Z-direction according to the displacements of the prismatic – in our case, Piezo-electric (PZT) - actuator.

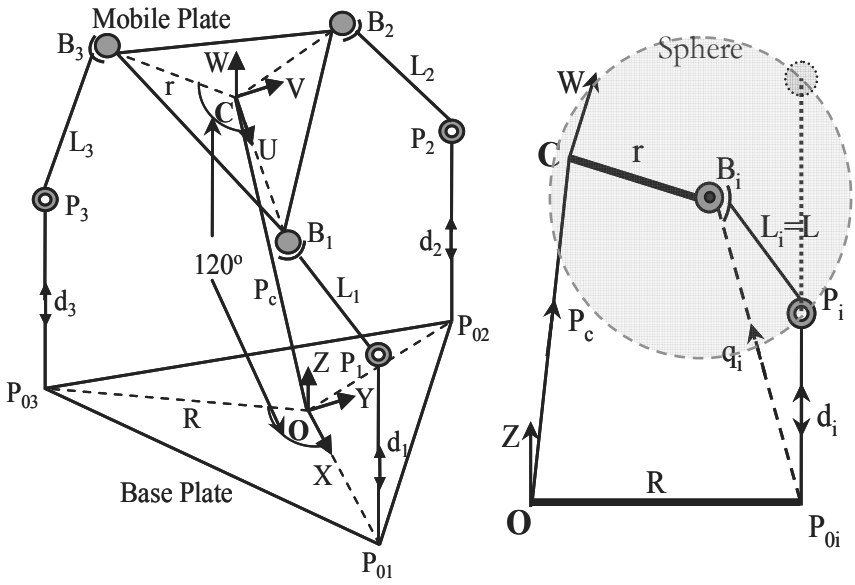

Fig. 2.5: Geometrical structure (left) and vector representation of a single chain (right) of the 3-DOF PRS parallel mechanism.

The considered 3-DOF PRS parallel mechanism has three degrees of freedom as the previous one. The IKP solution is similar in the first part to that of the 3-DOF RPS parallel mechanism of section 2.3.1. Many researchers investigated the IKP of 3-DOF RPS parallel mechanism but very few investigated the IKP of 3-DOF PRS parallel mechanism. In this

section we will drive a closed form solution for the IKP of 3-DOF PRS parallel mechanism in the form of simple equations [52, 55].

Using the geometrical structure for the 3-DOF PRS parallel mechanism in Fig. 2.5, the coordinates of the points P_{0i} and P_i referred to the fixed base reference frame XYZ are given by (2.20) and (2.21)

$$P_{01} = \begin{bmatrix} R \\ 0 \\ 0 \end{bmatrix}, \quad P_{02} = \begin{bmatrix} -0.5R \\ \frac{\sqrt{3}}{2} R \\ 0 \end{bmatrix}, \quad P_{03} = \begin{bmatrix} -0.5R \\ \frac{-\sqrt{3}}{2} R \\ 0 \end{bmatrix} \tag{2.20}$$

$$P_1 = \begin{bmatrix} R \\ 0 \\ d_1 \end{bmatrix}, \quad P_2 = \begin{bmatrix} -0.5R \\ \frac{\sqrt{3}}{2} R \\ d_2 \end{bmatrix}, \quad P_3 = \begin{bmatrix} -0.5R \\ \frac{-\sqrt{3}}{2} R \\ d_3 \end{bmatrix} \tag{2.21}$$

The solution steps are identical to the previous case of 3-DOF RPS parallel mechanism to get the orientation matrix ${}^{b}R_{m}$. For this case, only v_{y4} satisfies both mathematical and physical conditions. Solution v_{y3} give imaginary value for displacement due to physical condition violation. Once we get the orientation matrix ${}^{b}R_{m}$ and we have the center position vector P_c, using Fig. 2.5, we can proceed as follows:

$$\overrightarrow{q_i} = \overrightarrow{P_{0i}B_i} = \overrightarrow{B_i} - \overrightarrow{P_{0i}} = d_i \underline{z} + \overrightarrow{P_iB_i} \tag{2.22}$$

Dot product (2.22) by itself and simplify, we get (2.23).

$$\left\| P_{0i}B_i \right\|^2 = {q_i}^2 = {d_i}^2 + 2d_i \cdot \left(\overrightarrow{P_iB_i} \right)_z + L^2 \tag{2.23}$$

Equation (2.23) is a 2nd order equation in d_i. The two solutions of (2.23) can be expressed in simple form as;

$$d_i|_{1,2} = [B_i]_z \pm \sqrt{[B_i]_z^{\,2} - \left({q_i}^2 - L^2 \right)} \tag{2.24}$$

where d_i is the displacement of PZT actuator i, $[B_i]_z$ is the z-component of ball joint i, q_i is the magnitude of vector $P_{0i}B_i$, L is the link length from ball joint to revolute joint, and i=1,2,3. Equation (2.24) indicates that there are two solutions for the actuators displacements representing the intersection of the displacement vector $d_i\, z$ with the surface of a sphere of radius L and centered at B_i as shown in Fig. 2.5. For minimum displacement of PZT actuators, we choose the negative sign for the square root – which is the lower intersection point [54 - 56], thus;

$$d_i = [B_i]_z - \sqrt{[B_i]_z^{\,2} - \left(q_i^{\,2} - L^2\right)} \tag{2.25}$$

Equation (2.25) represents the closed form solution for the IKP of 3-DOF PRS parallel mechanism. It is worth stating that *there is a 1-to-4 relationship in between the position of the mobile plate center and the actuator displacements*. So, *the same mobile plate center position can be obtained using four alternatives of* d_1, d_2, *and* d_3 *each has a different orientation matrix* ${}^{b}R_m$. Equation (2.25) represents the general solution for the actuators displacements, from which we can determine the PZT actuator displacement in each leg as given by (2.26).

$$\begin{aligned} d_1 &= [B_1]_z - \sqrt{[B_1]_z^{\,2} - \left(q_1^{\,2} - L^2\right)} \\ d_2 &= [B_2]_z - \sqrt{[B_2]_z^{\,2} - \left(q_2^{\,2} - L^2\right)} \\ d_3 &= [B_3]_z - \sqrt{[B_3]_z^{\,2} - \left(q_3^{\,2} - L^2\right)} \end{aligned} \tag{2.26}$$

For the proposed architecture of our micro-manipulator hand, a glass pipette -of length L_e - as an end effector is attached to the center of the mobile plate in w-direction. The position of the tip of the glass pipette end effector P_e is given by (2.27).

$$P_e = {}^{b}R_m \cdot P_{em} + P_c$$
$$where\ , \quad P_{em} = \begin{bmatrix} 0 \\ 0 \\ L_e \end{bmatrix} \quad and \quad P_c = \begin{bmatrix} P_{cx} \\ P_{cy} \\ P_{cz} \end{bmatrix} \tag{2.27}$$

where P_{em} is the position of the glass pipette in the mobile frame, L_e is the length of glass pipette end effector, ${}^{b}R_m$ is the orientation matrix of the mobile frame relative to base frame, and P_c is the mobile frame center position.

It is also worth stating that there is a 1-to-1 relationship in between the end effector tip position and the actuator displacements. So, each position of P_e has only one set of d_1, d_2, and d_3 that is defined by a particular orientation matrix ${}^{b}R_m$. *Each orientation matrix* ${}^{b}R_m$ *locate the end effector in one of the four quarters of the upper half of the space*.

This 3-DOF PRS parallel mechanism has three degrees of freedom that are one translational and two rotational as can be proved in the same way as in section 2.3.1.

2.3.3 Feasible Workspace Volume of IKP Solution

If the limits of the prismatic, revolute and spherical joints are not taken into consideration, both 3-DOF RPS and 3-DOS PRS parallel structures have the same feasible workspace volume for their IKP solution which is the boundary of a vertical cylinder with radius ρ = r and Z-coordinate as its axis [53, 80]. This is shown in Fig. 2.6 and can be easily proved using (2.11).

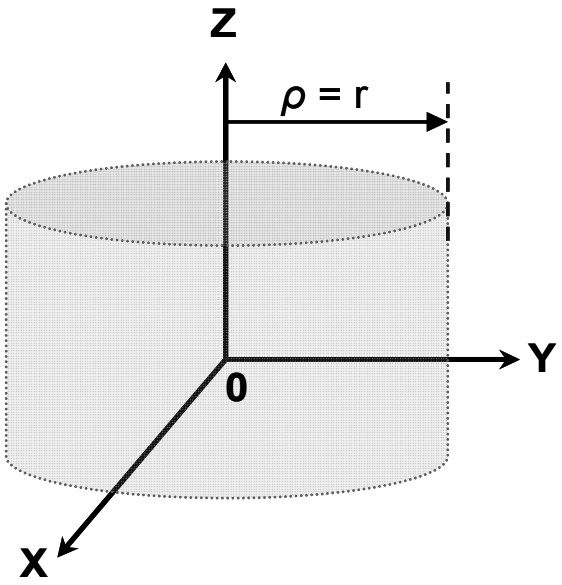

Fig. 2.6: Feasible workspace volume of the IKP solution

For the existence of a real solution, the under radicals' terms in (2.11) must be non-negative and real that can be expressed as the following two conditions in (2.28) [53].

$$\begin{aligned} &1-\left(2a+v_y\right)^2-b^2\geq 0 \quad \textit{and} \\ &1-b^2-v_y^2\geq 0 \end{aligned} \tag{2.28}$$

Substituting for a, b, and v_y from (2.12) and simplifying.

$$\begin{aligned} &r^2-P_{cy}^2-\left(r+P_{cy}-\sqrt{P_{cx}^2+P_{cy}^2}\right)^2\geq 0 \quad \textit{and} \\ &r^2-P_{cy}^2-\left(r-P_{cy}-\sqrt{P_{cx}^2+P_{cy}^2}\right)^2\geq 0 \end{aligned} \tag{2.29}$$

For simplicity, we can transform (2.29) to the cylindrical coordinates using the transformation equations given by (2.30) to get the new form of the conditions of (2.28) as given in (2.31).

$$P_{cz}=P_{cz} \qquad P_{cx}=\rho\cdot Cos\theta \qquad \textit{and} \qquad P_{cy}=\rho\cdot Sin\theta \tag{2.30}$$

$$\begin{aligned} &r^2-\rho^2\cdot Sin^2\theta-\left(\left[r-\rho\right]+\rho\cdot Cos\theta\right)^2\geq 0 \quad \textit{and} \\ &r^2-\rho^2\cdot Sin^2\theta-\left(\left[r-\rho\right]-\rho\cdot Cos\theta\right)^2\geq 0 \end{aligned} \tag{2.31}$$

The two conditions in (2.31) can be simplified to (2.32).

$$\begin{aligned} &2\rho\left(r-\rho\right)\left(1-Cos\theta\right)\geq 0 \quad \textit{and} \\ &2\rho\left(r-\rho\right)\left(1+Cos\theta\right)\geq 0 \end{aligned} \tag{2.32}$$

Both conditions of (2.32) are satisfied only for the value of ρ given by (2.33) which is represented in Fig. 2.6.

$$0\leq\rho\leq r \tag{2.33}$$

Due to large similarities in between 3-DOF RPS and 3-DOF PRS parallel mechanisms, either of them can be used in our proposed micro-manipulator hand. We decided to build the proposed hand based on 3-DOF PRS parallel mechanism. Also, the fabrication of small scale 3-DOF PRS parallel mechanism is easier than that of 3-DOF RPS parallel mechanism. The end effector will be a glass pipette attached to the center of the mobile plate of the chosen mechanism.

2.4 Solution Algorithm of 3-DOF PRS Parallel Mechanism IKP

The closed form solution derived in the previous section for the IKP of 3-DOF PRS parallel mechanism can be simplified into a series of steps – algorithm. This algorithm can be used to numerically calculate the actuators displacements - d_1, d_2, and d_3 - for a given position of the mobile plate center P_c - P_{cx}, P_{cy}, and P_{cz}.

Figure 2.7 shows the proposed 3-DOF PRS parallel finger module that uses a long glass pipette attached to the center of its mobile plate as an end effector. The algorithm steps to calculate the IKP solutions for 3-DOF PRS parallel finger module are [63]:

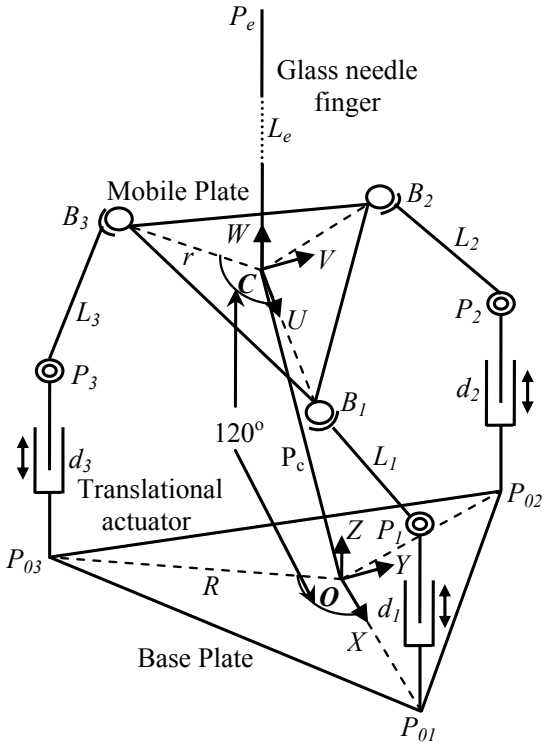

Fig. 2.7: Geometrical structure of the 3-DOF PRS parallel finger module.

1- *Define* the *parameters R, r, L,* and L_e *of the 3-DOF PRS parallel mechanism*.

2- *For a given position of mobile plate center* P_c - P_{cx}, P_{cy}, and P_{cz} - *calculate the direction cosine term* v_y *using*:

$$v_y = v_{y4} = -a + 1 - \sqrt{a^2 + b^2}, \quad a = \frac{P_{cx}}{r}, \quad b = \frac{P_{cy}}{r}$$

3- *Then determine the four alternatives of orientation matrix* ${}^bR_m$ *using:*

$$C_1 = \begin{bmatrix} 2a + v_y \\ -b \\ S_u\sqrt{1-(2a+v_y)^2 - b^2} \end{bmatrix}, \quad C_2 = \begin{bmatrix} -b \\ v_y \\ S_v\sqrt{1-b^2-v_y^2} \end{bmatrix}, \text{ where,}$$

$${}^bR_m = \begin{bmatrix} C_1 & C_2 & C_1 \times C_2 \end{bmatrix}$$

	${}^bR_{m1}$	${}^bR_{m2}$	${}^bR_{m3}$	${}^bR_{m4}$
S_u	+1	-1	-1	+1
S_v	+1	+1	-1	-1

4- *For each orientation matrix* ${}^bR_m$ *alternative*:

a. *Determine the position of the ball joints* B_i *and then calculate* q_i

$$B_i = {}^bR_m \cdot B_{im} + P_c \text{, and}$$

$$q_i = \overrightarrow{P_{0i}B_i} = \overrightarrow{B_i} - \overrightarrow{P_{0i}}$$

b. *Determine the actuator displacement* d_i *using:*

$$d_1 = [B_1]_z - \sqrt{[B_1]_z^2 - \left(q_1^2 - L^2\right)}$$

$$d_2 = [B_2]_z - \sqrt{[B_2]_z^2 - \left(q_2^2 - L^2\right)}$$

$$d_3 = [B_3]_z - \sqrt{[B_3]_z^2 - \left(q_3^2 - L^2\right)}$$

c. *Determine the corresponding end effector position* P_e *using:*

$$P_e = {}^bR_m \cdot P_{em} + P_c$$

$$where, \quad P_{em} = \begin{bmatrix} 0 \\ 0 \\ L_e \end{bmatrix} \quad and \quad P_c = \begin{bmatrix} P_{cx} \\ P_{cy} \\ P_{cz} \end{bmatrix}$$

The previous algorithm steps are applied to 3-DOF PRS parallel finger module having the parameters; R =10mm, r=3.5mm, L=13mm, and L_e=100mm and for a given mobile plate center position of P_c= [0.17, 0.03, 14.2583]^T. The results obtained from calculation have a clear symmetry due to the nature of the parallel mechanism structure and are summarized in table 2.2.

TABLE 2.2
IKP SOLUTION OF 3-DOF PRS PARALLEL MECHANISM

Parameters: R =10mm, r=3.5mm, L=13mm, L_e=100mm, and given the position of the mobile plate center:

$$P_c = \begin{bmatrix} 0.17 & 0.03 & 14.2583 \end{bmatrix}^T$$

$$v_y = 0.9021$$

$${}^b R_{m1} = \begin{bmatrix} 0.9992 & -0.0086 & -0.0378 \\ -0.0086 & 0.9021 & -0.4314 \\ 0.0378 & 0.4314 & 0.9014 \end{bmatrix}, \quad {}^b R_{m2} = \begin{bmatrix} 0.9992 & -0.0086 & 0.0304 \\ -0.0086 & 0.9021 & -0.4308 \\ -0.0378 & 0.4314 & 0.9014 \end{bmatrix}$$

$${}^b R_{m3} = \begin{bmatrix} 0.9992 & -0.0086 & 0.0378 \\ -0.0086 & 0.9021 & 0.4314 \\ -0.0378 & -0.4314 & 0.9014 \end{bmatrix}, \quad {}^b R_{m4} = \begin{bmatrix} 0.9992 & -0.0086 & -0.0304 \\ -0.0086 & 0.9021 & 0.4308 \\ 0.0378 & -0.4314 & 0.9014 \end{bmatrix}$$

$$\begin{bmatrix} d_1 \\ d_2 \\ d_3 \end{bmatrix}_1 = \begin{bmatrix} 3.0372 \\ 4.4145 \\ 1.8634 \end{bmatrix}, \quad \begin{bmatrix} d_1 \\ d_2 \\ d_3 \end{bmatrix}_2 = \begin{bmatrix} 2.7728 \\ 4.5467 \\ 1.9956 \end{bmatrix}, \quad \begin{bmatrix} d_1 \\ d_2 \\ d_3 \end{bmatrix}_3 = \begin{bmatrix} 2.7728 \\ 1.9313 \\ 4.6110 \end{bmatrix}, \quad \begin{bmatrix} d_1 \\ d_2 \\ d_3 \end{bmatrix}_4 = \begin{bmatrix} 3.0372 \\ 1.7991 \\ 4.4788 \end{bmatrix}$$

$$P_{e1} = \begin{bmatrix} -3.6075 \\ -43.1128 \\ 104.3939 \end{bmatrix}, \quad P_{e2} = \begin{bmatrix} 3.2079 \\ -43.0481 \\ 104.3939 \end{bmatrix}, \quad P_{e3} = \begin{bmatrix} 3.9475 \\ 43.1728 \\ 104.3939 \end{bmatrix}, \quad P_{e4} = \begin{bmatrix} -2.8679 \\ 43.1081 \\ 104.3939 \end{bmatrix}$$

2.5 An IKP Numerical Solution of 3-DOF PRS Parallel Mechanism for a Given End Effector Tip Position

The IKP solution given in the previous section is calculated based on the position of the mobile plate center. However, in practice the more convenient case is to give the position of the end effector tip not that of the mobile plate center. So, the outlined method in this section describes how to find the solution of the IKP starting from the given position of the end effector tip using the previous IKP in section 2.3 together with Newton-Raphson method [64, 80].

The proposed method depends on first calculating the position of the mobile plate center and then applies the algorithm presented in section 2.4 to calculate the actuators displacements that corresponds to the given position of the end effector. From equation (2.27) we can express P_e as a function of P_c - P_{cx}, P_{cy}, and P_{cz} - as described in (2.34).

$$
\begin{aligned}
& P_e = {}^{b}R_m \cdot P_{em} + P_c \\
\therefore \quad & P_e = \begin{bmatrix} C_1 & C_2 & C_1 \times C_2 \end{bmatrix} \cdot \begin{bmatrix} 0 \\ 0 \\ L_e \end{bmatrix} + \begin{bmatrix} P_{cx} \\ P_{cy} \\ P_{cz} \end{bmatrix} \\
\Rightarrow \quad & P_e = L_e.(C_1 \times C_2) + P_c \\
\therefore \quad & f(P_{cx}, P_{cy}, P_{cz}) = P_e - L_e.(C_1 \times C_2) - P_c = 0
\end{aligned}
\tag{2.34}
$$

The last equation is in the form required by Newton-Raphson method. In this form, the left hand side should be a function of the variables while the right hand side will be equal to zero. We can define the jacobian as:

$$
J(P_{cx}, P_{cy}, P_{cz}) = \frac{\partial f(P_{cx}, P_{cy}, P_{cz})}{\partial (P_{cx}, P_{cy}, P_{cz})} \tag{2.35}
$$

The solution for equation (2.34) can be found using repetitive calculation of the algorithm given by (2.36).

$$\begin{bmatrix} P_{cx} \\ P_{cy} \\ P_{cz} \end{bmatrix}^{k+1} = \begin{bmatrix} P_{cx} \\ P_{cy} \\ P_{cz} \end{bmatrix}^{k} - J^{-1}(P_{cx}, P_{cy}, P_{cz})^{k} . f(P_{cx}, P_{cy}, P_{cz})^{k} \tag{2.36}$$

where k+1 stands for the new/next solution and k stands for previous/old solution and provided that this solution equation is convergent.

This iterative algorithm can determine the final solution in about 4 or 5 iterations. A sequence of generated solutions for a given tip position of end effector [-3.6075, -43.1128, 104.3939]^{T} is presented in (2.37) – refer to table II.

$$\begin{bmatrix} P_{cx} \\ P_{cy} \\ P_{cz} \end{bmatrix}^{1\to 4} = \begin{bmatrix} 0.1263 \\ 0.0000 \\ 11.2237 \end{bmatrix} \Rightarrow \begin{bmatrix} 0.1674 \\ 0.0256 \\ 13.9585 \end{bmatrix} \Rightarrow \begin{bmatrix} 0.1700 \\ 0.0300 \\ 14.2558 \end{bmatrix} \Rightarrow \begin{bmatrix} 0.1700 \\ 0.0300 \\ 14.2583 \end{bmatrix} \tag{2.37}$$

After calculating the corresponding position of the mobile plate center, starting from this solution, we can proceed to find the actuators displacements using the algorithm of section 2.4 as in table II. From table II there are four solutions for the calculated position of the mobile plate center but only one of them matches the given position of the end effector. So, the solution for the given position of the end effector is presented in (2.38).

$$\begin{bmatrix} P_{ex} \\ P_{ey} \\ P_{ez} \end{bmatrix} = \begin{bmatrix} -3.6075 \\ -43.1128 \\ 104.3939 \end{bmatrix} \Rightarrow \begin{bmatrix} P_{cx} \\ P_{cy} \\ P_{cz} \end{bmatrix} = \begin{bmatrix} 0.1700 \\ 0.0300 \\ 14.2583 \end{bmatrix} \Rightarrow \begin{bmatrix} d_1 \\ d_2 \\ d_3 \end{bmatrix} = \begin{bmatrix} 3.0372 \\ 4.4145 \\ 1.8634 \end{bmatrix} \tag{2.38}$$

2.6 Solution Algorithm of the FKP of 3-DOF PRS Parallel Mechanism

The solution of FKP concerns with determining the position and orientation of the mobile plate center given the actuators displacements. Forward kinematics solution can be calculated using the Jacobian matrix, which is relating the generalized velocities of mobile platform to joint velocities [9, 12, and 22]. From (2.26), we have [56];

$$\begin{aligned} d_1 &= f_1\left(P_{cx}, P_{cy}, P_{cz}\right) \\ d_2 &= f_2\left(P_{cx}, P_{cy}, P_{cz}\right) \\ d_3 &= f_3\left(P_{cx}, P_{cy}, P_{cz}\right) \end{aligned} \tag{2.39}$$

Using (2.39), the derivatives with respect to time are;

$$\begin{aligned} d_1' &= \frac{df_1}{dP_{cx}} P_{cx}' + \frac{df_1}{dP_{cy}} P_{cy}' + \frac{df_1}{dP_{cz}} P_{cz}' \\ d_2' &= \frac{df_2}{dP_{cx}} P_{cx}' + \frac{df_2}{dP_{cy}} P_{cy}' + \frac{df_2}{dP_{cz}} P_{cz}' \\ d_3' &= \frac{df_3}{dP_{cx}} P_{cx}' + \frac{df_3}{dP_{cy}} P_{cy}' + \frac{df_3}{dP_{cz}} P_{cz}' \end{aligned} \tag{2.40}$$

Equation (2.40) can be expressed in matrix form as in (2.41).

$$\begin{bmatrix} d_1' \\ d_2' \\ d_3' \end{bmatrix} = \begin{bmatrix} \frac{df_1}{dP_{cx}} & \frac{df_1}{dP_{cy}} & \frac{df_1}{dP_{cz}} \\ \frac{df_2}{dP_{cx}} & \frac{df_2}{dP_{cy}} & \frac{df_2}{dP_{cz}} \\ \frac{df_3}{dP_{cx}} & \frac{df_3}{dP_{cy}} & \frac{df_3}{dP_{cz}} \end{bmatrix} \begin{bmatrix} P_{cx}' \\ P_{cy}' \\ P_{cz}' \end{bmatrix} \tag{2.41}$$

Matrix equation (2.41) takes the following form.

$$\begin{aligned} \Delta d &= J^{-1} \Delta P_c \\ \therefore \Delta P_c &= J \Delta d \end{aligned} \tag{2.42}$$

where J and J^{-1} are the Jacobian and Jacobian inverse matrices, Δd the displacement change, and ΔP_c the position change. For micro-manipulators, the variation in jacobian matrix values is very small and can be neglected over the entire workspace of the

manipulator. So, we can consider it constant inside the workspace. This assumption is acceptable only for small variations.

The derivatives of f_1, f_2, and f_3 with respect to P_{cx} and P_{cy} all are having the term $\sqrt{(Pcx^2 + P_{cy}^2)}$ as a common factor in their dominators while their derivatives with respect to P_{cz} are all equal to 1. So, the proposed parallel mechanism has only inverse kinematics singularities inside its workspace when all the piezo-electric actuators have the same displacement. This singularity takes place each time when *w*-axis is coincident with *z*-axis.

Unfortunately, the FKP equations are highly nonlinear and can not be decoupled to get a closed form solution [8, 11]. So, The FKP solution can be calculated based on the previous IKP closed form solution together with Newton-Raphson method [65].

The values of d_1, d_2, and d_3 are first used to determine one alternative for the orientation matrix ${}^{b}R_{m}$ to be used in the iterative solution algorithm. Then, the closed form solution given by (2.26) can be represented as in (2.43).

$$\vec{d} = \begin{bmatrix} d_1 \\ d_2 \\ d_3 \end{bmatrix} = g\left({}^{b}R_m(P_{cx}, P_{cy}, P_{cz}), \begin{bmatrix} P_{cx} \\ P_{cy} \\ P_{cz} \end{bmatrix} \right) = g(P_{cx}, P_{cy}, P_{cz})$$
$$\therefore \quad f(P_{cx}, P_{cy}, P_{cz}) = \vec{d} - g(P_{cx}, P_{cy}, P_{cz}) = 0 \tag{2.43}$$

Equation (2.43) is in the form required by Newton-Raphson method. We can define the jacobian as;

$$J(P_{cx}, P_{cy}, P_{cz}) = \frac{\partial f(P_{cx}, P_{cy}, P_{cz})}{\partial (P_{cx}, P_{cy}, P_{cz})} \tag{2.44}$$

The solution for equation (2.44) can be found using repetitive calculation of the algorithm given by (2.45).

$$\begin{bmatrix} P_{cx} \\ P_{cy} \\ P_{cz} \end{bmatrix}^{k+1} = \begin{bmatrix} P_{cx} \\ P_{cy} \\ P_{cz} \end{bmatrix}^{k} - J^{-1}(P_{cx}, P_{cy}, P_{cz})^{k} . f(P_{cx}, P_{cy}, P_{cz})^{k} \tag{2.45}$$

where *k+1* stands for new solution and *k* stands for previous solution provided that this solution equation is convergent.

This algorithm can calculate the final solution in about 4 or 5 iterations. A sequence of generated solutions for a given actuators' displacements $[3.0372, 4.4145, 1.8634]^{T}$ is;

$$\begin{bmatrix} P_{cx} \\ P_{cy} \\ P_{cz} \end{bmatrix}^{1\to 5} = \begin{bmatrix} 0.0500 \\ 0.0100 \\ 14.3634 \end{bmatrix} \Rightarrow \begin{bmatrix} 0.1305 \\ 0.0171 \\ 14.2952 \end{bmatrix} \Rightarrow \begin{bmatrix} 0.1663 \\ 0.0275 \\ 14.2619 \end{bmatrix} \Rightarrow \begin{bmatrix} 0.1700 \\ 0.0300 \\ 14.2584 \end{bmatrix} \Rightarrow \begin{bmatrix} 0.1700 \\ 0.0300 \\ 14.2583 \end{bmatrix} \tag{2.46}$$

Based on the calculated position of the mobile plate center, we can proceed to find the position of the end effector using the algorithm of section 2.4 as in table II. So, the solution for the given actuators' displacements is given by (2.47).

$$\begin{bmatrix} d_1 \\ d_2 \\ d_3 \end{bmatrix} = \begin{bmatrix} 3.0372 \\ 4.4145 \\ 1.8634 \end{bmatrix} \Rightarrow \begin{bmatrix} P_{cx} \\ P_{cy} \\ P_{cz} \end{bmatrix} = \begin{bmatrix} 0.1700 \\ 0.0300 \\ 14.2583 \end{bmatrix} \Rightarrow \begin{bmatrix} P_{ex} \\ P_{ey} \\ P_{ez} \end{bmatrix} = \begin{bmatrix} -3.6075 \\ -43.1128 \\ 104.3939 \end{bmatrix} \tag{2.47}$$

2.7 IKP Solution of Hybrid Structure Two-Fingered Hand

Based on the new IKP solution derived in section 2.3, the solution of single 3-DOF PRS parallel mechanism finger module is extended to the proposed hybrid motion mechanism of Fig. 2.8 to get the tip position of the two fingers [57-60]. The complete solution for the proposed two-fingered hybrid manipulator hand is divided into two parts:

first or lower module finger solution and second or upper module finger solution. Figure 5 shows a schematic architecture of hand mechanism.

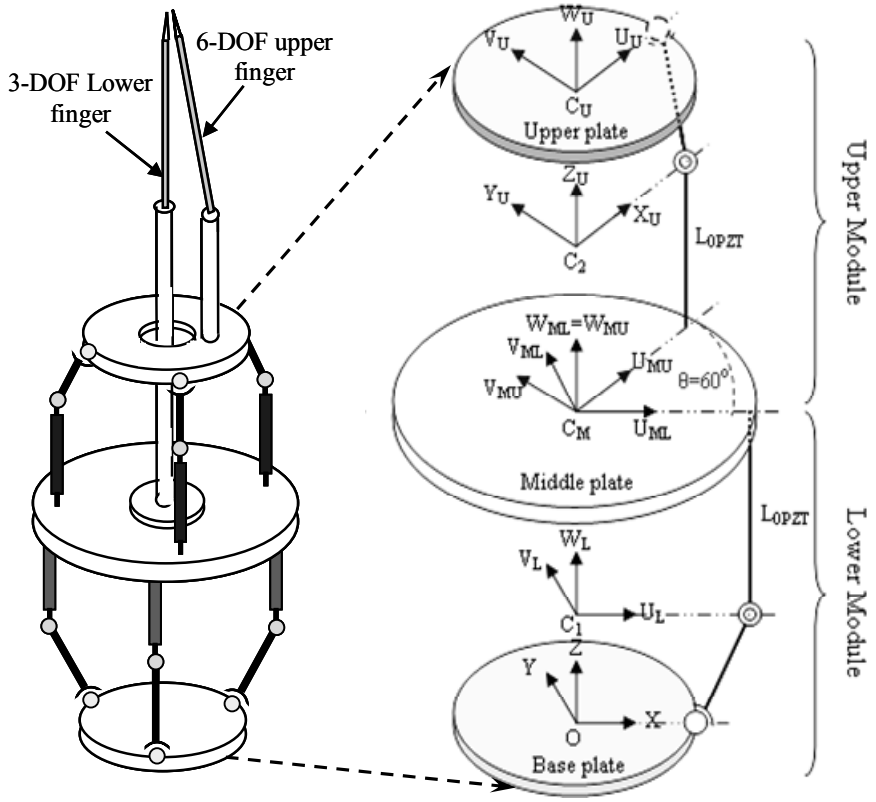

Fig. 2.8: Schematic diagram (left) and hybrid motion mechanism (right) of two-fingered micromanipulator hand.

The IKP solution of the lower module finger is the same as described above but with fixing mobile plate and moving base plate. This finger has 3-DOF and the position of the lower finger tip P_{e1} referred to base reference frame XYZ is given by (2.48).

$$P_{e1} = R_L \cdot \left(P_{e1m} + C_1C_M\right) + P_{C_1}$$
$$C_1C_M = \begin{bmatrix} 0 \\ 0 \\ L_{0PZT} \end{bmatrix} \tag{2.48}$$

where P_{e1m} is the finger tip position referred to mobile frame $U_{ML}V_{ML}W_{ML}$, R_L is the orientation matrix of lower module, C_1C_M is the vector connecting the two origins C_1 and

C_M referred to the mobile frame $U_L V_L W_L$, P_{C1} is the vector connecting origins C_1 and O referred to base frame XYZ, and L_{0PZT} is the initial length of PZT actuator which is in W_L-direction.

The IKP solution of the second or upper module finger is calculated in two steps. The first one is to calculate the finger position in its upper module and then refer it to the base reference frame. This finger has 6-DOF due to the serial connection in between the lower and upper modules. This can be proved using Grübler/Kutzbach criterion.

$$F = \lambda(n - j - 1) + \sum_{i=1}^{j} f_i$$
$$F = 6(15 - 18 - 1) + 6(1 + 1 + 3) = 6 \tag{2.49}$$

The tip position of upper mechanism finger referred to its upper mechanism reference frame $X_U Y_U Z_U$ is given by (2.50).

$$P_{e2U} = R_U \cdot P_{e2m} + P_{C_U} \tag{2.50}$$

where P_{e2U} is the upper finger tip referred to $X_U Y_U Z_U$ frame, P_{e2m} is the finger tip referred to mobile frame $U_U V_U W_U$, R_U is the orientation matrix of upper module, and P_{CU} is the vector connecting C_U and C_2 referred to $X_U Y_U Z_U$ frame.

Then, continue referring to subsequent frames till reaching the fixed base frame XYZ, we can drive the following equations to get the upper finger tip position referred to base reference frame XYZ.

$$P_{e2MU} = P_{e2U} + C_M C_2$$
$$C_M C_2 = \begin{bmatrix} 0 \\ 0 \\ L_{0PZT} \end{bmatrix} \tag{2.51}$$

$$
\begin{aligned}
&P_{e2ML} = R_{(W_{ML},-60^\circ)} \cdot P_{e2MU} \\
&P_{e2} = R_L \cdot \left(P_{e2ML} + C_1 C_M\right) + P_{C_1} \\
&\therefore\ P_{e2} = R_L \cdot \left[R_{(W_{ML},-60^\circ)} \cdot \left[P_{e2U} + C_M C_2\right] + C_1 C_M\right] + P_{C_1} \\
&\therefore P_{e2} = R_L \cdot R_{(W_{ML},-60^\circ)} \cdot \left[P_{e2U} + 2 \cdot C_M C_2\right] + P_{C_1} \\
&\therefore\ P_{e2} = R_L \cdot R_{(W_{ML},-60^\circ)} \cdot \left[R_U \cdot P_{e2m} + P_{C_U} + 2 \cdot C_1 C_M\right] + P_{C_1}
\end{aligned}
\qquad (27)
$$

where P_{e2} is the tip of second finger referred to base reference frame XYZ, $R_{(W\mathrm{ML},-60)}$ is the rotation matrix of upper module base frame $U_{\mathrm{MU}}V_{\mathrm{MU}}W_{\mathrm{MU}}$ to lower module mobile frame $U_{\mathrm{ML}}V_{\mathrm{ML}}W_{\mathrm{ML}}$.

2.8 Summary

In this chapter, the first phase of the development process of the hybrid structure two-fingered micro-manipulator hand. The first phase concerns with the mathematical analysis and modeling of the theoretical model of the building unit of our proposed micro-manipulator hand. This building unit is the 3-DOF PRS parallel mechanism.

In this phase, we began with a literature review of the research work in the area of solving the IKP of 3-DOF RPS and PRS parallel mechanisms. Then we proceeded to present the possible structures of the mechanism of the proposed micro-manipulator. Next, a novel solution of the IKP of both 3-DOF RPS and PRS parallel mechanisms is presented. The IKP solution derived takes the form of simple equations. The feasible workspace of both mechanisms is studied. A solution algorithm for the IKP of 3-DOF PRS parallel mechanism based on the closed form solution derived is presented and its application with a numerical example is presented.

A more practical case, which is the solution of the IKP for a given tip position of the end effector is presented with a numerical example. Moreover, the procedure to solve the FKP using the derived closed form solution is presented with a numerical example. Finally, this solution is extended to the hybrid structure mechanism of the proposed micro-manipulator hand.

CHAPTER 3

Phase Two: Optimization and Design

This chapter presents the details of the second phase of the development process of our proposed micro-manipulator hand. The second phase concerns with the optimization of the chosen design parameters of the micro finger module to be used in the final CAD design.

In this chapter a brief introduction on search techniques will be given at the beginning. The optimization process is carried out in two consecutive steps. First step carry out the optimization of the chosen design parameters of the theoretical 3-DOF PRS parallel mechanism model - based on the solution algorithm derived in chapter 2 - using discrete search method and Genetic and Evolutionary Algorithms (GEAs) for comparison purposes. The objective of the optimization process is to maximize the workspace volume of the end effector tip. Next, based on the output of first step, a CAD model for parallel 3-DOF PRS micro finger module is build. Then the optimization of the pin flexure hinge mechanical properties is carried out as a complementary step to decide the most suitable web thickness for the hinge. Finally, the CAD model for the hybrid micro-manipulator hand is build.

3.1 Overview of Search/Optimization Techniques

Algorithms for function optimization are generally limited to convex regular functions. However, many functions are multi-modal, discontinuous, and non-differentiable. Stochastic sampling methods have been used to optimize these functions. Whereas traditional search techniques use characteristics of the problem to determine the next sampling point (e.g. gradients, linearity, and continuity), stochastic search techniques make no such assumptions. Instead, the next sampled point/points is/are determined based

on stochastic sampling/decision rules rather than a set of deterministic decision rules [66]. Search techniques can be grouped into three broad categories as shown in Fig. 3.1.

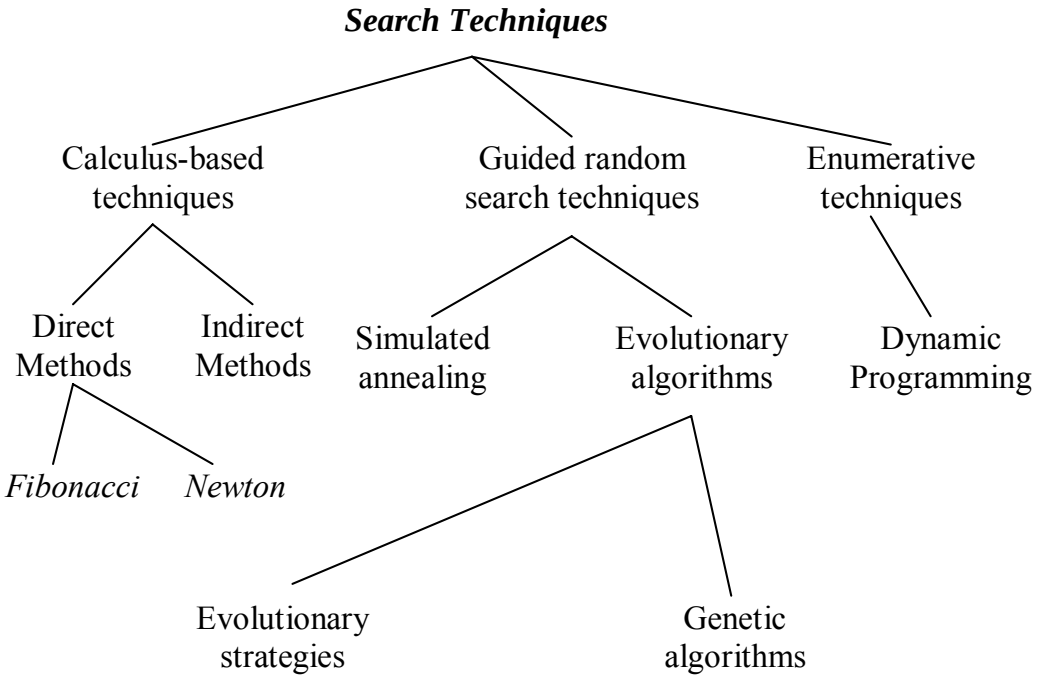

Fig. 3.1: Categories of search/optimization techniques.

Calculus-based techniques use a set of necessary and sufficient conditions to be satisfied by the solutions of an optimization problem. These techniques subdivide into indirect and direct methods. Indirect methods look for local extrema by solving the usually nonlinear set of equations resulting from setting the gradient of the objective function equal to zero. The search for possible solutions (function peaks) starts by restricting itself to points with zero slope in all directions. Direct methods, such as those of Newton and Fibonacci, seek extrema by *hopping* around the search space and assessing the gradient of the new point, which guides the search.

Enumerative techniques search every point related to an objective function's domain space (finite or discretized), one point at a time. They are very simple to implement but may require significant computation and time. The domain space of many applications is too large to search using these techniques. Dynamic programming is a good example of an enumerative technique.

Guided random search techniques are based on enumerative techniques but use additional information to guide the search. They are quite general in scope and can solve very complex problems. Two major subclasses are simulated annealing and evolutionary algorithms. Both are evolutionary processes, but simulated annealing uses a thermodynamic evolution process to search minimum energy states. Evolutionary algorithms, on the other hand, are based on natural-selection principals. This form of search evolves throughout generations, improving the features of potential solutions by means of biologically inspired operations. These techniques subdivide, in turn, into evolutionary strategies and genetic algorithms. Evolutionary strategies were proposed by Rechenberg [67] and Schwefel [68] in the early 1970s. They can adapt the process of artificial evolution to the requirements of the local response surface. This means that unlike traditional genetic algorithms, evolutionary strategies can adapt their major strategy parameters according to the local topology of the objective function [69].

Following Holland's original genetic algorithm proposal, many variations of the basic algorithm have been introduced [70]. However, an important and distinctive feature of all genetic algorithms is the population-handling technique. The original genetic algorithm adopted a generational replacement policy, according to which the whole population is replaced in each generation. Conversely, the steady-state policy used by many subsequent genetic algorithms selectively replaces the population. It is possible, for example, to keep one or more population members for several generations, while those individuals sustain a better fitness than the rest of the population.

In this chapter, we used two search techniques for the optimization of the design parameters of the 3-DOF PRS parallel mechanism. The first one is *direct search method* which is an *Enumerative technique* and the second one is GEAs which is a *Guided random search technique*.

3.2 Introduction to Genetic and Evolutionary Algorithms (GEAs)

GEAs are stochastic search techniques based on the mechanics of natural genetics. They combine survival of the fittest strategy among string structures with a structured yet

randomized information exchange to form a search algorithm with some of the innovative flair of human search. So, GEAs emulate biological evolutionary theories to solve optimization problems. One of the important features of GEAs is that it works with a coding of the parameter set not the parameters themselves. The GEAs comprise a set of individual elements (the population) and a set of biologically inspired operators (selection, crossover, and mutation) defined over the population itself. According to evolutionary theories, only the most fitted elements in a population are likely to survive and generate offspring, thus transmitting their biological heredity to new generations. In computing terms, the GEAs map a problem onto a set of (typically binary) strings, each string representing a potential solution. The GEAs then manipulate the most promising strings in its search for improved solutions [69 -72].

GEAs are different from most of the normal optimization and search procedures in some very fundamental ways [69 -76]:

- GEAs work with a coding of the parameter set not the parameters themselves.
- GEAs search from a population of points, not a single point.
- GEAs use payoff (objective / fitness function) information, not derivatives or other auxiliary knowledge. So it can handle all search spaces, including non-smooth, multi-modal, and discontinuous spaces.
- GEAs use probabilistic transition rules, not deterministic rules.
- GEAs are robust in the sense that they are applicable to a variety of problems with little or no modifications to the technique.
- GEAs are generally straightforward to apply, because no restrictions for the definition of the objective function exist.
- GEAs can handle multiple objectives and identify multiple optimal solutions.

The standard GEA operates through a simple cycle of steps, as shown in Fig. 3.2:

- Start with a randomly generated population of N strings.
- Calculate the fitness $f(x)$ of each string x in the population.
- Repeat the following steps until N (or % of N) offspring have been created:
    - Select a pair of parent strings from the current population, the probability of selection being an increasing function of fitness.

- With probability P_c (the crossover probability), cross over the pair by taking part of the string from one parent and the other part from the other parent. This forms a single offspring as in Fig. 3.3 (a).
- Mutate the resulting offspring at each locus with probability P_m (the mutation probability), and place the resulting string in the new population as in Fig. 3.3 (b).
- Replace the current population with the new population.

- Go to the second step until termination criterion or maximum number of generation is reached.
- Print out the best solution found.

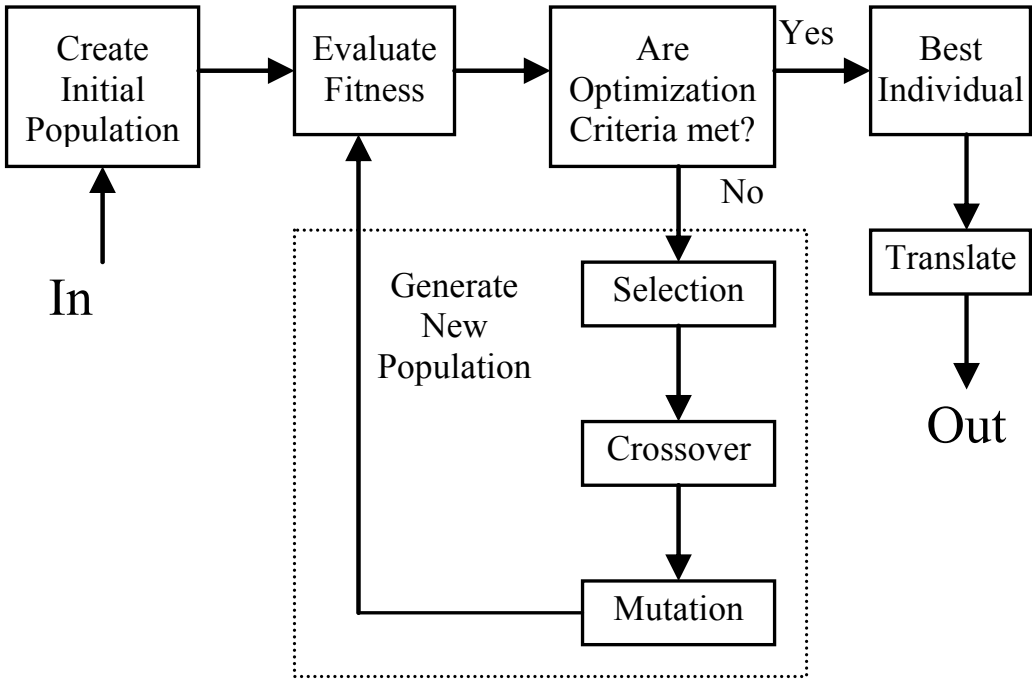

Fig. 3.2: The Standard Procedure of the Genetic and Evolutionary Algorithm (GEA).

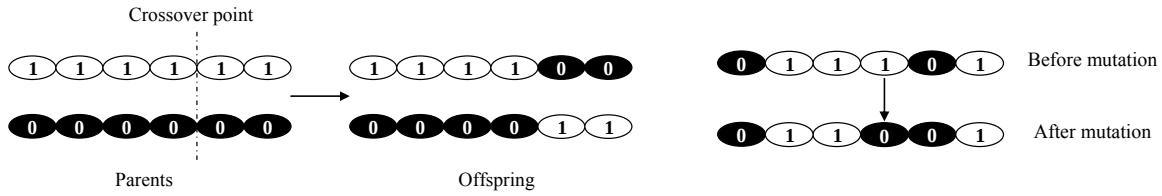

(a) (b)

Fig. 3.3: GEAs operators (a) Crossover and (b) Mutation

The type of GEAs that uses real numbers coding is called evolutionary algorithms (EAs) or real-valued genetic algorithms. So, the main difference between genetic algorithms and evolutionary algorithms is in the coding format of the parameters to be optimized but the strategies used in both techniques are similar to each other. Michalewicz [73] has done extensive experimentation comparing real-valued and binary genetic algorithm and shows that the real-valued genetic algorithm is an order of magnitude more efficient in terms of CPU time. He also showed that a real-valued representation moves the problem closer to the problem representation, which offers higher precision with more consistent results across replication [73-75]

Major issues in designing successful GEAs include the following points:

1- *The choice of encoding (representation) scheme.* When generating initial population, a coding structure for a solution has to be chosen. The coding scheme is a sequence of genes. These genes could be binary digits, floating point numbers, integers, symbols, etc. This scheme determines how the problem is structured, and which genetic operators (crossover and mutation) are to be used.

2- *The choice of selection probability.* Selection is a process where two parents from the current population are carried through into a new population with probabilities depending on their fitness values using one of the selection schemes - roulette wheel, linear ranking, or tournament. This models nature's survival of the fittest principle.

3- *The choice of mutation and crossover probability***.** Genetic operators provide the basic search mechanism of the GEAs to create new solutions based on existing solutions in the population. Crossover takes two individuals (parent) and produces two new individuals (offspring) while mutation alters one individual to produce a single new solution as in Fig. 3.3. Crossover probability is typically around 0.9 while mutation probability is around 0.001.

4- *The design of fitness (objective) function***.** A good design of fitness function is probably the most important factor in a successful application of GEAs. The fitness function (performance index) is the driving force of the search

(evolution) mechanism in GEAs. It should reflect the desired characteristics of the system being optimized [77].

3.3 Design Requirements and Design Parameters

To achieve accurate motion, micro-manipulators usually use flexure hinges offering several advantages over classical rotation joints such as no friction, no need for lubrication and no assembly. So, to fabricate the proposed two-fingered micro-manipulator hand presented in chapter 2, we adapt two types of flexure joints as shown in Fig. 3.4. The wire acts as a ball joint, while the indicated pin joint acts as a revolute joint. Based on the closed form solution developed in chapter 2 for the kinematics problem [52], we can build a simulation program that can be used in the optimization process.

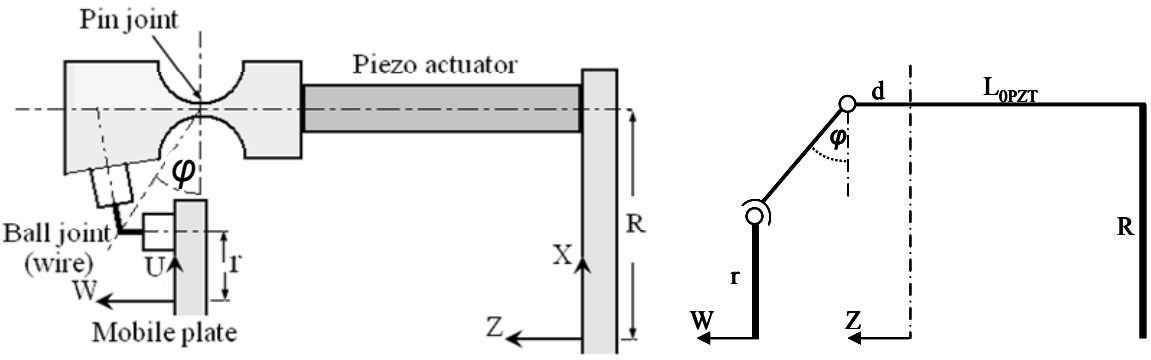

Fig. 3.4: Schematic diagram of a single kinematics chain – theoretical and practical – indicating the chosen design parameters.

The building unit of our proposed micro-manipulator hand is 3-DOF PRS parallel mechanism. We examined the behavior of the 3-DOF PRS micro finger module that will use piezo-electric actuators having maximum displacements of 40μm, for different values of three design parameters that completely define the mechanism [57]. The chosen design parameters are:

1- The fixed base platform radius *R*,
2- The mobile platform radius *r*, and
3- The angle φ which is the angle of the line connecting the center of revolute joint and the center of ball joint with the *XY*-plane, as indicated in Fig. 3.4.

The design requirements that should be satisfied by the proposed design of micro-manipulator hand can be listed as:

1- *Large workspace volume*. This can be achieved by choosing the best values for the design parameters of the micro-manipulator hand through optimization process.
2- *Small size and light in weight*. This can be achieved by considering different configurations for the arrangements of the chain components and the connection way of the two-finger modules.
3- The size of the objects to be manipulated by the micro-manipulator hand may be in the range of few microns up to hundred of microns.
4- The manipulation tasks will include grasping, holding, rotating, moving, picking, placing, ….etc.
5- The manipulation environment may be air, liquid, or vacuum.
6- The objects to be manipulated by the micro-manipulator hand may be hard materials or soft and deformable materials like biological cells and tissues.

The first design requirement - large workspace volume – is the main requirement that can be achieved through optimization of design parameters. The second design requirement can be achieved through the new architecture of the two-fingered micro manipulator hand in which the two modules are connected back-to-back in a mirror image style. The remaining design requirements are to be fulfilled while operation with the micro-manipulator hand.

3.4 Optimization of 3-DOF PRS Parallel Motion Mechanism of Micro-Finger Theoretical Model

In this section, the optimization process of the theoretical model of 3-DOF PRS micro finger module is presented using two different approaches for the purpose of comparison. The first approach is the discrete search method while the second is GEAs.

The theoretical model of 3-DOF PRS micro finger module is derived in chapter 2. As stated in the previous section, the chosen design parameters that are completely defining

the mechanism are: base plate and mobile plate radii R and r plus angle φ. A simulation program is built to simulate the behaviour of the 3-DOF PRS micro finger based on the solution algorithm presented in chapter 2, section 2.4. The behaviour of the 3-DOF PRS micro finger is examined for different values of the design parameters to select the design parameters that correspond to the largest workspace.

3.4.1 Discrete Search Technique

In this technique, we explore the whole chosen range of design parameters depending on a certain step. As the selected step becomes smaller, this technique takes a long time and the computation work will be heavy and this is the main disadvantage of all enumerative search techniques. Also, this technique can not catch a better solution that can exist in between the points it explores. So, this technique can only check certain points – relative to the decided step values – within the workspace volume of the manipulator.

The ranges of design parameters used are; base plate radius R from 8mm to 13mm with 0.5mm step, mobile plate radius r from 1 to 8mm with 0.5mm step, and the angle φ from 10^o to 80^o with 5^o step. The volume index to be maximized is given by (3.1) and is defined as the product of the X-, Y-, and Z-ranges.

$$VolumeIndex = (x_{\max} - x_{\min}) \cdot (y_{\max} - y_{\min}) \cdot (z_{\max} - z_{\min}) \tag{3.1}$$

We can summarize the results obtained for the behavior of the 3-DOF PRS micro finger module over its entire workspace volume as:

1- The workspace volume of the micro manipulator hand almost does not change with changing the base radius R while both of r and φ are fixed at constant values. So, we choose R to be 10mm.

2- By changing the mobile plate radius r, the workspace volume increases as r decreases down to r equal to 3.5mm and then it becomes almost constant as shown in Fig. 3.5.

3- By changing the value of angle φ, the workspace volume alternates between two maximum and minimum values as φ increases as shown in Fig. 3.6.

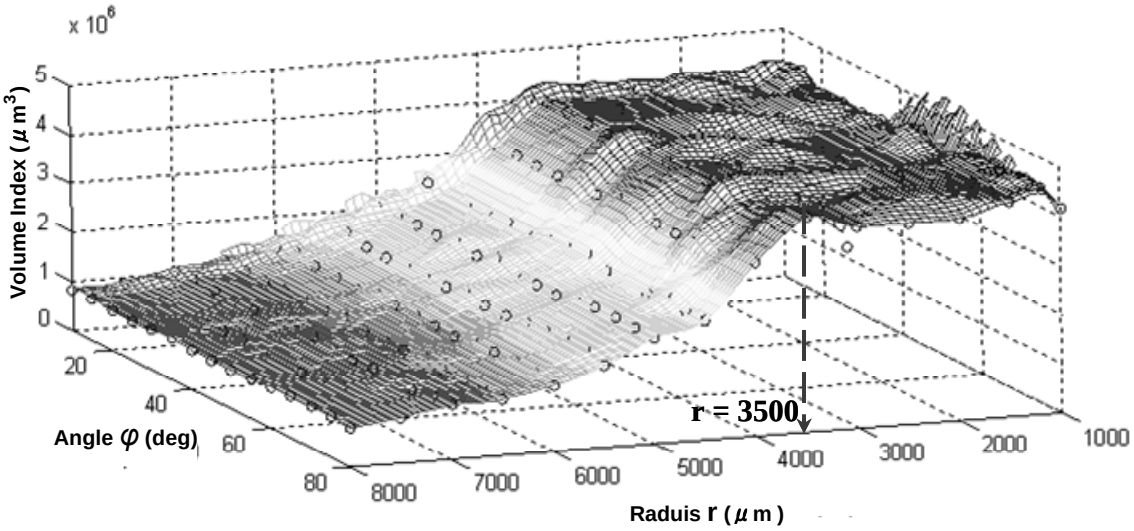

Fig. 3.5: Volume index surface variation vs. *r* and *φ* parameters. *R*=10mm

Fig. 3.5 shows the surface variation of workspace volume as *r* changing from 1mm up to 8mm and φ changing from 10° to 80° degrees while Fig. 3.6 shows the variation of workspace volume versus φ for different values of *r* in between 1mm and 8mm with 0.5mm step value. Both figures are for *R* equal to 10mm.

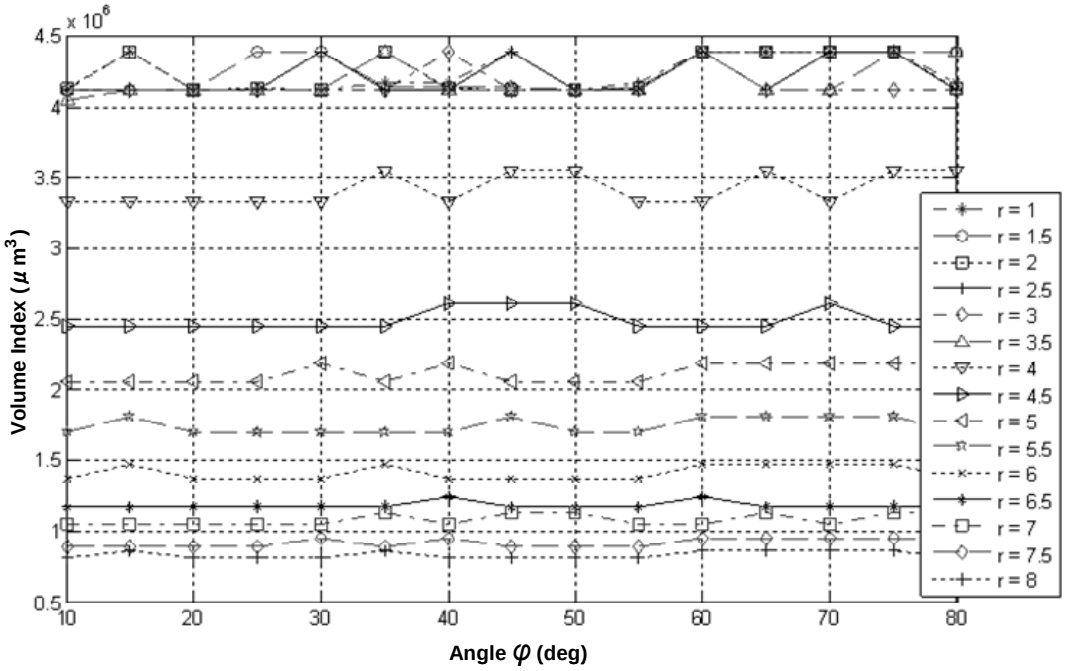

Fig. 3.6: Workspace volume variation vs. *φ* for different values of mobile radius *r*. *R*=10mm

Based on the results obtained from the optimization program using discrete search technique, we found that the best values for the design parameters of the theoretical model of 3-DOF PRS micro finger module are [59]:

- Fixed frame radius R = 10mm
- Mobile frame radius r = 3.5mm
- Angle $\varphi = 35^{o}$ or 60^{o} or 75^{o}.

Using the simulation program, the behavior of the two-fingered micro-manipulator hybrid hand – see Fig. 3.7 - using the set of design parameters mentioned above is evaluated based on the module behavior over the entire workspace and the extremes of the workspace volume. The length of lower finger is set to 10cm and that of the upper finger is set to 5cm. The maximum displacement of the piezo-electric actuator used is 40μm and L_{0ZPT} is constant at 4.5cm. The evaluation results are given in table 3.1.

TABLE 3.1
DISCRETE SEARCH METHOD: WORKSPACE EXTREMES FOR TWO-FINGERED MICRO-MANIPULATOR HAND

	Lower Finger (10 cm) in fixed frame	Upper Finger (5 cm) in mobile frame	Upper Finger (5 cm) in fixed frame
$\boldsymbol{X}_{min}$ μm	-1078.9	-370.92	-1445.9
$\boldsymbol{X}_{max}$ μm	1078.8	370.83	1445.9
$\boldsymbol{Y}_{min}$ μm	-961. 3279	-330.49	-1289.9
$\boldsymbol{Y}_{max}$ μm	961.2500	330.42	1289.8
$\boldsymbol{Z}_{min}$ μm	-20	-20	-40
$\boldsymbol{Z}_{max}$ μm	20	20	40

The workspace volumes of lower finger tip in fixed frame, upper finger tip in mobile frame, and upper finger tip in fixed frame are shown in Fig. 3.8, Fig. 3.9, and Fig. 3.10 respectively. From these results and figures, we can notice that the hybrid two-fingered micro-manipulator hand has a large workspace volume.

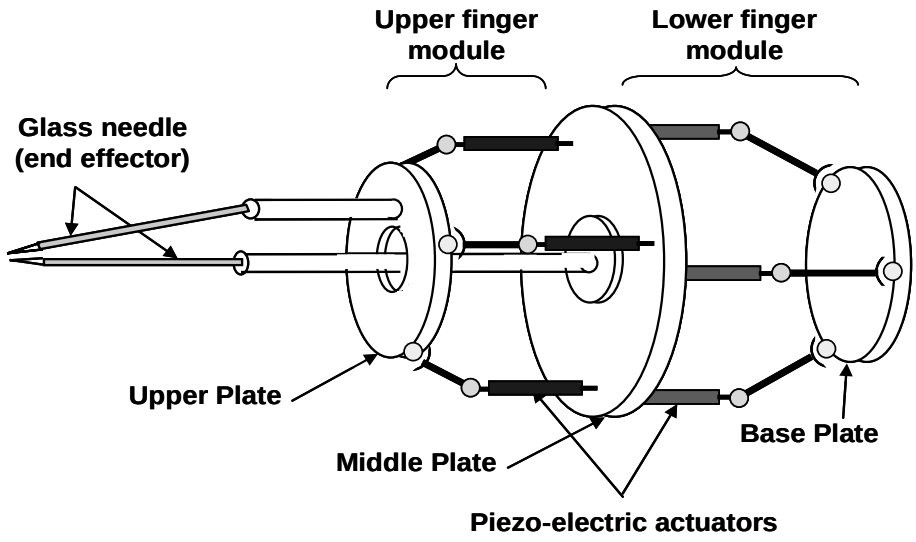

Fig. 3.7: Two-fingered micro-manipulator hybrid hand model

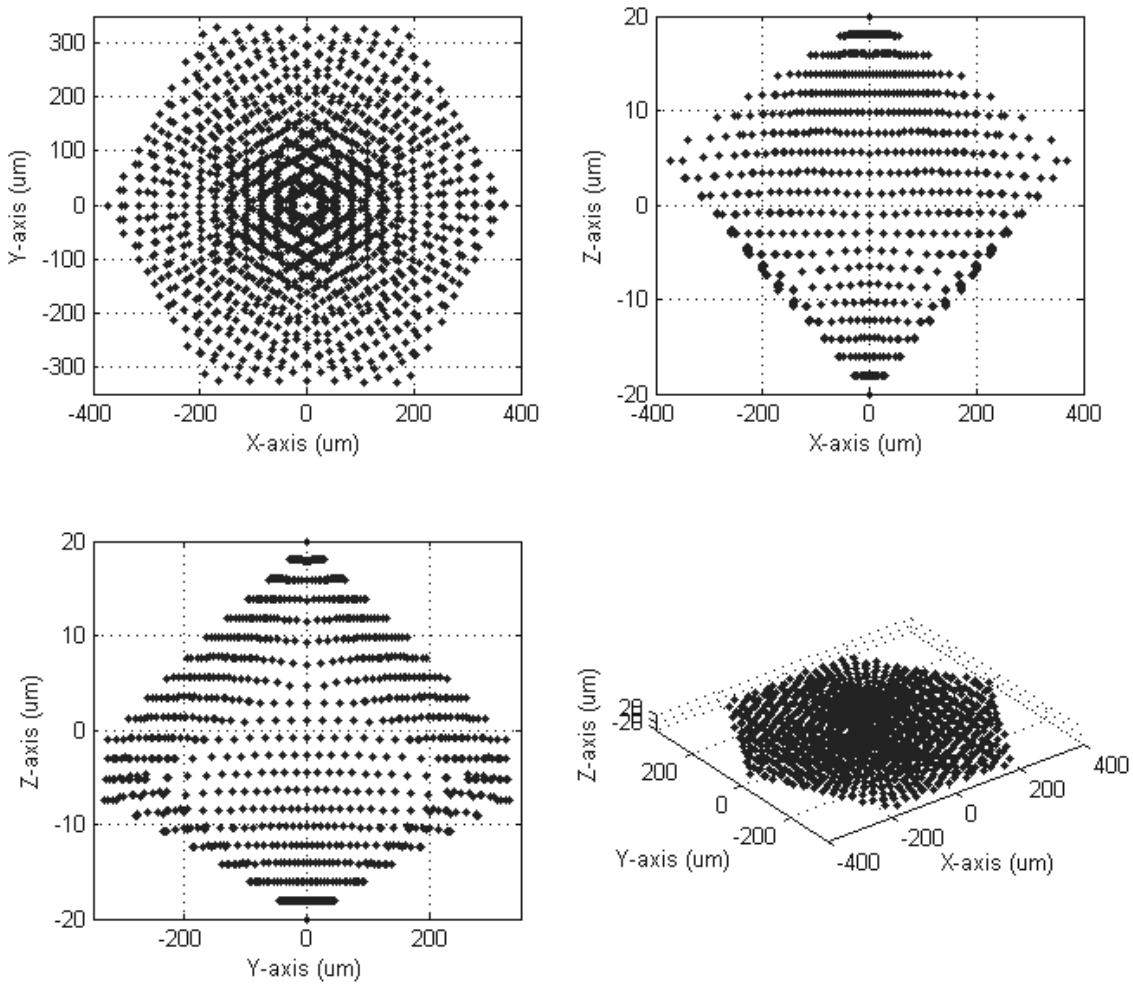

Fig. 3.8: Discrete search method: workspace volume of lower finger tip in fixed base frame

Also we can see that the two fingers will have a maximum opening range of about 370μm and 330μm in both *X*-axis and *Y*-axis respectively.

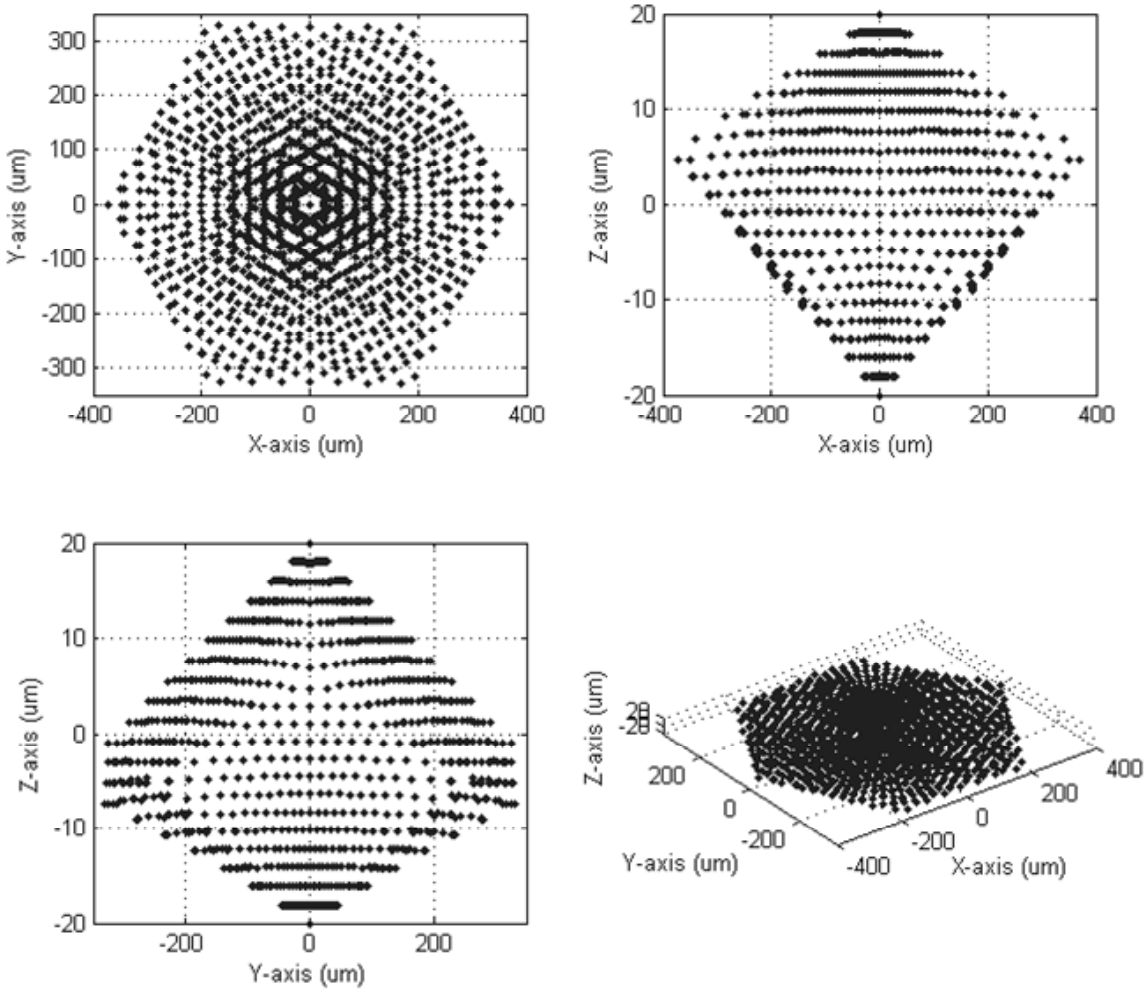

Fig. 3.9: Discrete search method: workspace volume of upper finger tip in its mobile frame

From Fig. 3.8 and Fig. 3.9, we notice that the workspace volume of the lower finger tip is more than twice that of the upper finger tip in its mobile frame. This is because the added length of L_{0ZPT} to the lower finger length due to the SRP structure of the lower mechanism. Also, Fig. 3.10 indicates that the motion of the upper finger tip referred to the base fixed frame will be very large as it will extend from 1445.9μm to -1445.9μm in *X*-direction and from 1289.8μm to -1289.9μm in *Y*-direction. This is due to the serial connection in between the upper and lower finger modules. The displacement in the Z-direction is limited to the maximum displacement of the piezo-electric actuators.

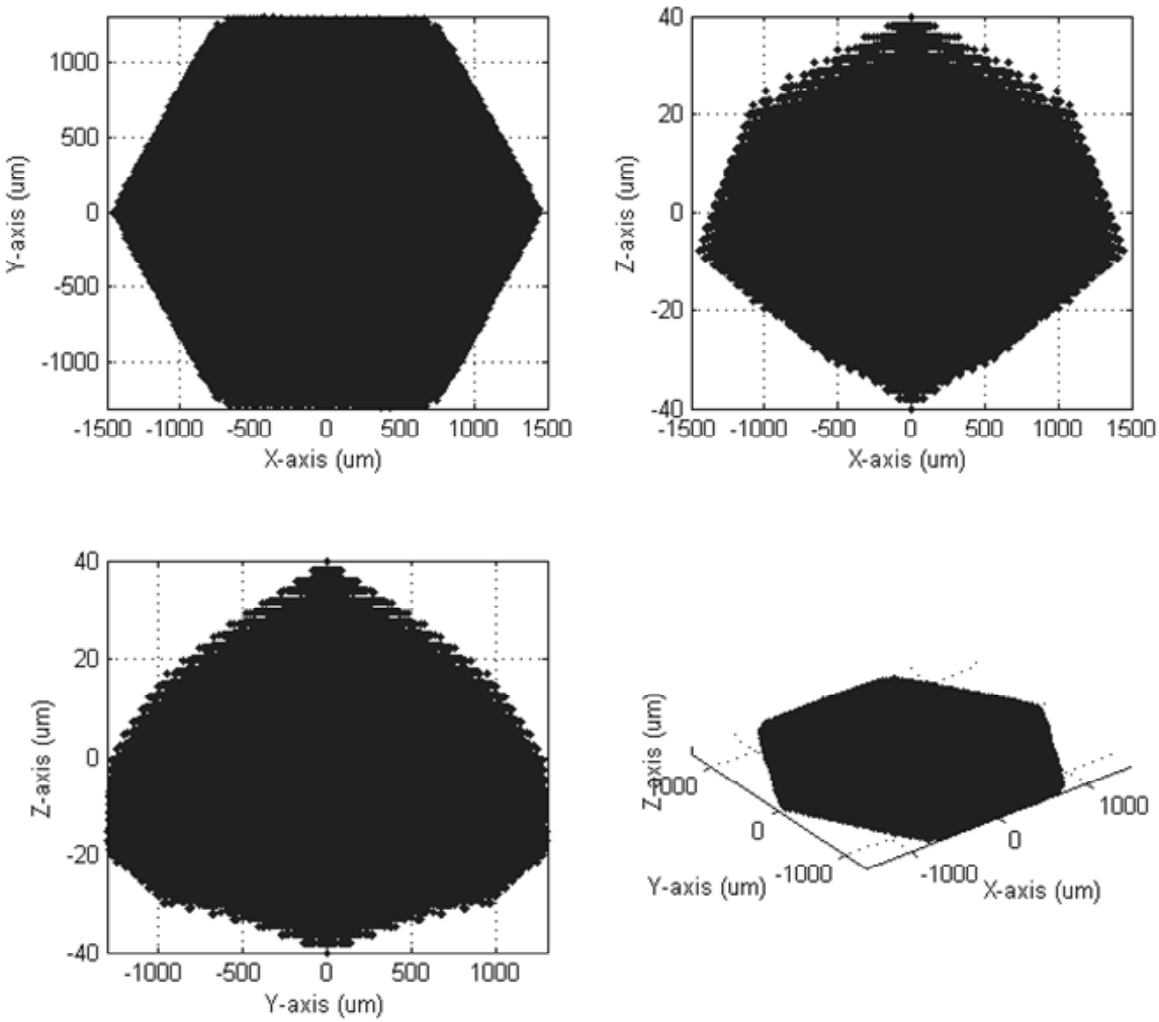

Fig. 3.10: Discrete search method: workspace volume of upper finger tip in fixed base frame

3.4.2 Genetic and Evolutionary Algorithms Method

In this method, the whole chosen range of design parameters can be explored for the optimal or at least the near optimal values. This method can find the best solution inside the specified ranges. There is no limitation due to step value in GEAs. In GEAs, a population of solutions is examined at a time and improved from generation to generation based on stochastic sampling rules till we reach the best solution. As the specified ranges become wider, this technique takes a considerable time and it can reach a near optimal solution, not the absolute optimal one. One disadvantage of GEAs is that this method mostly can be used off-line for simulation purposes but not on-line with the system. This is because it evaluates many solutions till convergence happen.

GEA is typically iterated for anywhere from 250 to 2500 or more generations. The entire set of generations is called a *run*. At the end of a run, there are typically one or more highly fit candidate solutions in the population. Since randomness plays a large role in each run, two runs with different random-number seeds will generally produce different detailed behavior [75].

There are several methods to criticize the fitness value of individual [73-77]. In this thesis, the main objective is to maximize the workspace volume of the two fingers of the micro-manipulator hand. So, the fitness function *f (indv)* to be maximized by the GEA is described by (3.2).

$$f(indv) = \alpha(x_{\max} - x_{\min}) + \beta(y_{\max} - y_{\min}) + \delta(z_{\max} - z_{\min}) \qquad (3.2)$$

where $x_{\min}$, $x_{\max}$, $y_{\min}$, $y_{\max}$, $z_{\min}$, and $z_{\max}$ are extremities of the workspace volume in *X*-, *Y*-, and *Z*-directions and α , β, and δ are weighting factors that enable us to make the fitness function more sensitive to one factor more than the others.

In our proposed architecture of micro-manipulator hand, the movement of the fingers in the *Z*-direction is limited to the maximum displacement that can be achieved by the piezo-electric actuators used. This is a physical constraint imposed by piezo-electric actuator. So, the weighting factor δ is chosen to be equal to 1 because we can not maximize the *Z*-range. Both of the weighting factors α and β are chosen to be equal to 75 to make the fitness function sensitive to the variations in the *X*- and *Y*-ranges.

We run the algorithm for several times with almost the same parameters. The real-valued GA parameters used are:

Population size = 20
Subpopulations = 2
Max. Generations = 500
Generation gap = 0.9

Selection algorithm is stochastic universal sampling

Mutation algorithm is real mutation

Selection pressure is linear ranking algorithm

The results of three different runs of GEAs are given in table 3.2. Almost all the three runs have the same symmetric shape of workspace, although they have different values for design parameters. The workspace volume extremities in *X*-, *Y*- and *Z*-directions for the design parameters of the third run are presented in table 3.3.

TABLE 3.2
RESULTS OF THREE RUNS OF REAL-VALUED GA

	Base Radius R mm	Mobile Plate Radius r mm	Angle φ deg.
1st run	13.91298966	2.58639530	20.41681615
2nd run	6.31714531	2.74854940	73.72764676
3rd run	6.50890671	2.48691089	38.63278709

TABLE 3.3
GEAS METHOD: WORKSPACE EXTREMES FOR TWO-FINGERED MICRO-MANIPULATOR HAND

	Lower Finger (10 cm) in fixed frame	Upper Finger (5 cm) in mobile frame	Upper Finger (5 cm) in fixed frame
$\boldsymbol{X}_{min}$ μm	-1078.941	-370.9133	-1439.7
$\boldsymbol{X}_{max}$ μm	1078.845	370.8449	1439.7
$\boldsymbol{Y}_{min}$ μm	-1078.8798	-370.8791	-1439.71
$\boldsymbol{Y}_{max}$ μm	1078.8798	370.8791	1439.71
$\boldsymbol{Z}_{min}$ μm	-20	-20	-40
$\boldsymbol{Z}_{max}$ μm	20	20	40

The fingers motion in z-direction is restricted due to the limited movement of the piezo-electric actuators. The workspace extremities of genetically optimized design parameters are better than that of first method in the *Y*-axis. There is an improvement in the *Y*-range by about 12%.

The workspace volumes of lower finger tip in fixed frame, upper finger tip in mobile frame, and upper finger tip in fixed frame are shown in Fig. 3.11, Fig. 3.12, and Fig. 3.13 respectively. From these results and figures, we can notice that the hybrid two-fingered micro-manipulator hand has an improvement in the *Y*-range of the workspace volume.

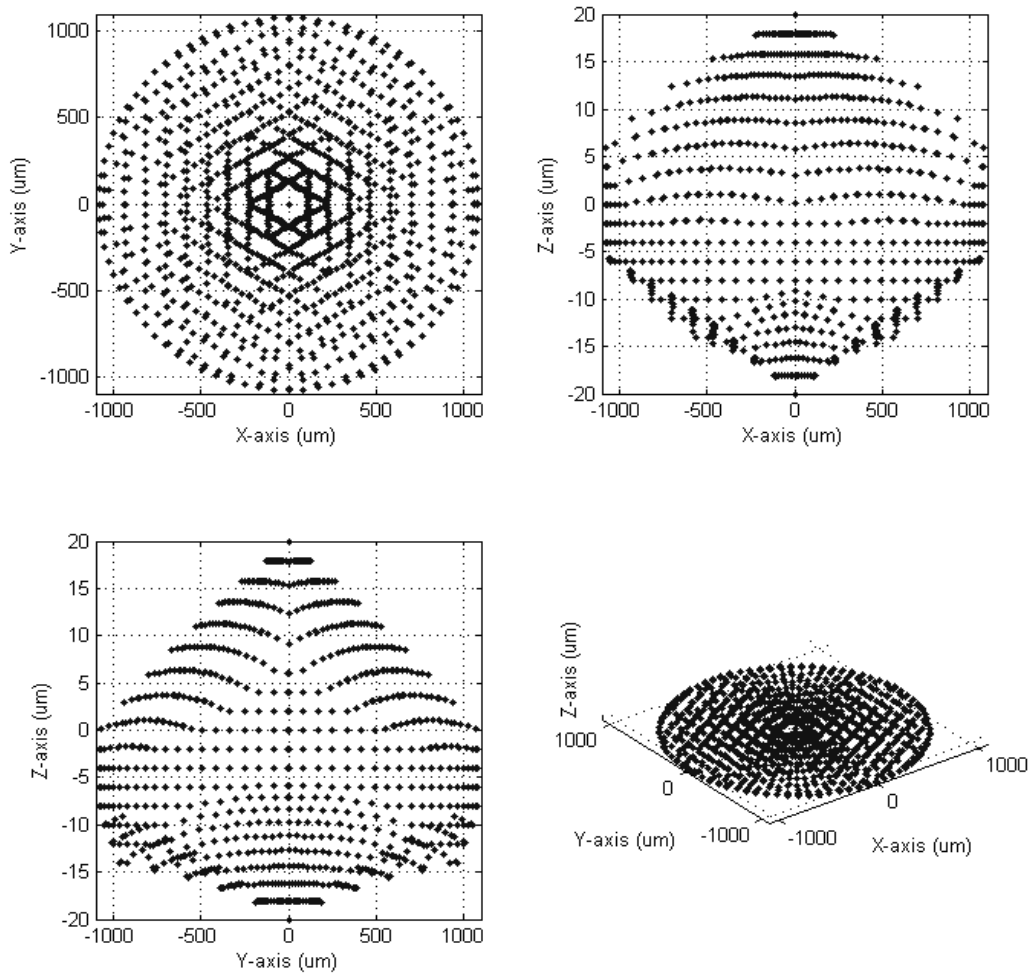

Fig. 3.11: GEAs method: workspace volume of lower finger tip in fixed base frame

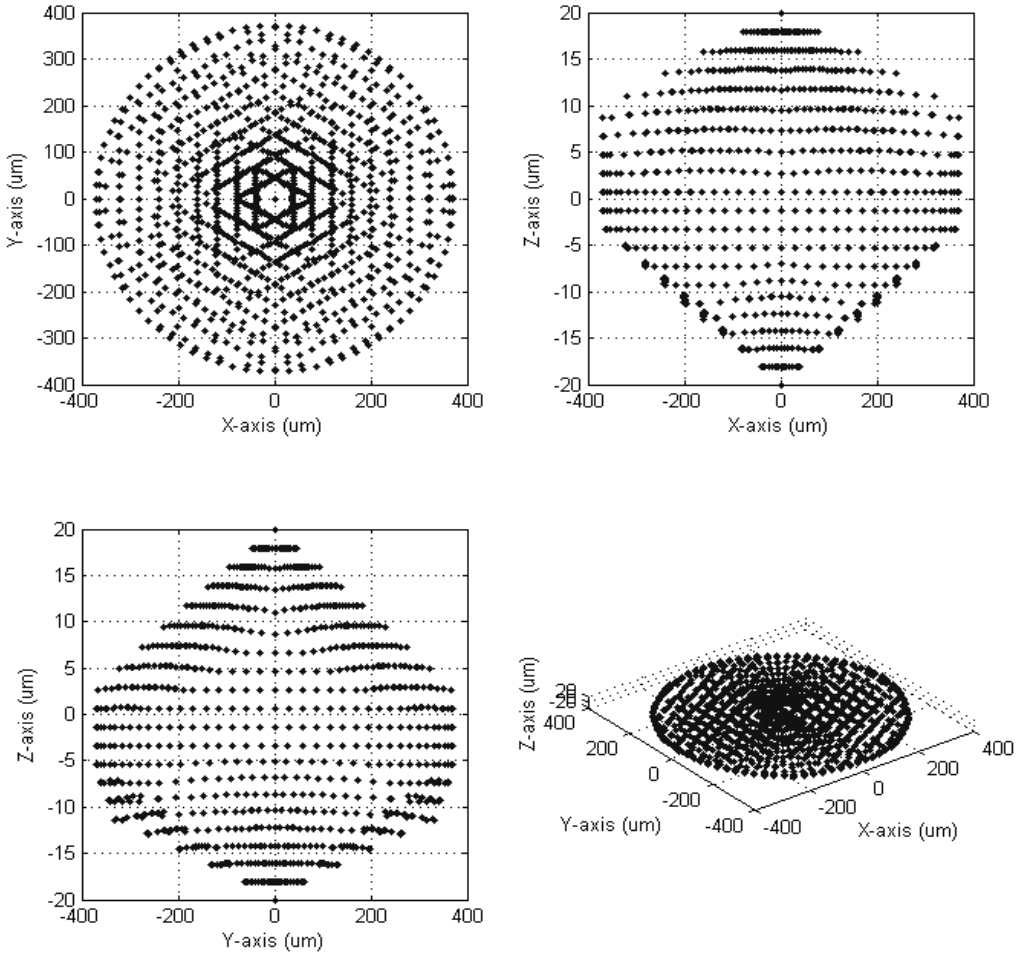

Fig. 3.12: GEAs method: workspace volume of Upper finger tip in its mobile frame

From Fig. 3.11, Fig. 3.12, and Fig. 3.13, we notice that the workspace volume of the two fingers in the *X*-direction is almost the same but there is an improvement in the *Y*-direction by about 12%. Also, we can notice that for genetically optimized design parameters the workspace is nearly circular, i.e. both *X*- and *Y*-ranges are equal in value. From Fig. 3.12 we can see that the two fingers will have a maximum opening range of about 370µm and 370µm in both *X*-axis and *Y*-axis respectively. Unfortunately, the values of the design parameters produced by the GEAs are difficult to be practically implemented because it needs high accuracy that can not be achieved nowadays. So, we thought to use discrete search method with a small range of parameters to solve this problem.

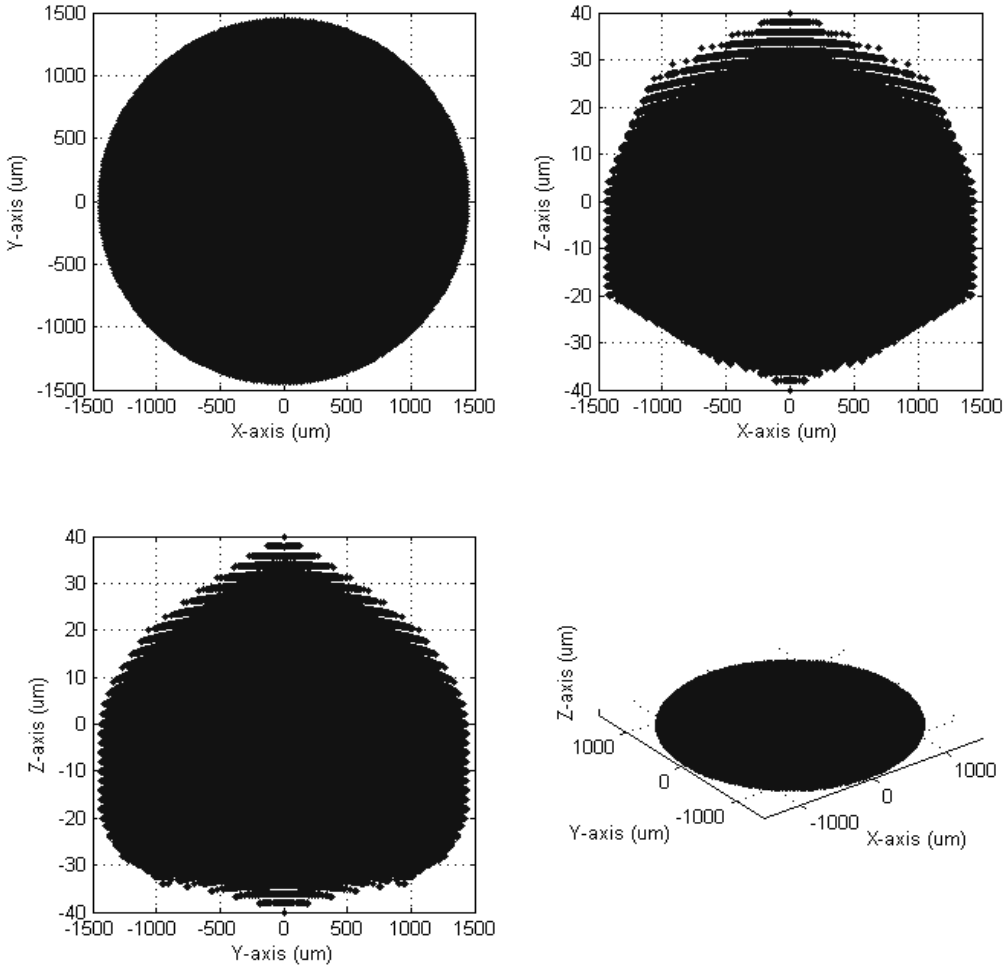

Fig. 3.13: GEAs method: workspace volume of Upper finger tip in fixed base frame

3.4.3 Comparison of Results for Both Methods

From the results of both discrete search method and GEAs method, we can see that there is an improvement – especially if the *Y*-range – in the workspace volume of the design parameters produced by GEAs method. But unfortunately the values of the genetically optimized design parameters are difficult to be implemented.

In this section we will compare the results of both optimization methods for a 3-DOF PRS micro finger module with 5cm finger length, i.e. the same as the upper finger.

Table IV lists the workspace extremities of both methods. The results of several runs of GEAs are given in table 3.3. The workspace volume extremities in both *X*-, *Y*- and *Z*-directions for the design parameters of both methods are presented in Table 3.4.

TABLE 3.4
WORKSPACE EXTREMITIES FOR BOTH OPTIMIZATION METHODS

	Discrete Search Technique	GEAs Method, 1st run	GEAs Method, 2nd run	GEAs Method, 3rd run
$\boldsymbol{X}_{min}$ μm	-370.9272	-370.9146	-370.9169	-370.9133
$\boldsymbol{X}_{max}$ μm	370.8309	370.8435	370.8413	370.8449
$\boldsymbol{Y}_{min}$ μm	-330.4946	-370.8791	-370.8791	-370.8791
$\boldsymbol{Y}_{max}$ μm	330.4167	370.8791	370.8791	370.8791
$\boldsymbol{Z}_{min}$ μm	-20	-20	-20	-20
$\boldsymbol{Z}_{max}$ μm	20	20	20	20

Fig. 3.14 shows the workspace volume of the optimized design parameters of first method and that of 3rd run of the GEAs method. As we can see, the GEAs technique have superior behaviour to find the optimal or near optimal solutions inside the search space of

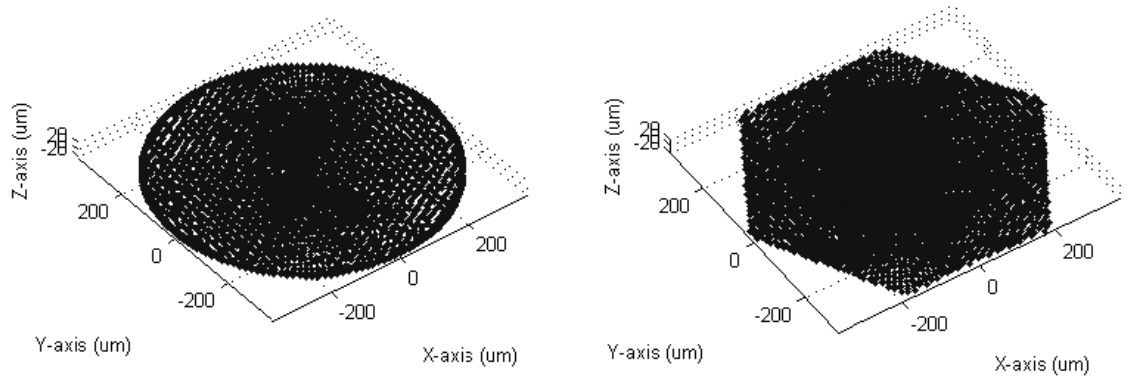

Fig. 3.14: Workspace of 3-DOF PRS micro finger module: Genetically optimized (left) and discrete search method optimized (right)

the problem. But, GEAs can mostly be used off-line for simulation purposes and in our case its solution values are difficult to be practically implemented.

3.4.4 Discrete Search Method for Narrow Range

To get a more easily to be practically implemented design parameters, we again use the discrete search method but with narrow range for *mobile plate radius r*. The chosen range of r is from 2 to 3.5mm with 0.1mm step and that of φ is from 10^o to 80^o with a step value of 5^o while fixing the base radius R to 8mm. The surface of the design parameters changes is presented in Fig. 3.15.

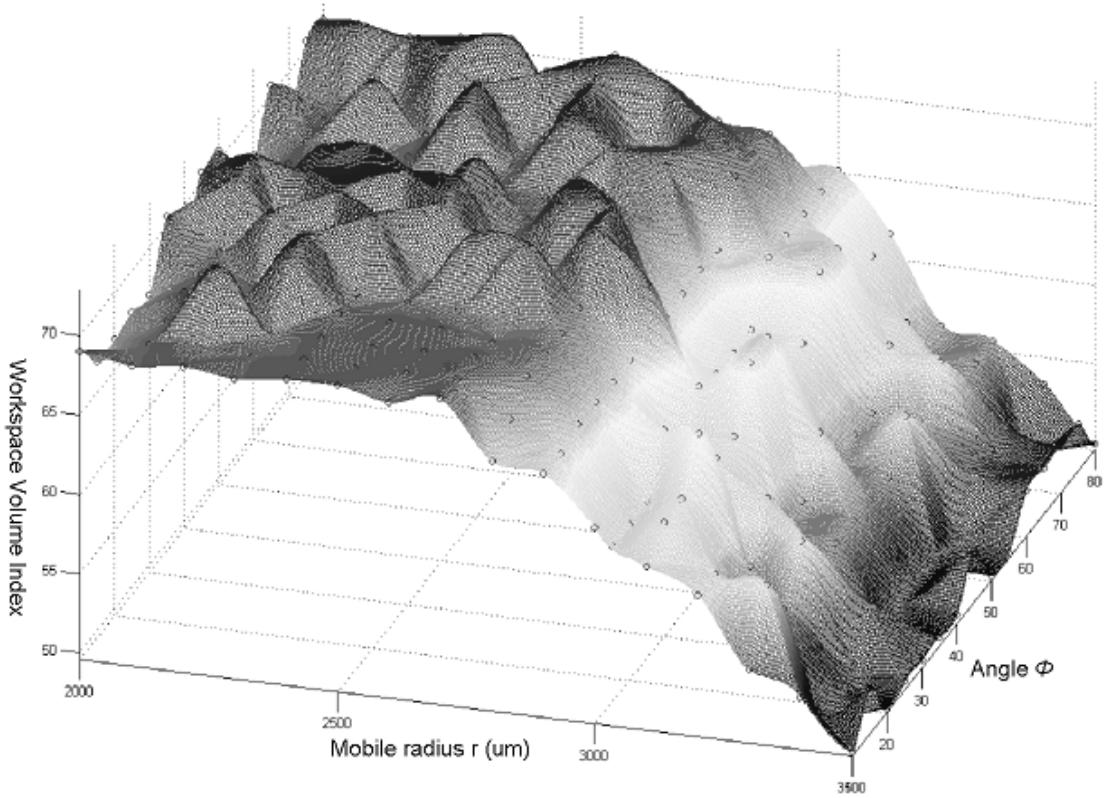

Fig. 3.15: Workspace volume index surface variation vs. r and φ parameters. R=8mm

Based on the results obtained from the optimization program using discrete search technique for narrow range, we found that the best values for the design parameters of the theoretical model of 3-DOF PRS micro finger module are [63]:

- Fixed frame radius R = 8mm
- Mobile frame radius r = 2.4mm

- Angle $\varphi = 12^o$ or 35^o.

These design parameters set are suitable to be practically implemented but this small value for the mobile radius *r* is still difficult to be realized. Using the simulation program, the behavior of the two-fingered micro-manipulator hybrid hand using the set of design parameters mentioned above is evaluated. The evaluation results are given in table 3.5. Again, the workspace volume in this case is almost circular in shape.

TABLE 3.5
DISCRETE SEARCH METHOD FOR NARROW RANGE: WORKSPACE EXTREMES FOR TWO-FINGERED MICRO-MANIPULATOR HAND

	Lower Finger (10 cm) in fixed frame	Upper Finger (5 cm) in mobile frame	Upper Finger (5 cm) in fixed frame
$\boldsymbol{X}_{min}$ μm	-1078.913	-370.912	-1444.95
$\boldsymbol{X}_{max}$ μm	1078.847	370.846	1444.95
$\boldsymbol{Y}_{min}$ μm	-1078.88	-370.879	-1444.97
$\boldsymbol{Y}_{max}$ μm	1078.88	370.879	1444.967
$\boldsymbol{Z}_{min}$ μm	-20	-20	-40
$\boldsymbol{Z}_{max}$ μm	20	20	40

The workspace volumes of lower finger tip in fixed frame, upper finger tip in mobile frame, and upper finger tip in fixed frame are shown in Fig. 3.16, Fig. 3.17, and Fig. 3.18 respectively. From these results and figures, we can notice that the hybrid two-fingered micro-manipulator hand has an improvement in the *Y*-range of the workspace volume. This case is almost the same as that of the GEAs. For the design parameters in this case, the workspace volume is very large and the two-fingers have a maximum opening range of 370 μm and 370 μm in both *X*-direction and *Y*-direction respectively.

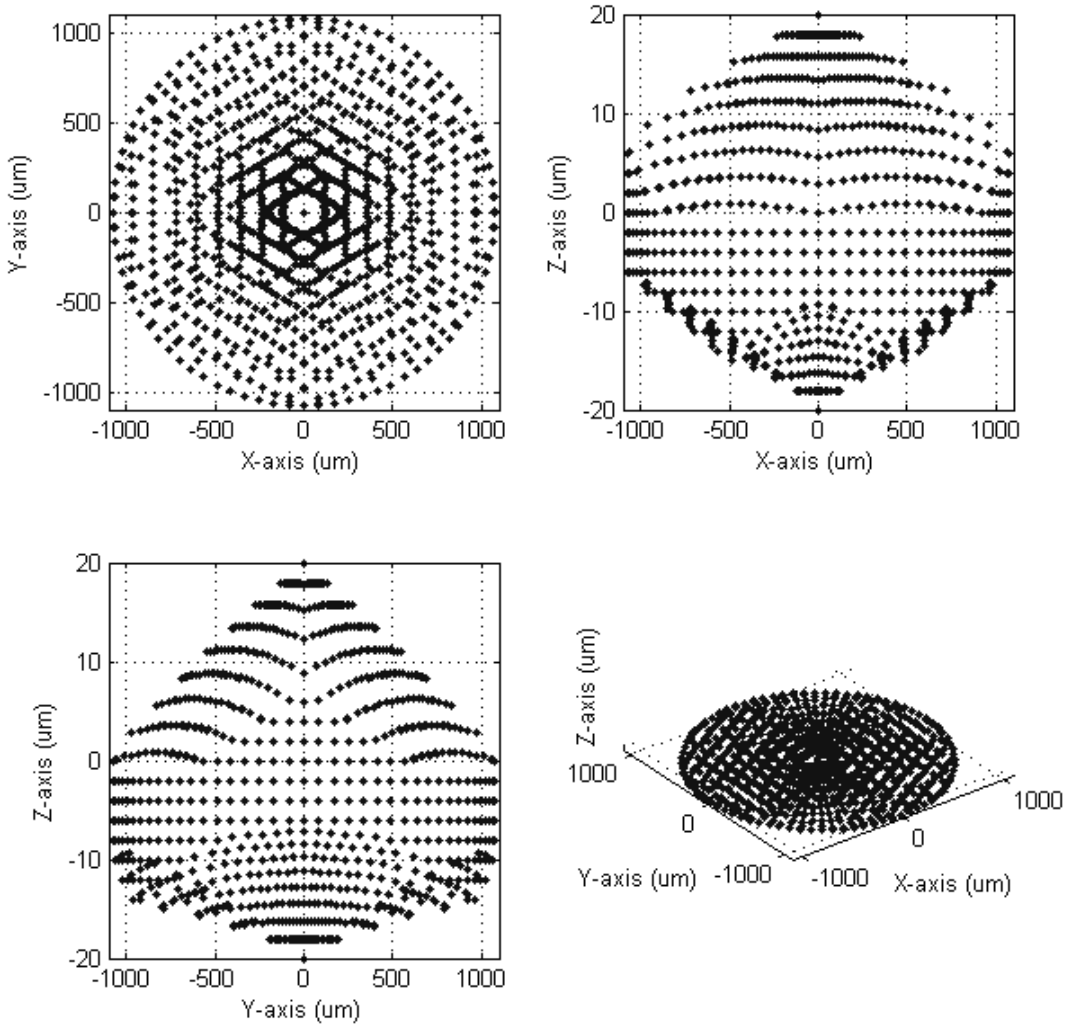

Fig. 3.16: Discrete search method with narrow range: workspace volume of lower finger tip in base fixed frame

These design values improve the workspace volume by about 12% than the first method – Discrete search method - but unfortunately they are also difficult to be realized with good accuracy. So, we decided to use the design parameters of the first method to build our CAD model and keep these values to a future CAD realization.

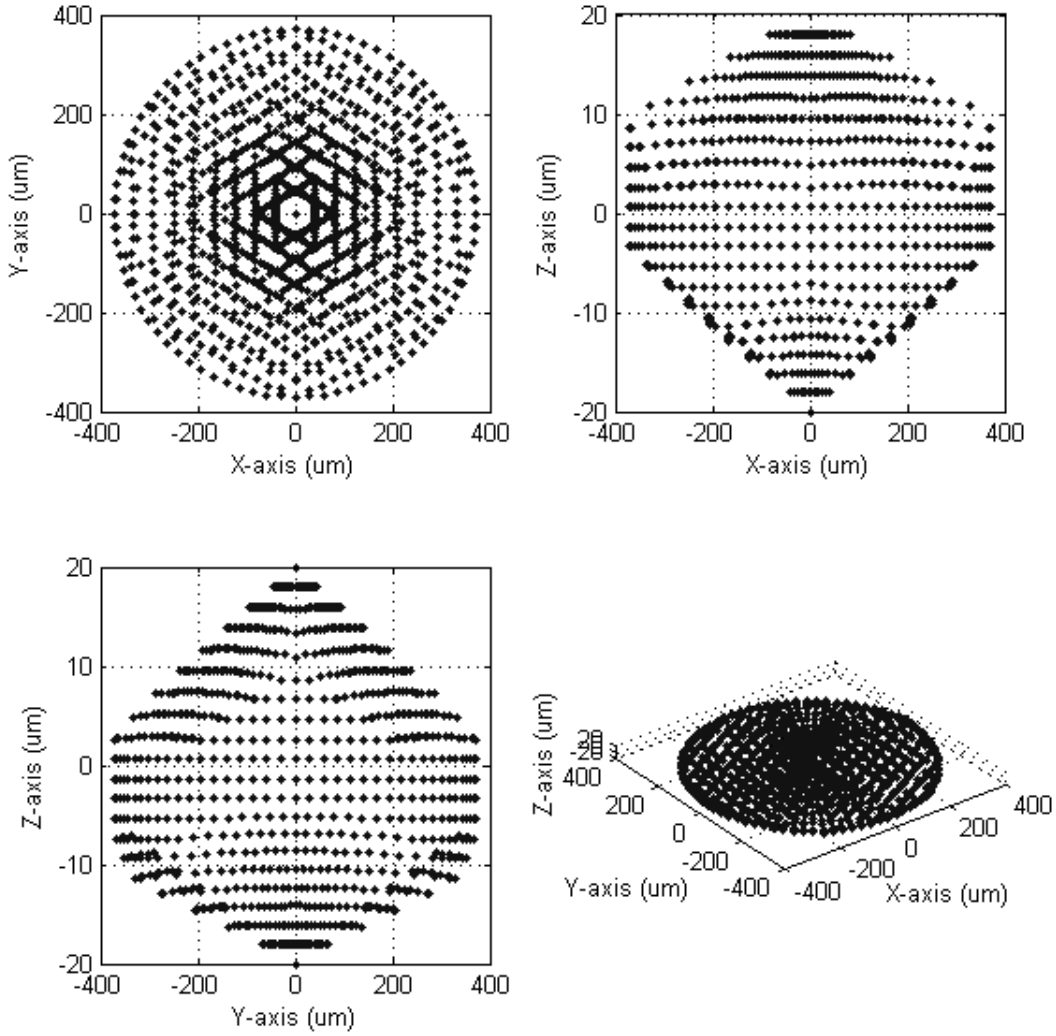

Fig. 3.17: Discrete search method with narrow range: workspace volume of upper finger tip in its mobile frame

3.5 Optimization of 3-DOF PRS parallel Motion Mechanism of Micro-Finger CAD Model

To built the 3-DOF PRS micro finger module, we decided to use the design parameters of first method – Discrete search method - in building our CAD model because these parameters have more easily to be practically implemented values than that of genetically

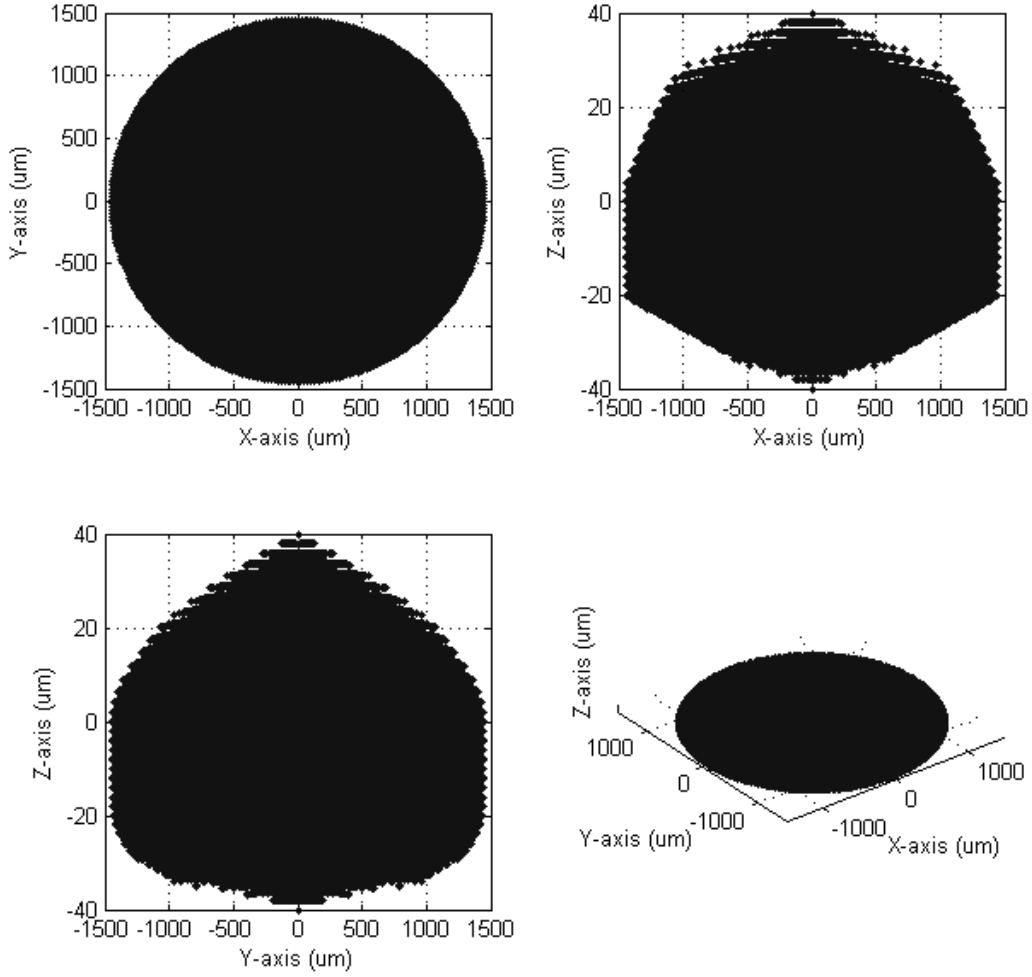

Fig. 3.18: Discrete search method with narrow range: workspace volume of upper finger tip in base fixed frame

optimized one. The angle φ is decided to be 35^{o}. So, the final design parameters for the 3-DOF PRS micro finger module are:

- Fixed frame radius $R = 10$mm
- Mobile frame radius $r = 3.5$mm
- Angle $\varphi = 35^{o}$.

The proposed design of the CAD model for the 3-DOF PRS micro finger module is shown in Fig. 3.19.

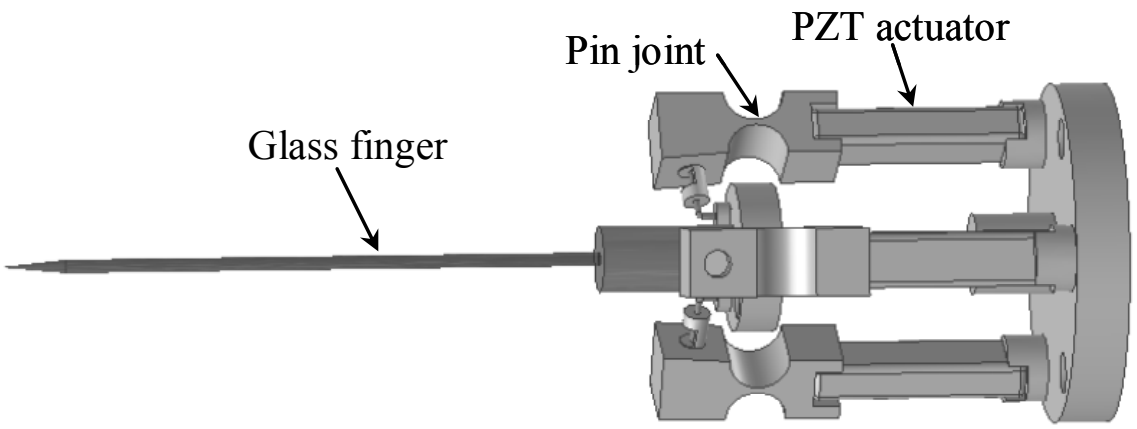

Fig. 3.19: 3-DOF PRS micro finger CAD model

A complementary optimization step is carried out for the CAD model of the 3-DOF PRS micro finger module to determine the most suitable mechanical properties of the pin flexure hinge used. The 3-DOF PRS micro-finger CAD model is analyzed using ANSYS workbench program for a 5cm finger length for different values of the web thickness of the pin joint and 0.5mm wire as ball joint. The results of this optimization step are depicted in table 3.6.

TABLE 3.6
WORKSPACE EXTREMES FOR MICRO-FINGER MODULE CAD MODEL

	0.2mm Case	0.3mm Case	0.4mm Case	0.5mm Case	0.6mm Case
X_{min} μm	-301	-324	-343	-353	-361
X_{max} μm	308	329	342	353	361
Y_{min} μm	-265	-284	-295	-307	-315
Y_{max} μm	264	285	296	307	315
Z_{min} μm	0	0	0	0	0
Z_{max} μm	40	40	40	40	40

From table 3.6, we decided to choose the thickness of pin joint web to be comparable to that of the wire diameter. So, we designed the pin joint web thickness to be 0.5mm and that of the wire to be 0.5mm also but from different material. The material of the pin joint is chosen to be Aluminum and that of the wire to be Copper. The Aluminum has higher stiffness than the Copper, so the motion of the piezo electric actuator will be transmitted through the pin joint – almost without losses - to the ball joint to produce bigger angular displacement in the finger. The analysis shows that the extreme values in *X*-axis will be from -353μm to 353μm and that in *Y*-axis from -307μm to 307μm for a design with 0.5mm web thickness. The difference in between practical and theoretical values is about 5% less. This is due to the use of pin flexure hinge and wire which they are neither an ideal revolute joint nor an ideal ball joint. The practical values are close to the theoretical values and this is promising in the design stage.

The complete workspace analysis of the 0.5mm case of 3-DOF PRS micro-finger CAD model using the ANSYS workbench program is given in table 3.7. Due to the symmetry of the manipulator workspace, we only considered changing of d_1 alone and d_2 alone and then $d_1$with d_2 and finally d_2 with d_3. The case of d_3 alone is similar to d_2 alone while the case of $d_1$with d_3 is similar to d_1 with d_2.

TABLE 3.7
WORKSPACE ANALYSIS FOR 0.5 MM CASE OF MICRO-FINGER CAD MODULE

d_1 μm	d_2 μm	d_3 μm	X μm	Y μm	Z μm
0	0	0	0	0	0
0	0	10	44.3	76.8	3.36
0	0	20	88.6	154	6.71
0	0	30	133	230	10.1
0	0	40	177	307	13.4
10	0	0	-88.4	-0.167	3.33
20	0	0	-177	-0.334	6.65
30	0	0	-265	-0.501	9.98
40	0	0	-353	-0.668	13.3

TABLE 3.7 – CONT.
WORKSPACE ANALYSIS FOR 0.5 MM CASE OF MICRO-FINGER CAD MODULE

d_1 µm	d_2 µm	d_3 µm	X µm	Y µm	Z µm
10	10	0	-44.3	-76.8	6.64
10	20	0	-0.235	-153	9.96
10	30	0	43.8	-230	13.3
10	40	0	87.9	-307	16.6
20	10	0	-133	-77	9.97
20	20	0	-88.6	-154	13.3
20	30	0	-44.5	-230	16.6
20	40	0	-0.47	-307	19.9
30	10	0	-221	-77.1	13.3
30	20	0	-177	-154	16.6
30	30	0	-133	-230	19.9
30	40	0	-88.8	-307	23.3
40	10	0	-309	-77.3	16.6
40	20	0	-265	-154	19.9
40	30	0	-221	-231	23.3
40	40	0	-177	-307	26.6
0	10	10	88.4	0.166	6.67
0	10	20	133	77	10
0	10	30	177	154	13.4
0	10	40	221	231	16.7
0	20	10	132	-76.5	9.99
0	20	20	177	0.331	13.3
0	20	30	221	77.1	16.7
0	20	40	265	154	20.1
0	30	10	176	-153	13.3
0	30	20	221	-76.3	16.7
0	30	30	265	0.497	20

TABLE 3.7 – CONT.
WORKSPACE ANALYSIS FOR 0.5 MM CASE OF MICRO-FINGER CAD MODULE

d_1 µm	d_2 µm	d_3 µm	X µm	Y µm	Z µm
0	30	40	309	77.3	23.4
0	40	10	221	-230	16.6
0	40	20	265	-153	20
0	40	30	309	-76.1	23.3
0	40	40	353	0.663	26.7
40	40	40	0	0	40

3.6 Final Design of Hybrid Two-Fingered Micro-Manipulator Hand

Based on the results obtained from the previous sections, the proposed new architecture CAD model of the hybrid two-fingered micro-manipulator hand, in which angle φ is chosen to be 35^o is given in Fig. 3.20. It is composed from two 3-DOF PRS parallel mechanisms connected in series to enlarge the workspace of the micro-manipulator.

The final design parameters and wire and flexure hinge characteristics for our proposed two-fingered micro-manipulator hand are:

- Fixed frame radius $R = 10$mm
- Mobile frame radius $r = 3.5$mm

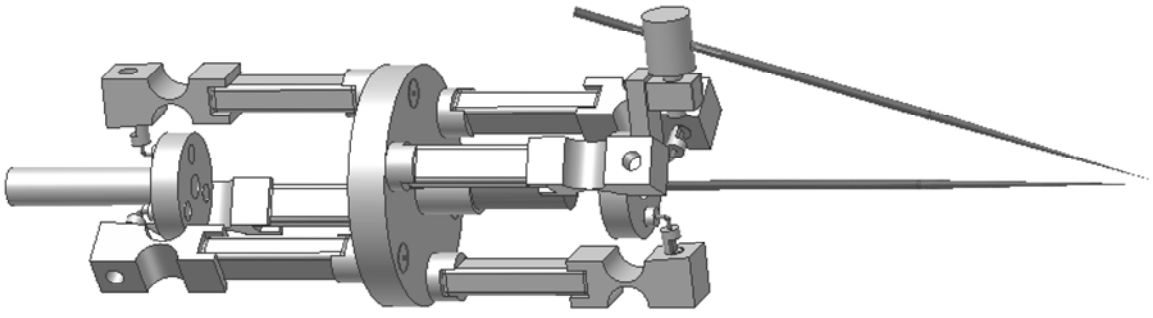

Fig. 3.20: CAD model of the hybrid two-fingered micro-manipulator hand

- Angle $\varphi = 35^{o}$.
- Thickness of flexure hinge is 0.5mm and it is fabricated from Aluminum.
- Wire thickness is 0.5mm and its material is Copper.

The proposed architecture of the two-fingered micro-manipulator hand is consists of two 3-DOF PRS parallel mechanism modules, upper and lower, connected serially back to back. It is driven by three PZT actuators in the three legs of the kinematics chain of each module. Each leg of the kinematics chain has PRS joints structure. Two glass pipettes are used as two-finger end effector in a chopstick-like manner. As the length of the glass pipette end effector is decreased, the resolution and accuracy of the micro-manipulator hand is increased.

3.7 Summary

This chapter presents a detailed discussion about the optimization and design phase. It starts with an overview of optimization/search techniques followed by and Introduction to Genetic and Evolutionary Algorithms including its merits, its standard procedure, and briefly discussing some major issues for designing successful GEAs.

The optimization process of our proposed 3-DOF PRS micro finger model is divided into two main parts:

1- Optimization of the theoretical model of 3-DOF PRS micro finger module: In this part, the optimization process is carried out using Discrete Search method first. Then the same optimization is repeated using GEAs. In the comparison in between the two methods, we noticed that the GEAs technique is superior in finding the best solution but its solution values are needs high accuracy for practical implementation. So, to find more easily to be practically implemented design parameters we used the discrete search method with narrow range for design parameters. Then the CAD model of 3-DOF PRS micro finger module is designed using Autodesk Inventor program.

2- Optimization of the Practical CAD model of 3-DOF PRS micro finger module: In this part, a complementary optimization process is carried out using ANSYS

workbench program to decide the suitable mechanical properties for the flexure hinge used in the CAD model. The most suitable thickness of the thickness of the flexure hinge is found to be 0.5mm to be comparable to that of the wire thickness and its material is decided to be of Aluminum. The workspace volume of the practical CAD model is about 5% less than that of the theoretical model.

Table 3.8 presents the *X*-, *Y*-, and *Z*-extremities for a 3-DOF PRS micro finger module having a 5cm glass pipette finger as its end effector for all methods used.

TABLE 3.8
WORKSPACE EXTREMITIES FOR ALL OPTIMIZATION METHODS

	Discrete Search Technique	GEAs Method, 3rd run	Discrete Search Narrow Range	CAD Model of Micro Finger
$\boldsymbol{X}_{min}$ μm	-370.9272	-370.9133	-370.912	-353
$\boldsymbol{X}_{max}$ μm	370.8309	370.8449	370.846	353
$\boldsymbol{Y}_{min}$ μm	-330.4946	-370.8791	-370.879	-307
$\boldsymbol{Y}_{max}$ μm	330.4167	370.8791	370.879	307
$\boldsymbol{Z}_{min}$ μm	-20	-20	-20	-20
$\boldsymbol{Z}_{max}$ μm	20	20	20	20

Finally, based on the results obtained from the optimization process we could design the CAD model for the proposed two-fingered hybrid micro-manipulator hand. In next chapter, the realization and implementation of this CAD model will be explained.

CHAPTER 4

Phase Three: Realization and Implementation

This chapter presents the details of the third and last phase in the development process of micro-manipulator hand which is realization and implementation phase. First, the prototype realization of the two-fingered hybrid micro-manipulator hand CAD model designed in chapter 3 is presented. Then the description of the practical hardware system for the two-fingered micro-manipulator hybrid hand is discussed. Next, the program description, practical calibration method, practical jacobian matrices, practical workspace, and error analysis of the prototype are discussed and presented.

4.1 Introduction

By the end of chapter 3, we could design a CAD model for the micro-manipulator hand based on the optimization results. The proposed new architecture CAD model of the hybrid structure two-fingered micro-manipulator hand, in which angle φ is chosen to be 35^{o} is given in Fig. 4.1.

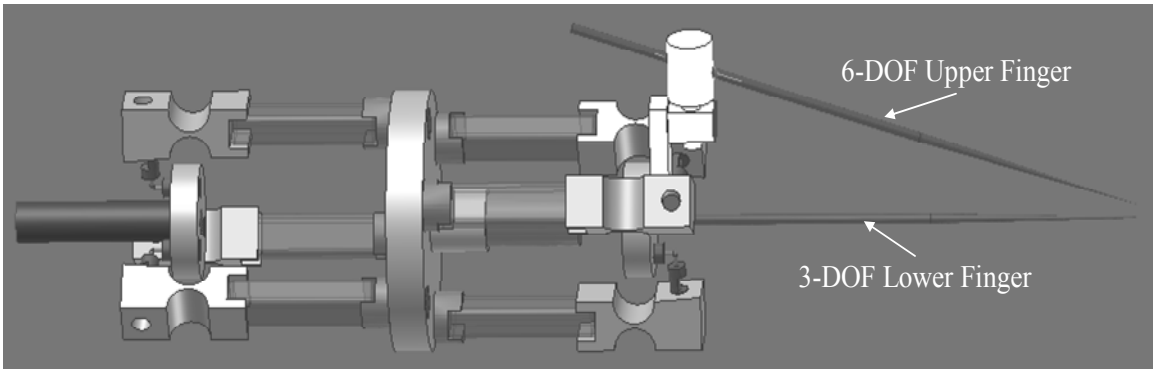

Fig. 4.1: Final design of CAD model for hybrid two-fingered micro-manipulator hand.

The realization of this CAD model is shown in Fig. 4.2. For this prototype, the length of the actuating mechanism is about 10.5cm and the total length of the hand with two glass fingers is about 15.5cm. The total weight of this prototype is about 50gm. In this prototype, two perpendicular strain gages are used for each piezo-electric actuator, one for measuring displacement and the other for temperature change compensation. The flexure hinges of upper module are made thinner than that of lower module to make the prototype more rigid and to give more flexibility to upper module finger [59].

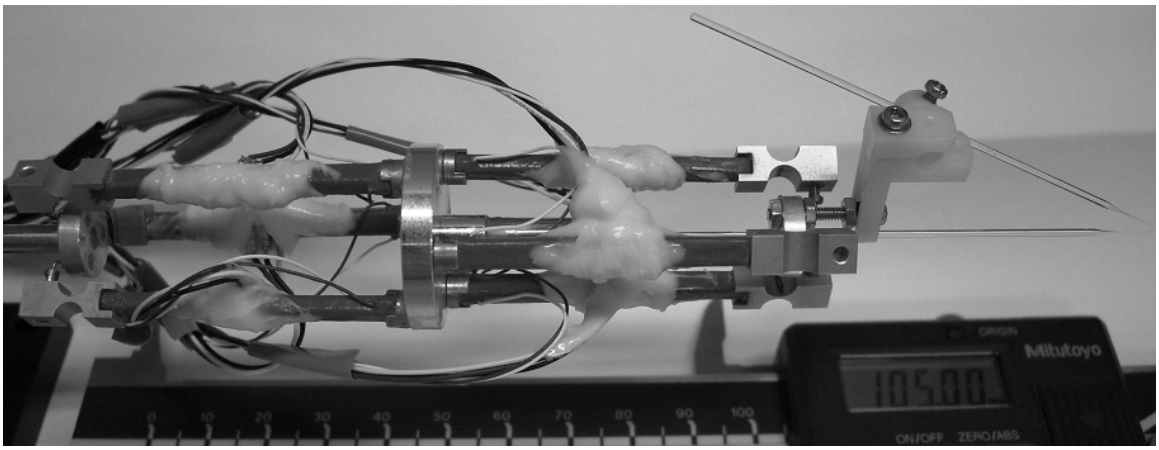

Fig. 4.2: Hybrid two-fingered micro-manipulator hand prototype.

Fig. 4.3 shows the old prototype parallel mechanism with thin plate for the two-fingered micro-manipulator [39]. Table 4.1 gives a brief comparison between the old prototype mechanism and the new two-fingered micro-manipulator hand proposed in this thesis from different aspects like; workspace extremities, weight of the mechanism, and length of actuation mechanism. From table 4.1, we can conclude [52]:

1- The proposed mechanism has larger workspace volume, lighter weight, and smaller length.
2- The proposed mechanism has two rotational degrees of freedom and one translational degree of freedom while the old one has three translational degrees of freedom. So, the proposed mechanism has a wider *XY*-range.
3- The thin plate parallel links in old mechanism is easier to fabricate than the flexure hinges in proposed new mechanism.

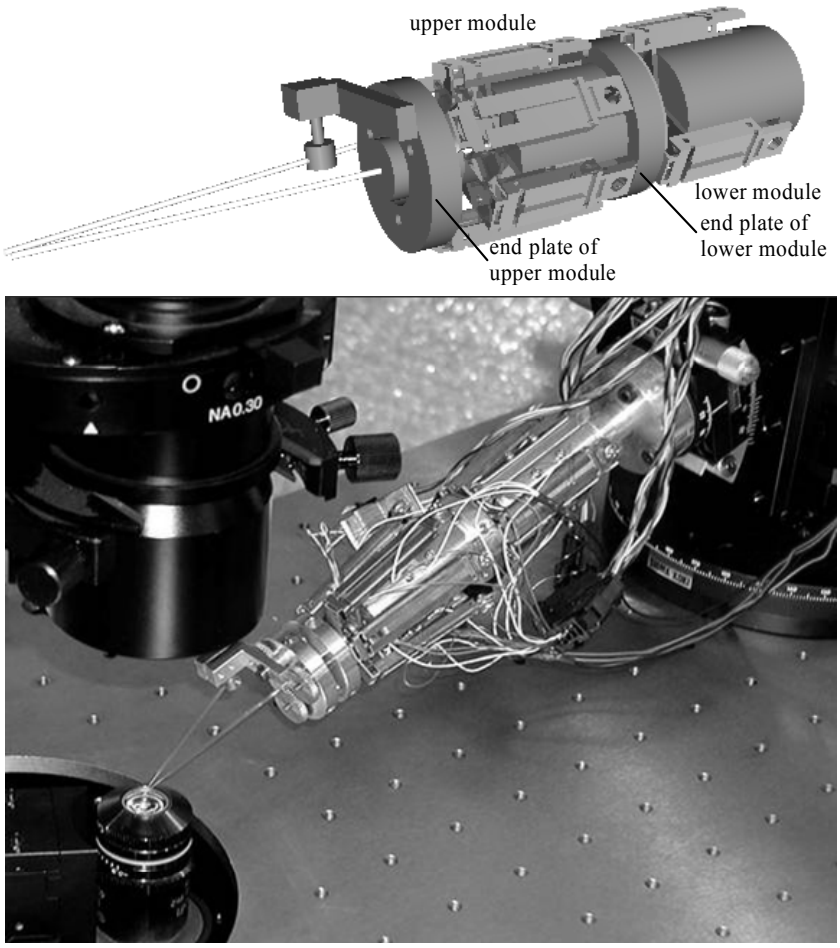

Fig. 4.3: Old prototype of two-fingered micro mechanism with thin plate.

TABLE 4.1
COMPARISON BETWEEN THIN PLATE MECHANISM AND PROPOSED NEW MECHANISM

	Thin plate mechanism	Proposed new mechanism
Workspace of one finger	Small	Large
X-axis extremes	From -240 μm to 240 μm	From -370.9 μm to 370.8 μm
Y-axis extremes	From -200 μm to 200 μm	From -330.5 μm to 330.4 μm
Weight	Heavy (200gm)	Light (50gm)
Degrees of freedom (DOF)	3-DOF Translational	1-DOF Translational plus 2-DOF Rotational
Actuating mechanism length	Tall (14cm)	Short (10.5cm)
Fabrication	Easy	Difficult

The comparison given in table 4.1 is for a 3-DOF micro manipulator having a 5cm glass pipette finger as an end effector. Both mechanisms are using three piezo-electric actuators as the active joints. The maximum displacement of the piezo-electric actuator is 40 μm. The details of the hardware system are given in next section.

4.2 System Hardware Setup of Hybrid Structure Two-Fingered Micro-Manipulator Hand

Figure 4.4 shows the details of the two-fingered micro-manipulator hand system hardware setup. The proposed system is almost the same as the old one. It consists of two control loops; the first one is for controlling the motion of the two fingers of the micro-manipulator hand while the second one is for image processing with auto focusing and auto tracking capabilities [53, 80].

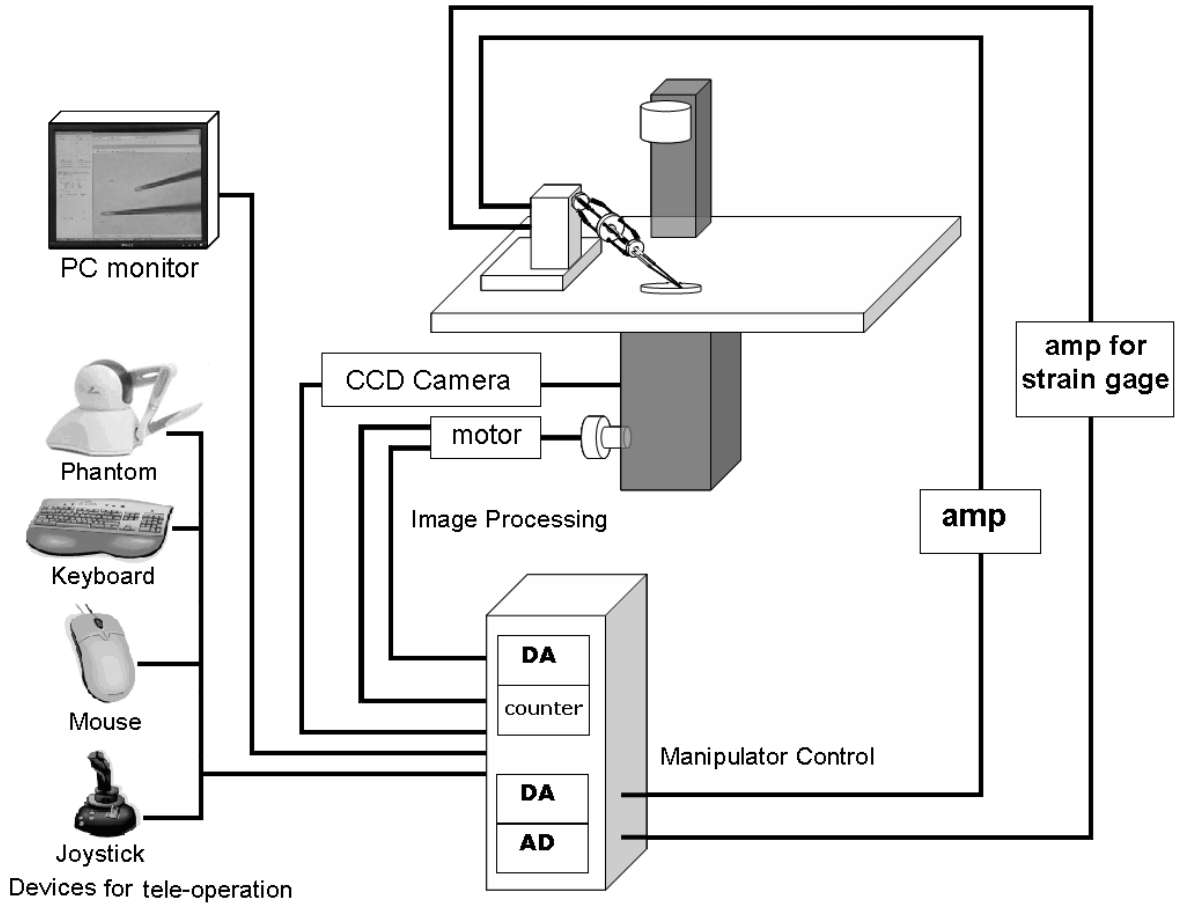

Fig. 4.4: Schematic diagram for the architecture of system hardware setup for the two-fingered micro-manipulator hand.

The micro-manipulator motion control loop controls the pose of the mobile plate by controlling the command voltage signals to the PZT actuators (TOKIN AE0203D44H40, max. displacement is 40μm). These actuators are driven by a high voltage amplifier (Matsusada 3Channel piezo driver) that cancels out the hysteresis behavior of PZT actuators. Their elongations are measured by using strain gages (NEC N11-FA-1-120-23) that are directly mounted on their surfaces. The strain gages are connected to a bridge that is connected to Multi-Conditioner (MCD-16A) for dynamic amplification of measurements. We use two strain gages perpendicularly mounted on the surface of every PZT to cancel the effect of temperature changes. The output of the multi-conditioner is connected to the PC through AD card [Contec AD16-16(PCI)EV]. The command signals to control the PZT actuators are outputted from PC through DA-card [Contec DA16-16(LPCI)L] to the PZT actuators driver. The hardware setup details of this loop are shown in Fig. 4.5.

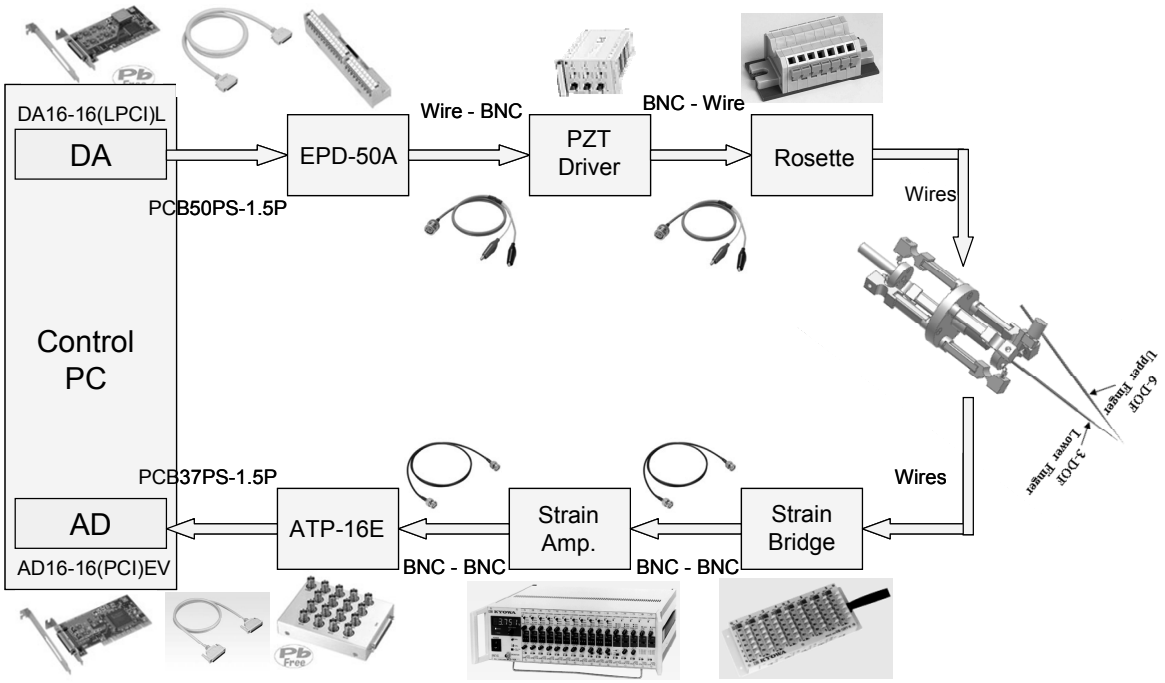

Fig. 4.5: Details of hardware system setup for manipulator motion control loop.

The image processing loop uses a Dragon Fly2 camera – connected to the PC through standard IEEE 1394 connection interface and programmed using Intel OpenCV library –

to get real time images from the microscope. This interface is used to locate the *XY*-coordinates of the fingertip glass needle graphically – i.e. from the captured image. The *Z*-coordinate is read from the automatic focusing stage with a counter board [Contec CNT24-4(PCI)H] that is interfaced to the encoder output of servomotor controller board (HS-230-05). This servomotor controller board is controlled by the output of the PC to operate a servomotor (RA-05) to auto focus the image depth under microscope. This image depth is the *Z*-coordinate. Keyboard, joystick, haptic device "Phantom", or graphical user interface (GUI) window can be used for tele-operation control of fingertips position of the micro-manipulator hand. The hardware setup details of this loop are shown in Fig. 4.6.

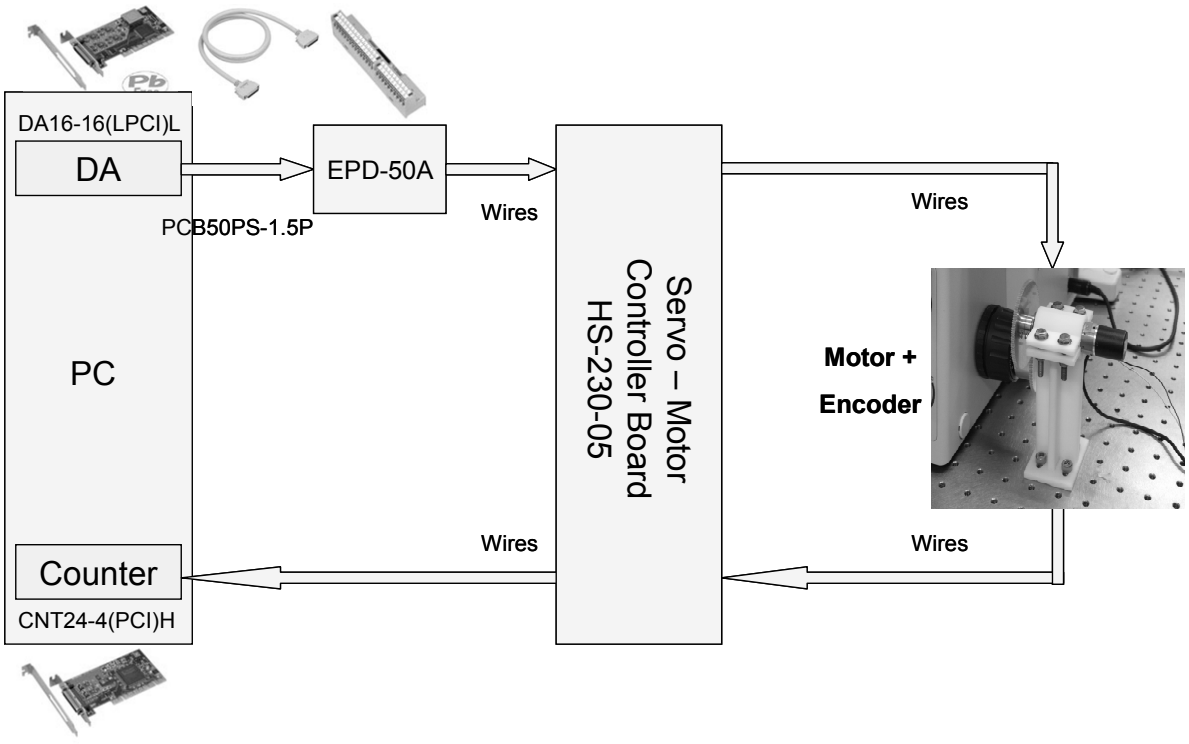

Fig. 4.6: Details of hardware system setup for image processing loop.

The design of the CAD model for the motor holder that is used in our system is given in Fig. 4.7 (a). The realization of this CAD model is given in Fig. 4.7 (b). The combination of the two control loops are presented in Fig. 4.4 which shows the complete micro-manipulation system for our newly developed micro-manipulator hand.

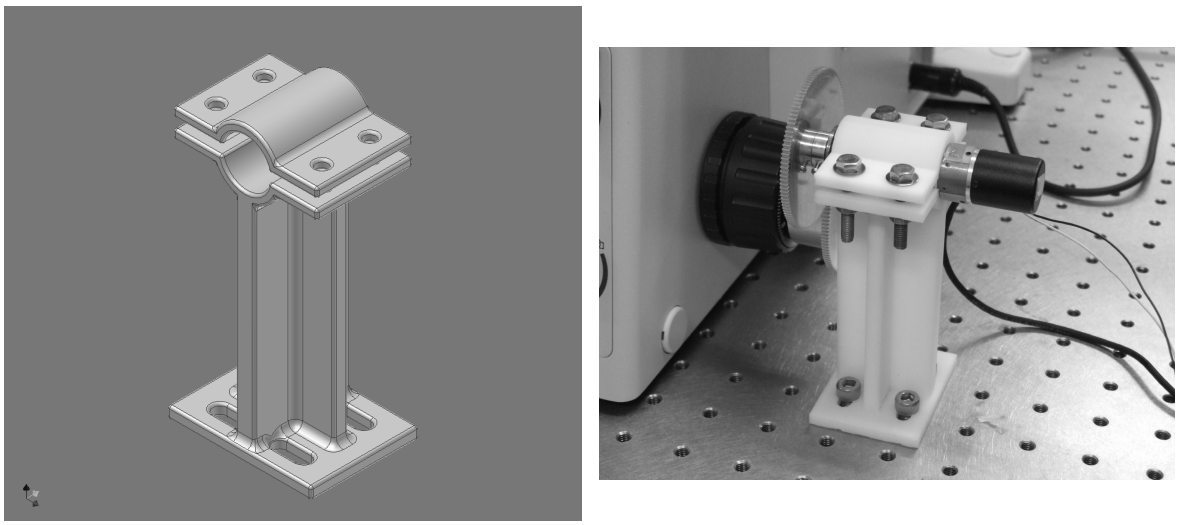

(a) CAD model (b) Real motor holder

Fig. 4.7: The design of the CAD model for motor holder (a) and its realization (b)

4.3 Description of Software Program

The graphical user interface (GUI) for overall control of the system functions is presented in this section. User can control the motion of the two fingers of the hand using one of the tele-operation devices at a time and the GUI interface. The GUI interface provides the user with many functions like initial calibration, auto calibration, auto focusing, auto tracking, and position detection. The program starts with initializing the image processing loop and the hardware devices. Then using the GUI interface, the user can choose to calibrate the two fingers – one at a time – or to use a previously determined jacobian matrix. After calibration, using the GUI interface, the user can control the motion of the two fingers individually in *X*-, *Y*-, and *Z*-directions with one of the tele-operation devices. When choosing to control the motion of the lower module, both fingers will move. This is due to the serial connection in between the upper and lower modules. But, when choosing to control the motion of the upper module, only the upper finger will move. The two fingers are in a chopstick like style. The lower finger is for support while the upper one is for fine motion. Different manipulation tasks are shown in Fig. 4.8. The GUI interface provides the user with the *X*-, *Y*-, and *Z*-coordinates of the finger being used and the measurements of the strain gages of the module of that finger in real time.

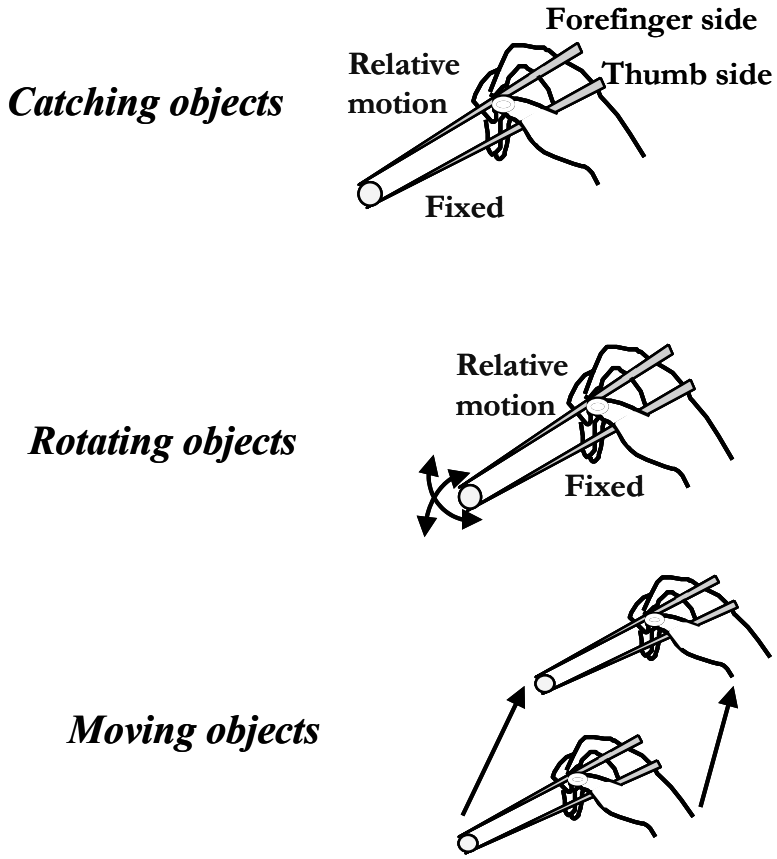

Fig. 4.8: Different manipulation tasks using two chopsticks

The evaluations of using different tele-operation devices are given in table 4.2. From this table we can conclude that joystick is better than keyboard at low speed but Phantom haptic device is better at high speed [53].

TABLE 4.2
AVERAGE RESULTS OF TELE-OPERATION DEVICES

	Max Speed 30μm/s		Max Speed 60μm/s	
	Keyboard	Joystick	Joystick	Phantom
Average time [sec]	11.791	9.028	12.007	10.111
Standard Deviation	0.529	0.547	0.678	2.472
No. of Samples	20	20	20	9

4.4 Practical Calibration Method -LSE

In calibration process, the starting position of the finger tip is defined as the zero or origin position relative to finger tip coordinates. Then we start to give commands to the PZT actuators to move the finger tip in grid points for different planes as shown in Fig. 4.9. The link displacements are measured using strain gages that have resolution of about 30nm. The corresponding finger tip position is determined using template matching technique that gives *X*- and *Y*-coordinates and counter board gives *Z*-coordinate so that the finger tip is clearly visible. All coordinates are relative to the microscope reference frame. After stacking N measurements for the PZT actuator displacements and corresponding finger tip positions, we can proceed for calculating the jacobian matrix using least squares errors (LSE) Technique [78].

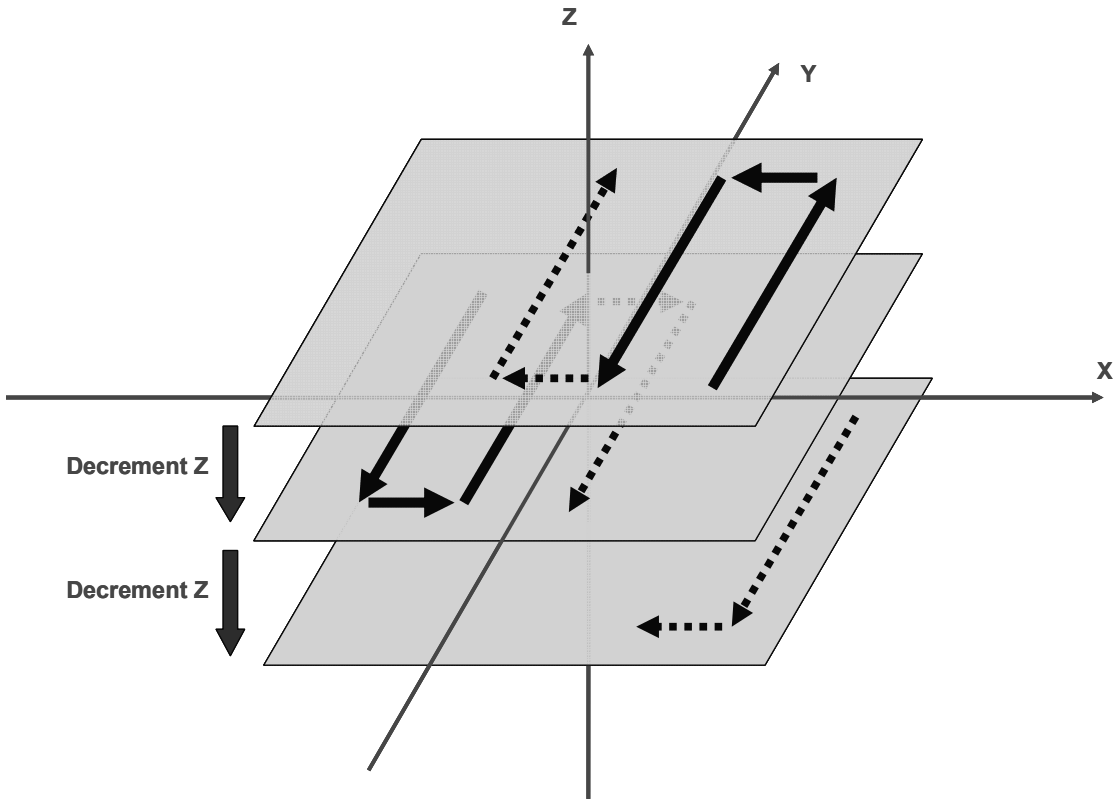

Fig. 4.9: The path taken by end effector in practical calibration process

We know that the relationship between PZT actuator displacements and finger tip position is as given in (4.1).

$$\begin{bmatrix} d_1 \\ d_2 \\ d_3 \end{bmatrix} = J \begin{bmatrix} x \\ y \\ z \end{bmatrix} \Rightarrow \begin{bmatrix} d_1 & d_2 & d_3 \end{bmatrix} = \begin{bmatrix} x & y & z \end{bmatrix} J^T$$
$$Let \quad G = J^T$$
$$\therefore \begin{bmatrix} d_1 & d_2 & d_3 \end{bmatrix} = \begin{bmatrix} x & y & z \end{bmatrix} G \tag{4.1}$$

For N measurements data sets – that for sure include an error in the measurements, - it follows that;

$$\begin{bmatrix} d_{11} & d_{21} & d_{31} \\ d_{12} & d_{22} & d_{32} \\ \vdots & \vdots & \vdots \\ d_{1N} & d_{2N} & d_{3N} \end{bmatrix}_{N\times 3} = \begin{bmatrix} x_1 & y_1 & z_1 \\ x_2 & y_2 & z_2 \\ \vdots & \vdots & \vdots \\ x_N & y_N & z_N \end{bmatrix}_{N\times 3} G_{3\times 3} + \begin{bmatrix} e_1 \\ e_1 \\ \vdots \\ e_N \end{bmatrix}_{N\times 3} \tag{4.2}$$

In matrix form, it will take the form of (4.3).

$$D = PG + e$$
$$\therefore e = D - PG \tag{4.3}$$

From (4.3), the sum of squared error is defined as;

$$S = e^T e = \left(D - PG\right)^T \left(D - PG\right) \tag{4.4}$$

To calculate the matrix G that minimizes the sum of squared errors S, we can proceed as follows;

$$\frac{\partial S}{\partial G} = 0 = -2P^T D + 2P^T PG$$
$$\therefore G = \left(P^T P\right)^{-1} P^T D$$
$$and \qquad J = G^T \tag{4.5}$$

Finally, we can use this jacobian matrix in controlling the finger tip position of the parallel mechanism. For micro-manipulators, the variation in jacobian matrix values is very small and can be neglected over the entire workspace of the micro-manipulator. So, we can consider it constant. This is acceptable only for small variations [55, 62].

4.5 Evaluation Results

In our micro-manipulator hand, the two fingers act like two chopsticks. The lower module finger will act as the thumb side chopstick while the upper module finger will act as the forefinger side chopstick, see Fig. 4.8. This arrangement for the micro-manipulator hand has the advantage of having dexterous motions by coordinating the two glass pipettes end effectors using simple control algorithm.

The calibration process described before is carried out for each finger individually to determine its jacobian matrix. The practical jacobian inverse matrices of lower and upper finger tips based on a set of calibration data points are given by (4.6) and (4.7) respectively and shown in Fig. 4.10. These two jacobian inverse matrices are used to control the position of the tip of two fingers while operation [61, 63].

$$G_{Lower} = \begin{bmatrix} 0.032847 & -0.005085 & -0.080528 & -0.261982 \\ 0.041115 & -0.001436 & -0.094133 & -0.309697 \\ 0.032582 & -0.001688 & -0.087255 & -0.302800 \end{bmatrix} \tag{4.6}$$

$$G_{Upper} = \begin{bmatrix} 0.064003 & -0.006038 & -0.116110 & 0.065692 \\ 0.039538 & 0.010491 & -0.098198 & 0.058805 \\ 0.033672 & -0.007968 & -0.105055 & 0.097967 \end{bmatrix} \tag{4.7}$$

The two practical jacobian inverse matrices given are 3×4 matrices. The first three columns constitute the jacobian inverse matrix. The last column is the initial position of the finger tip relative to the image processing – microscope - system coordinates when the calibration process starts. This initial position serves as the origin for the motion of the finger tip relative to finger tip coordinates. So, each time we give an order to the finger tip

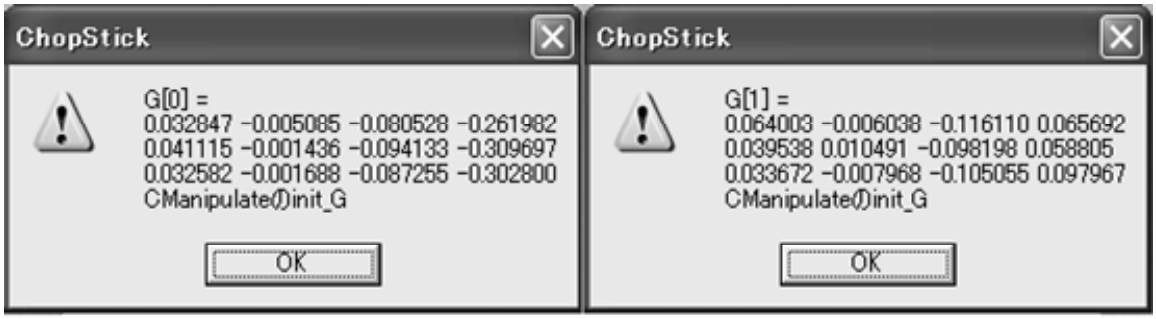

Fig. 4.10: Practical jacobian matrices of lower and upper finger tips

to return to the origin position, it will return to its initial position at which the calibration process is done.

An image of the system setup of the prototype of the hybrid two-fingered micro-manipulator hand proposed in this thesis with a closer look at the two finger tips after calibration process is done is shown in Fig. 4.11.

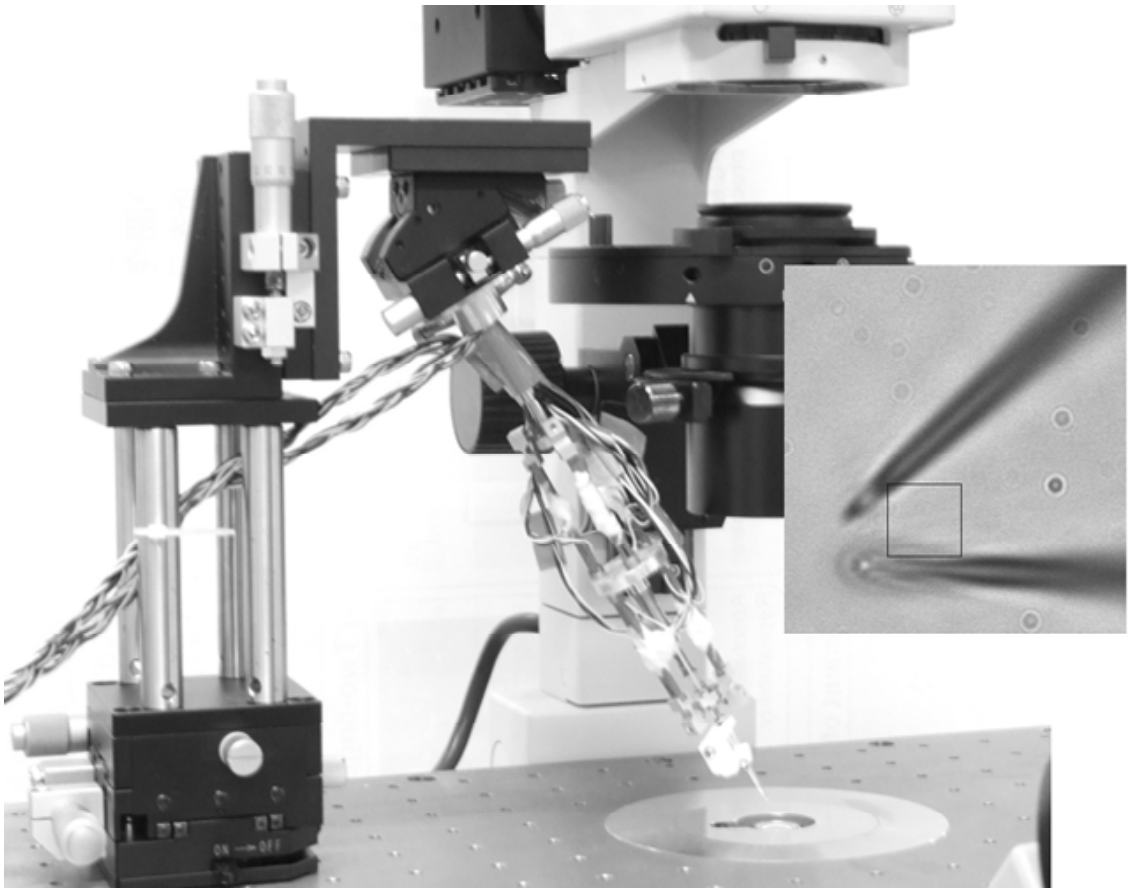

Fig. 4.11: Setup of the two-fingered micro-manipulator hybrid hand

Figure 4.12 shows the practical workspace of the upper and lower fingers calculated using the obtained Jacobian inverse matrices. The workspace looks rotated because the axis of the micro-manipulator is not adjusted at the beginning. Even though, we can see that both fingers have large workspaces.

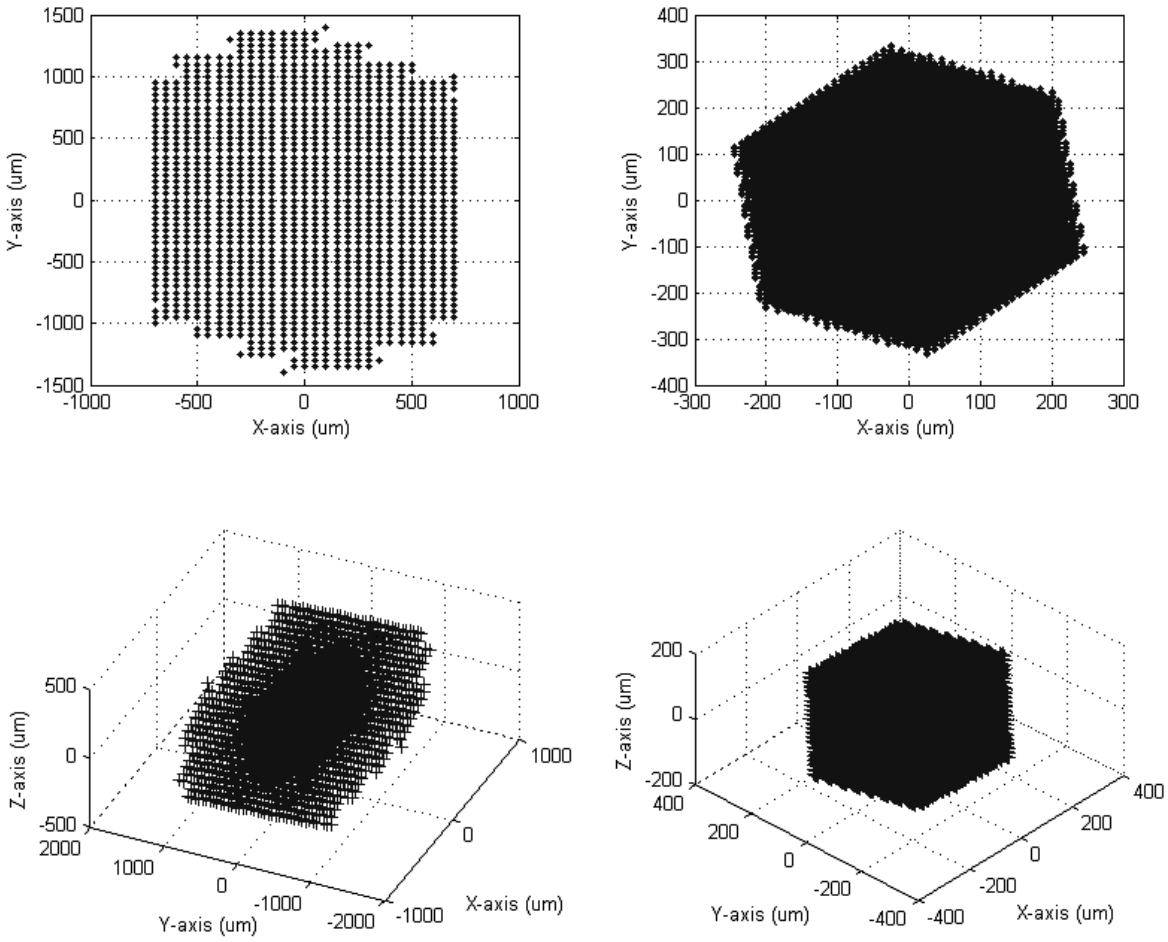

Fig. 4.12: Practical workspaces and its *XY*-projection for both fingers. Lower finger (left) and upper finger (right)

Fig. 4.13 shows the error norm in μm of some test data points after calibration process. The hybrid structure two-fingered micromanipulator hand has a maximum error norm of about 0.866μm – i.e. 0.5μm in each direction – small range displacements while operation. The maximum error can reach 1.5 to 2μm in the workspace of the finger.

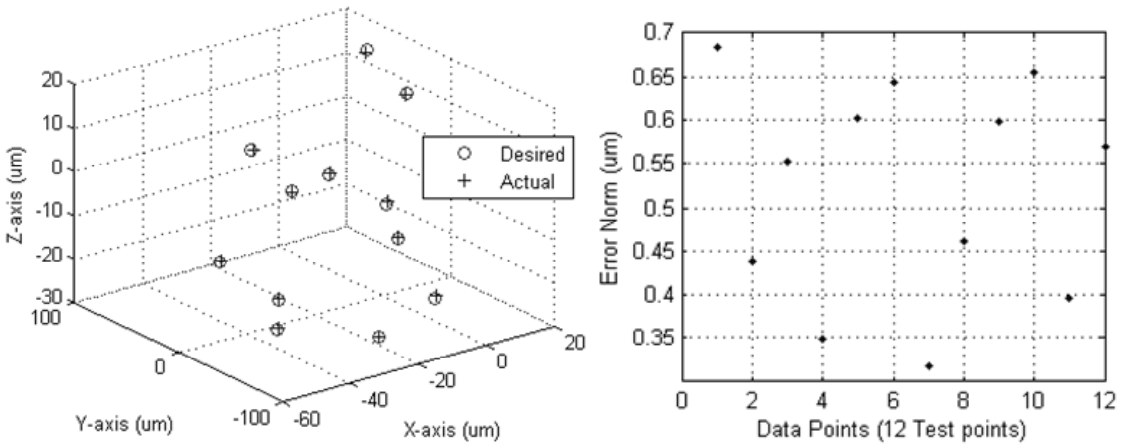

Fig. 4.13: Test data points and its Error norm values

4.6 Practical workspace determination of the two-fingered micro-manipulator hand prototype

Based on the least squares error (LSE) method, the practical jacobian matrices in between the voltage commands and the actuators displacements are calculated. The procedure is as follows;

1- Give the voltage commands to the PZT actuators through the DA card.
2- Measure the *X*- and *Y*-coordinates from the screen scale - see Fig. 414 - and *Z*-coordinates of the finger tip from the fine focus knob of the microscope.
3- Repeat the previous two steps N times.
4- Using the N measurements data sets, calculate the Jacobian matrix using LSE technique.

The previous procedure is carried out for each finger individually. The practical jacobian matrix obtained for the lower finger is given in (4.8).

$$J_{Lower} = \begin{bmatrix} 0.06572770699707 & -0.02904285573233 & -0.11941747568728 \\ 0.05631514824361 & -0.03185941685346 & -0.12673161182001 \\ 0.06960909378744 & -0.02250674173875 & -0.14196609470309 \end{bmatrix} \quad (4.8)$$

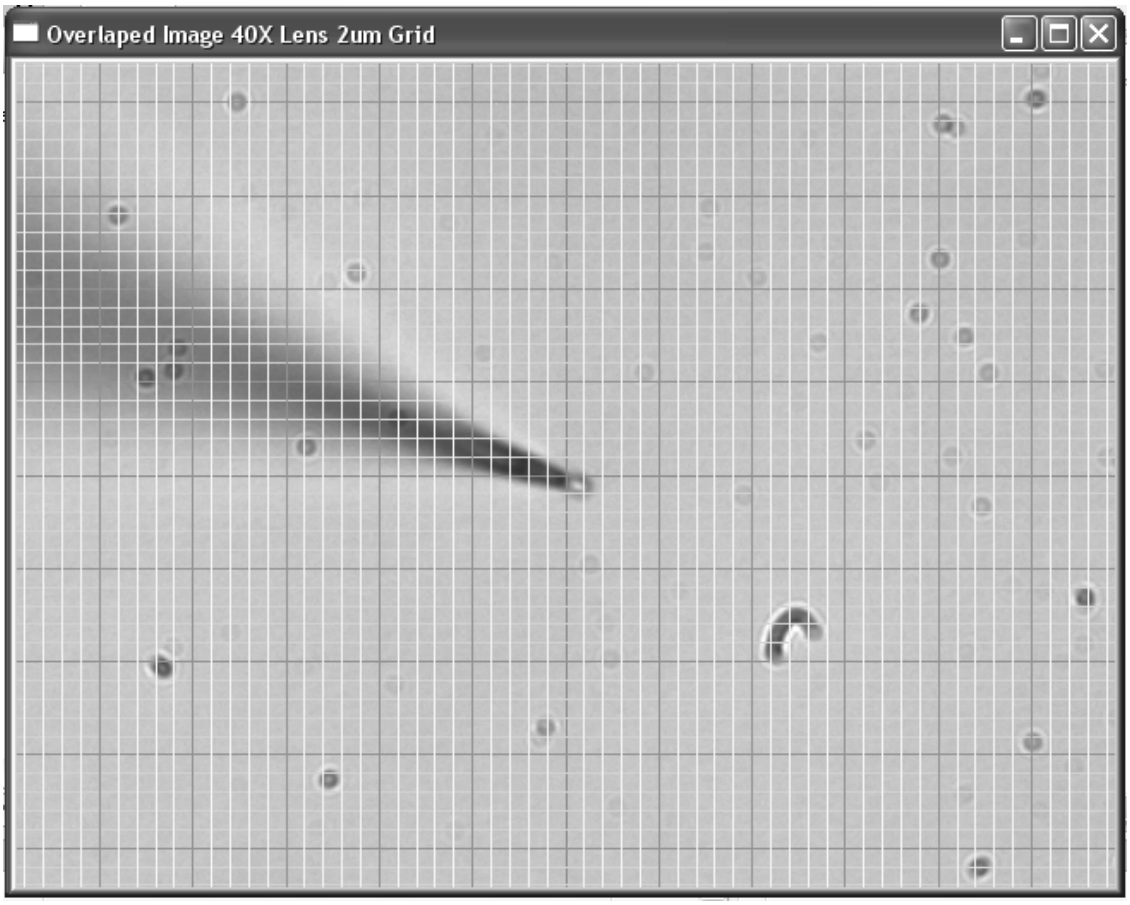

Fig. 4.14: On screen scale for determining *XY*-coordinates

The error norm of some test data is presented in Fig. 4.15 and the calculated practical workspace of the lower finger is shown in Fig. 4.16.

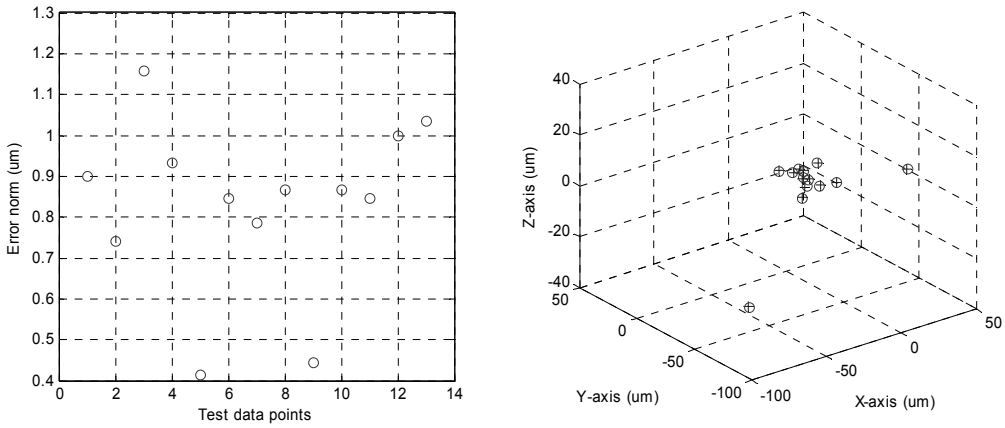

Fig. 4.15: Error norm for some test data points of lower finger tip and their location in 3D

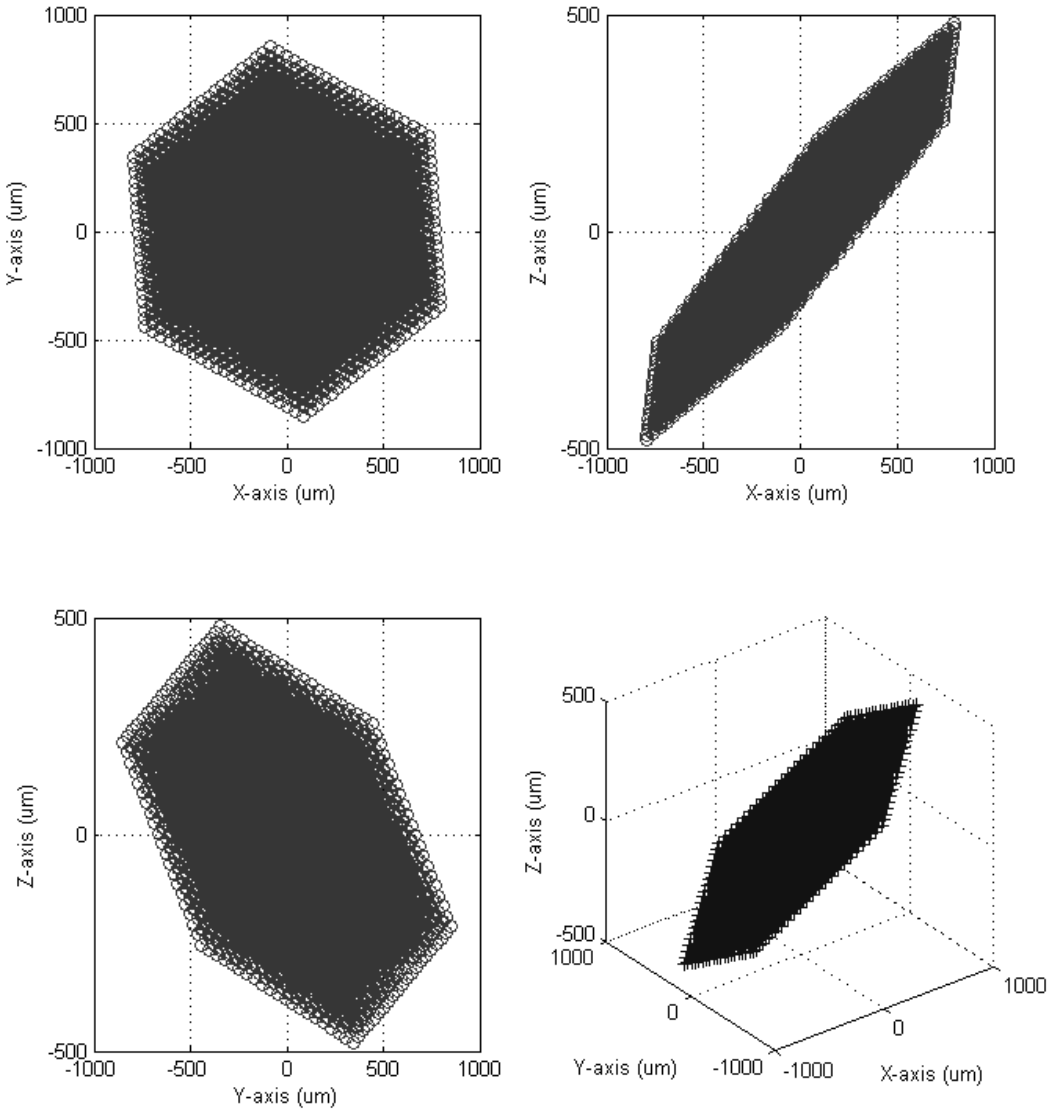

Fig. 4.16: Practical workspace volume of lower finger tip

From Fig. 4.15 we can notice that the maximum error norm is about 1.2μm. Also from Fig. 4.16 we can see that the practical *X*-range is from about -1000μm to 1000μm and the practical *Y*-range is from about -890μm to 890μm. The practical *X*-range is about 7% less than that of theoretical value and the practical *Y*-range is about 7% less than that of theoretical values.

The practical jacobian matrix obtained for the upper finger is given in (4.9).

$$J_{Upper} = \begin{bmatrix} 0.11732026415979 & -0.06323286222513 & -0.20461512105290 \\ 0.09143336512546 & -0.02747733712544 & -0.20691939522632 \\ 0.13515220388994 & -0.02512005676001 & -0.20145941632885 \end{bmatrix} \quad (4.9)$$

The calculated practical workspace of the upper finger is shown in Fig. 4.17 and the error norm of some test data is presented in Fig. 4.18.

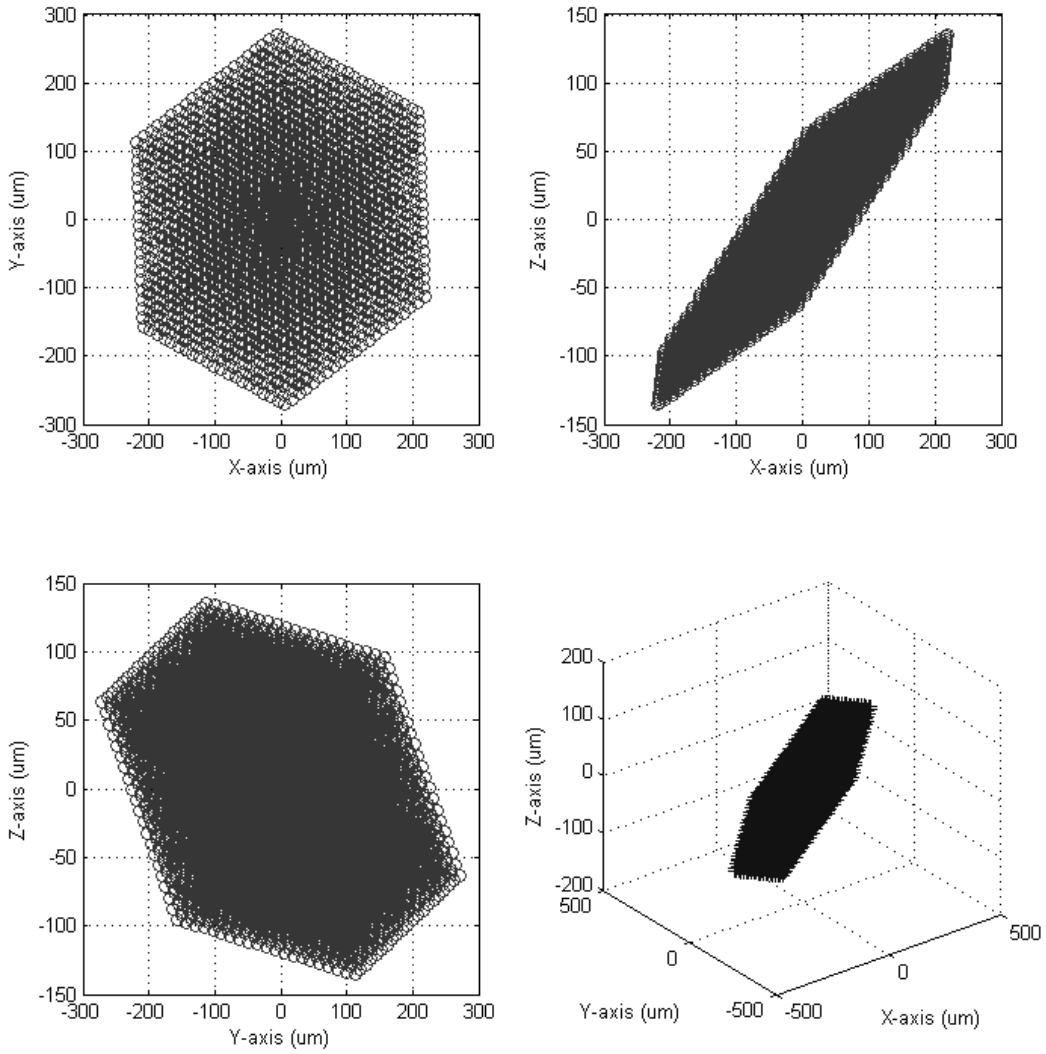

Fig. 4.17: Practical workspace volume of upper finger tip

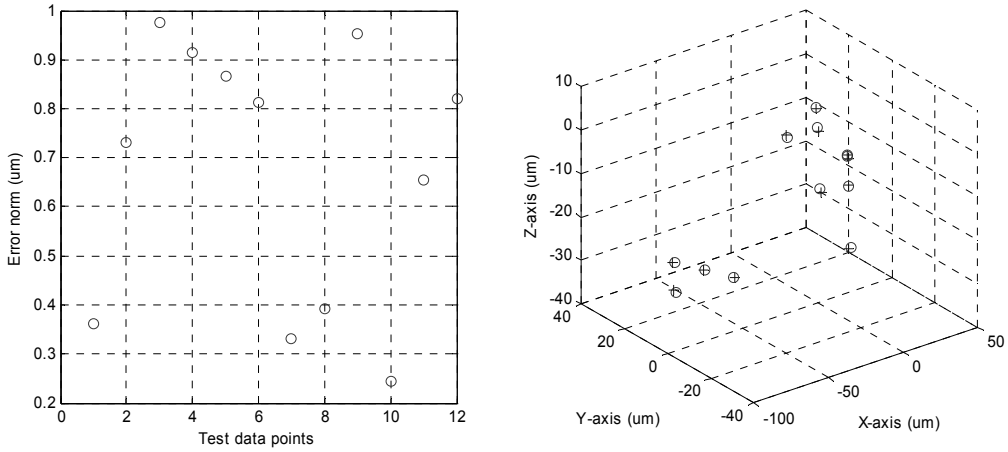

Fig. 4.18: Error norm for some test data points of upper finger tip and their location in 3D

From Fig. 4.17 we can see that the practical *X*-range is from about -320μm to 320μm and the practical *Y*-range is from about -295μm to 295μm. The practical *X*-range is about 13% less than that of theoretical value and the practical *Y*-range is about 10% less than that of theoretical value. These values are about 5 to 6% less than that of the CAD model values. Also from Fig. 4.18 we can notice that the maximum error norm is about 1μm.

The small deviation of the results of the practical prototype from the theoretical value is due to the use of pin flexure joint as a revolute joint and wire as a spherical ball joint which they are neither an ideal revolute joint nor an ideal spherical ball joint. The workspaces of the lower and upper fingers of practical prototype are in general about 5% less than that of CAD model.

4.7 Target Application: Setup for Tissue Micro-injection Experiment

As a target application of the developed micro-manipulator hand, we plan to use two micro-manipulator hands for micro-injection of high-density cell suspension of epithelium and Mesenchyme tissues in a collagen gel environment with precise positioning of cytokines [79]. The setup of this proposed experiment of tissues micro-injection is presented in Fig. 4.19.

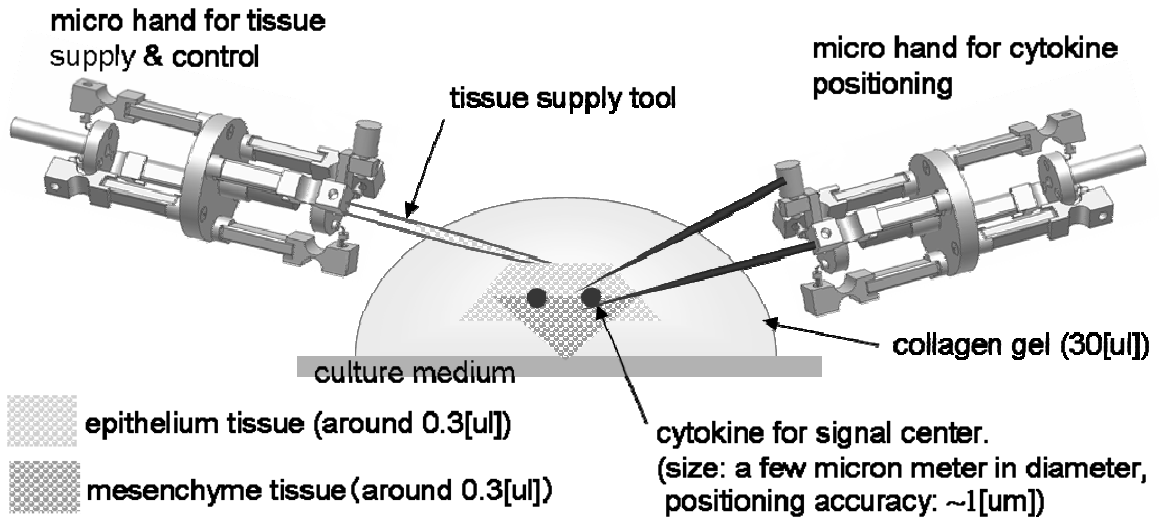

Fig. 4.19: Proposed setup of tissue micro-injection experiment

In this experiment, one micro-manipulator hand will be used to supply 0.3µl high-density cell suspension of each of epithelium and Mesenchyme tissues in a 30µl collagen gel environment while the other micro-manipulator hand will be used to precisely position cytokines in the same medium. The supply of high-density cell suspension of tissues will be provided by a syringe pump KDS270 through a hollow glass pipette which can be produced using PC-10 puller, see Fig. 4.20. The KDS270 syringe pump can hold up to four syringes; two of them will operate in fusion mode while the others are for withdrawal at the same time with a minimum flow rate of 0.001µl/h.

Fig. 4.20: PC-10 puller (left) and KDS270 syringe pump (right)

The PC-10 puller produces micro-tip glass pipette using one step procedure or two step procedure. The length and diameter of the tip produced is controlled by adjusting the number of weights used and the temperature of heater 1 and heater 2. For high heater temperature or heavy weight or both, the tip produced tends to be long and the time of production is small. Table 4.3 presents some guidelines for producing glass pipettes using PC-10 puller using regular 1mm outer diameter glass pipettes.

TABLE 4.3
GUIDELINES FOR USING PC-10 PULLER TO PRODUCE DIFFERENT TIPS

Method	H1 °C	H2 °C	Sliders position	Weights	Result Tip
One step	--	70	--	Full (4)	~<= 0.5 μm
One step	--	55~60	--	Full (4)	~ >= 0.5 μm
Two step	72.5	55	8 – 4 mm	Full (4)	~ >= 50 μm
Two step	66	84	8 – 4 mm	2L + 1H	~ 0.5 μm
Two step	65	85	7 – 4 mm	Full (4)	~ >= 50 μm
Two step	60	85	7 – 4 mm 6 – 4 mm 8 – 5 mm	Full (4)	0.5 μm - 1 μm

Figure 4.21 shows sample tips produced using one step procedure in the first row and two step procedure in the second row. In general two step procedure is much better in producing the shape and diameter of the tip you need.

4.8 Summary

In this chapter, we presented the third and last phase of the development process of our proposed micro-manipulator hand which is realization and implementation. First the real prototype of the two-fingered micro-manipulator hand CAD model designed in chapter 3

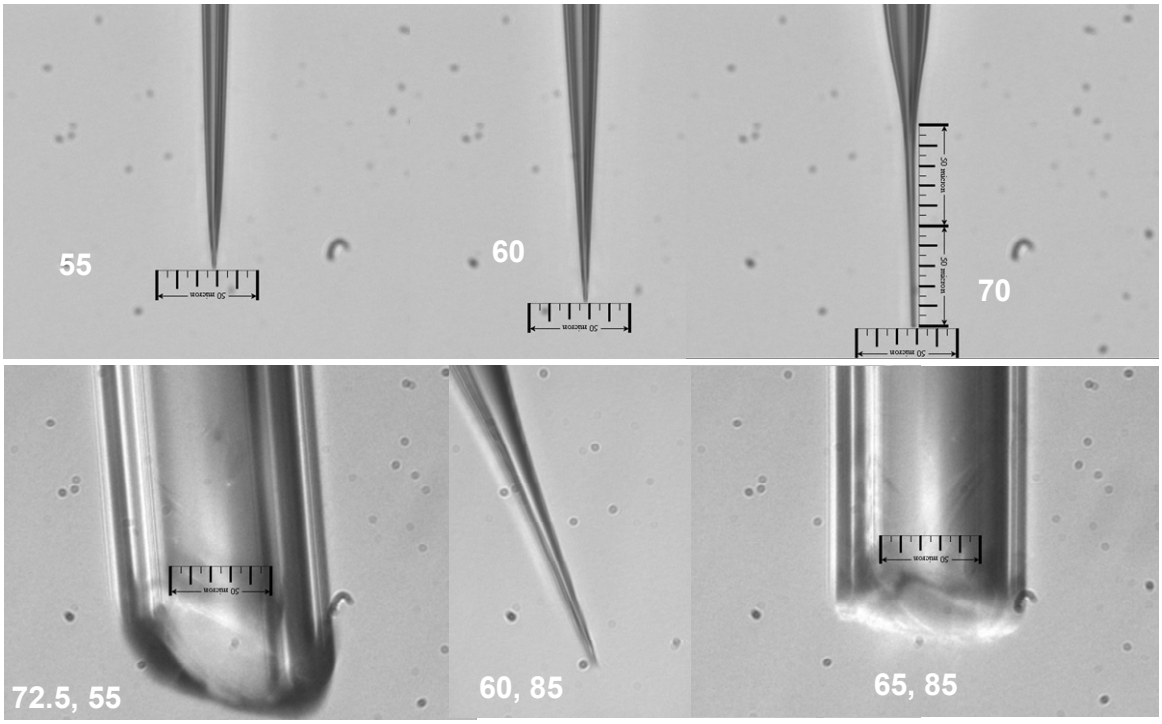

Fig. 4.21: Sample tips produced by PC-10 puller

is presented. Then, the details of the hardware system setup of the micro-manipulation system are discussed. The control loops – manipulator motion control loop and image processing loop - inside the hardware system are presented. A brief comparison in between the old micro-manipulator hand mechanism and the newly designed one is introduced.

The program description along with evaluation results is presented. The method of least squares errors – LSE – is briefly discussed to be used in the determination of the practical jacobian matrices of both the lower and upper fingers. Finally, the workspaces of both the lower and upper finger tips are determined based on the practical jacobian matrices. We found that the workspaces of the lower and upper fingers of practical prototype are in general about 5% less than that of CAD model. This is because of the use of pin flexure hinge as a revolute joint and a wire as a spherical ball joint. Table 4.4 shows the *X*-, *Y*-, and *Z*-ranges for theoretical model, CAD model, and practical prototype.

TABLE 4.4
COMPARISON BETWEEN THEORETICAL, CAD, AND PRACTICAL PROTOTYPE RANGES

	Theoretical Model (5cm finger)	CAD Model (5cm finger)	Practical Prototype (5cm finger)
X_{min} μm	-370.9272	-353	-320
X_{max} μm	370.8309	353	320
Y_{min} μm	-330.4946	-307	-295
Y_{max} μm	330.4167	307	295
Z_{min} μm	-20	-20	-20
Z_{max} μm	20	20	20

At the end of this chapter, we introduce a target application as a future work of our developed two-fingered micro-manipulator hand which is the setup of tissue micro-injection experiment. A brief description of the setup that will be used is presented.

CHAPTER 5

Conclusion and Future Work

This thesis has presented the three phases of the development process of a two-fingered hybrid micro-manipulator hand. The proposed new architecture of our micro-manipulator hand is based hybrid motion mechanism. The hybrid mechanism is consisting from two 3-DOF PRS parallel mechanisms connected in series to enlarge the workspace of the micro-manipulator hand. Two glass pipettes in a chopstick like manner are used as the end effector of our micro-manipulator hand.

A novel solution for the IKP of 3-DOF PRS parallel mechanism is derived. Based on this solution, we could solve the FKP of the 3-DOF PRS parallel mechanism and the IKP giving the tip position of the finger. An optimization process is carried out based on the new kinematics problem solution to optimally choose the design parameters. Finally, we could design and realize the two-fingered micro-manipulator CAD model. The real prototype is checked to determine how close it is to the theoretical model.

5.1 Thesis Summary

Following the introductory chapter, the first phase of the development process of our proposed micro-manipulator hand starts with literature review about research work concerning the solution of 3-DOF RPS and PRS parallel mechanisms. A novel solution for the IKP of both 3-DOF RPS and PRS parallel mechanisms is derived. The feasible workspaces of both mechanisms are checked. Then, we decided to use the 3-DOF PRS parallel mechanism as the basic building unit in our design of the two-fingered micro-manipulator hand. The derived IKP solution is extended to the hybrid motion mechanism of the proposed architecture of micro-manipulator hand.

In chapter 3, the optimization and design of the proposed micro-manipulator hand is carried out based on the mathematical analysis achieved in chapter 2. The main target of the optimization process is to enlarge the workspace volume of the two-fingered micro-manipulator hand. The optimization of the design parameters is done first to the theoretical model using discrete search method and GEAs method for comparison purposes. The discrete search method with narrow range is introduced to get a more easily to be practically implemented design parameters than that of GEAs. Then another optimization step is done for the CAD model to find the best thickness of the pin flexure hinge used in the micro finger CAD model. Finally, the CAD model of the two-fingered hybrid micro-manipulator hand is designed and built.

In chapter 4, the final phase of the development process of our micro-manipulator hand, the real prototype of the proposed design is assembled and tested. The hardware system setup of the micro-manipulation system is discussed. The practical jacobian matrices of the two fingers tips are determined using LSE method. The workspaces of the lower and upper finger tips are also calculated based on the jacobian matrices. The error norm for some test data points is calculated. A brief comparison in between the *X*-, *Y*-, and *Z*-extremities of theoretical model, CAD model, and practical prototype is given at the end of this chapter.

The design procedure of the proposed two-fingered hybrid micro-manipulator hand based on a concrete mathematical analysis and using optimization techniques showed several improvements especially in enlarging the workspace of the manipulator. Besides by the new architecture proposed for the manipulator, the compactness and small size of the manipulator are achieved.

5.2 Achievements and Conclusions

The main achievement of the research work presented in this thesis is that a systematic development process of two-fingered micro-manipulator hand is developed based on a novel IKP solution and using optimization techniques to mainly enlarge the workspace of

the micro-manipulator. Simulation and practical results demonstrate the efficiency of the proposed technique.

The development process of the two-fingered micro-manipulator hand with hybrid structure mechanism is presented. The micro-manipulator hand is assembled of two 3-DOF PRS parallel mechanisms in series connection. The mechanism is actuated by PZT actuators in each leg of the kinematics chain. The end effector is chosen to be two long glass pipettes tapered to a sharp edge in a chopstick-like style. The synthesis and design optimization issues are deeply discussed. An algorithm for the new solution of the 3-DOF PRS IKP is presented with a numerical example. Then the FKP solution based on the closed form IKP together with Newton-Raphson numerical approach is discussed with a numerical example. Moreover the IKP solution based on the tip position of the end effector is presented using the same approach used in FKP solution.

The optimization of the theoretical model design parameters using discrete search method and GEAs are discussed. The GEAs shows better performance in determining the design parameters but unfortunately its values can not be practically realized with a good accuracy. As a result, we decided to build our proposed micro finger using the design parameters out from the discrete search method. Then a complementary optimization step is carried out to determine the suitable mechanical properties of the pin flexure hinge used. A complete CAD model based on the optimized design parameters has been built. The practical CAD model *X*-, *Y*-, and *Z*-extremities are about only 5% less that of theoretical one. The hardware system setup for the micro-manipulator hand prototype is built and used to calibrate both finger modules. Also the real system is checked for the maximum possible error norm and it is found to be about 1μm. Also, the practical prototype workspace volumes are about 7 to 10% less that of the theoretical results and about 5%less that of CAD model values. One problem arises in aligning the two finger tips at the beginning but it can be handled manually.

The following conclusions are the main achievements from this thesis:

- ✓ A novel 3-DOF RPS and PRS parallel mechanisms inverse kinematics problem closed form solution is derived. The solution is in the form of simple equations.

So, given the position of the mobile plate center, we can easily determine the possible solutions for the displacements of the actuators.

- ✓ The inverse kinematics problem of either 3-DOF RPS or PRS parallel mechanisms has ***eight*** mathematically accepted solutions. But only ***four*** of them are physically accepted due to actuators limitation and physical constrains.

- ✓ A numerical solution of the 3-DOF PRS parallel mechanism forward kinematics problem is presented. This solution is based on the closed from solution of the inverse kinematics problem and the Newton-Raphson method.

- ✓ A more practical case, the numerical solution of the 3-DOF PRS parallel mechanism inverse kinematics problem given the tip position of the end effector is presented. This solution is based on the closed from solution of the inverse kinematics problem and the Newton-Raphson method.

- ✓ There is a *1-to-4* relationship in between the *position of the mobile plate center* and the *actuator displacements*. So, the same mobile plate center position can be obtained using four alternatives of d_1, d_2, and d_3 each has a different orientation matrix ${}^{b}R_{m}$ –i.e. different pose.

- ✓ Each orientation matrix ${}^{b}R_{m}$ locate the end effector in one of the four quarters of the upper half of the space.

- ✓ There is a *1-to-1* relationship in between the *end effector tip position* and the *actuator displacements*. So, each end effector tip position has only one set of d_1, d_2, and d_3 that is defined by a particular orientation matrix ${}^{b}R_{m}$.

- ✓ If the limitations of the joints are not taken in consideration, both 3-DOF RPS and PRS parallel mechanisms have the same feasible workspace volume for their inverse kinematics problem solution which is the *boundary of a vertical cylinder with radius $\rho = r$ and Z-coordinate as its axis*.

- ✓ A new architecture for the two-fingered hybrid micro-manipulator hand is designed and realized in this thesis in which two 3-DOF PRS parallel mechanisms are connected in series back-to-back to form the motion mechanism.

- ✓ The use of optimization techniques – Discrete Search Method and Genetic and Evolutionary Algorithms – is very essential to determine the optimal – or at least the near optimal - design parameters. So, a simulation program is developed to help in optimization process.

- ✓ Genetic and Evolutionary Algorithms prove superiority in finding optimal solution of design parameters over traditional method like discrete search method. But unfortunately the genetically optimized design parameters are difficult to be practically implemented. So, we decided to use the design parameters out from the discrete search method.

- ✓ A complementary optimization step for the micro finger CAD model is carried out using ANSYS workbench program to find the suitable thickness of the pin flexure hinge used.

- ✓ The CAD model designed has a workspace that is 5% less than that of the theoretical model values.

- ✓ Due to the proposed serial connection of the motion mechanism, the lower finger has 3-DOF and the upper finger has 6-DOF. So, lower finger will be used for support while the upper finger will be used for fine motion.

- ✓ The final CAD model design of the two-fingered micro-manipulator hand is realized and a prototype is assembled and built.

- ✓ The practical two-fingered micro-manipulator hand prototype has a workspace that is about 5% less than that of the CAD model and that is about 10% less than that of the theoretical values.

- ✓ The practical two-fingered micro-manipulator hand prototype is checked for the maximum error and it is found to be around 1μm for small range and it can be as 2μm for large movements.

5.3 Future Work and Directions

Future work will focus on the system hardware setup improvement of the hand with the optimized parameters to solve the alignment problem for better performance and completing the tissue micro-injection experiment setup.

For future work, the following points can be approached:

- ➢ To solve the problem of alignment of the two finger tips at the beginning, a fine adjustment mechanism can be designed for adjusting the two finger tips. The fine adjustment mechanism should not be bulky and it should be capable of moving either fingers – or at least one of them – in the three directions *X*, *Y*, and *Z* to adjust the two finger tips.

- ➢ To solve the problem of limited movements in the *Z*-direction, the connection in between the upper and lower modules can be serially in perpendicular to each other not in straight.

- ➢ Developing a new software program to fine controlling the new two-fingered micro-manipulator hand with the feature of auto tracking both of the finger tip and the microscopic object to be manipulated.

- ➢ Designing or finding a micro force sensor to be attached to our two-fingered micro-manipulator hand for sensing and measuring the forces exerted by the finger tips to the manipulated microscopic object.

- ➢ Completing the setup of the tissue micro-injection experiment in which all components will be assembled together.

REFERENCES

[1] V. E. Gough and S.G. Whitehall, Universal tyre test machine, in *Proc. of the FISITA Ninth Int. Technical Congress*, pp. 117-137 (1962)

[2] D. Stewart, A platform with six degrees of freedom, *Proc. of the IMechE*, **180,** Pt. 1, No. 5, pp. 371-385 (1965-66)

[3] E. F. Fichter, "A Stewart platform-based manipulator: General theory and practical consideration," Int. J. of Robotics Research, vol. 5, no. 2, pp. 157-182, 1986.

[4] R. S. Stoughton, T. Arai, "A modified Stewart platform manipulator with improved dexterity," IEEE Trans. on Robotics and Automation, vol. 9, no. 2, pp. 166-173, April 1993

[5] G. Yang, I. Chen, W. Chen, W. Lin, "Kinematic design of a six-DOF parallel-kinematics machine with decoupled-motion architecture," IEEE Trans. on Robotics, vol. 20, no. 5, pp. 876-884, Oct. 2004

[6] O. Didrit, M. Petitot, and E. Walter, Guaranteed solution of direct kinematic problems for general configurations of parallel manipulators, IEEE Trans. Robotics and Automation, 14, 259-266 (1998)

[7] J. Nielsen, and B. Roth, On the kinematic analysis of robotic mechanisms, Int. J. of Robotics Research, 18, 1147-1160 (1999)

[8] H. Sadjadian, H. D. Taghirad, and A. Fatehi, Neural networks approaches for computing the forward kinematics of a redundant parallel manipulator, Int. J. computational intelligence, 2, 40-47 (2005)

[9] X. Liu, J. Wang, F. Gao, and L. Wang, On the analysis of a new spatial three-degrees-of-freedom parallel manipulator, IEEE Trans. Robotics and Automation, 17, 959-968 (2001)

[10] J. A. Carretero, R. P. Podhorodeski, M. A. Nahon, and C. M. Gosselin, Kinematic Analysis and Optimization of a New Three Degree-of-Freedom Spatial Parallel Manipulator, ASME Trans. J. Mechanical Design, 122, 17-24 (2000)

[11] J. P. Merlet, Parallel Robots, Springer (2006)

[12] L. W. Tsai, Robot analysis: the mechanics of serial and parallel manipulators, Wiley-science publications (1999)

[13] S. M. Song and M. D. Zhang, A Study of Reaction Force Compensation Based on Three-Degrees-of-Freedom Parallel Platform, J. Robotic Systems, 12, 783-794 (1995)

[14] K. M. Lee and D. K. Shah, Kinematic analysis of a three-degree- of- freedom in-parallel actuated manipulator, IEEE J. Robotics and Automation, 4, 354-360 (1988)

[15] C. H. Liu and S. Cheng, Direct Singular Positions of 3RPS Parallel Manipulators, ASME Trans. J. Mechanical Design, 126, 1006-1016 (2004)

[16] J. P. Merlet, "Still a long way to go on the road for parallel mechanisms," ASME 2002 DETC Conference, Montreal, Canada, 2002. Available: http://www-sop.inria.fr

[17] J. P. Merlet, "Parallel Robots: Open Problems," In 9th Int. Symp. of Robotics Research, Snowbird, 9-12 October 1999. Available: http://www-sop.inria.fr

[18] Y. Lu and T. Leinonen, Solution and Simulation of Position-Orientation for Multi-Spatial 3-RPS Parallel Mechanisms in Series Connection, J. Multibody systems dynamics, 14, 47-60 (2005)

[19] T. Tanikawa and T. Arai, Development of a Micro-Manipulation System Having a Two-Fingered Micro-Hand, IEEE Trans. Robotics and Automation, 15, 152-162 (1999)

[20] J-P Merlet, Micro parallel robot MIPS for medical applications, Proc. of 8th IEEE Int. Conf. on Emerging Technologies and Factory Automation, France, 2, pp. 611-619 (2001)

[21] T. Fukuda and W. Menz, Micro Mechanical systems principles and technology, Elsevier, vol. 6, Handbook of sensors and actuators, pp. 146-153, 161-175, and 215-251 (1998)

[22] P. Liu and Q. Li, Kinematics and dynamics of a general-purpose, parallel, compliant micromanipulator, Proc. of the IMechE, 217, pp. 39-50 (2003)

[23] T. Lu, D. C. Handley, Y. K. Yong, and C. Eales, A three-DOF compliant micromotion stage with flexure hinges, Int. J. Industrial Robot, 31, 355-361 (2004)

[24] W. Zhang, et al, "The constant-Jacobian method for kinematics of a three-DOF planar micro-motion stage," J. of Robotic sys., vol. 19, no. 2, pp. 63-72, Feb. 2002.

[25] Y. Ohya, T. Arai, Y. Mae, K. Inoue, T. Tanikawa, "Development of 3-DOF Finger Module for Micro Manipulation," Proceeding of the 1999 IEEE/RSJ International Conference on Intelligent Robots and Systems, pp. 894-899, 1999.

[26] A. Menciassi, A. Eisinberg, I. Izzo, P. Dario, "From "Macro" to "Micro" manipulation: Models and experiments," IEEE/ASME Trans. on Mechatronics, vol. 9, no. 2, pp. 311-319, June 2004.

[27] R. S. Fearing, “Survey of sticking effects for micro parts handling,” In International workshop on Intelligent Robots and Systems, Pittsburg,USA, 1995

[28] M. Gauthier, S. Rgnier, P. Rougeot, and N. Chaillet, “Forces analysis for micromanipulation in dry and liquid media,” Journal of Micromechatronics, 3(3-4):389–413, September 2006.

[29] P. Lambert and A. Delchambre, “Design rules for a capillary gripper in microassembly,” In International Symposium on Assembly and Task Planning, Montr´eal, Canada, July 2005.

[30] Y. Zhou and B. J. Nelson, “Force controlled microgripping,” In SPIE Conference on Microrobotics and Microassembly, pages 211–221, Boston, USA, September 1999

[31] J.P. Merlet, “Optimal design for the micro parallel robot MIPS,” Proceedings of the 2002 IEEE international Conference on Robotics and Automation, Washington, DC, May 2002

[32] Dezhong Liu, Yihua Xu, and Renyuan Fei, “Study of an intelligent micro-manipulator,” Journal of Materials Processing Technology, vol. 139, pp. 77–80, (2003)

[33] D. Sinan Haliyo, Yves Rollot and St´ephane R´egnier, “Manipulation of micro-objects using adhesion forces and dynamical effects,” Proceedings of the 2002 IEEE International Conference on Robotics and Automation, Washington DC, USA, May, 2002

[34] D. Sinan Haliyo, Gentiane Venture, St´ephane R´egnier and Jean-Claude Guinot,” An overview of the micro-manipulation system [m¨u]MAD,” Proceedings of the 2005 IEEE/ASME International Conference on Advanced Intelligent Mechatronics, Monterey, California, USA, 24-28 July, 2005

[35] Yangmin Li and Qingsong Xu, “Optimal Design of a Novel 2-DOF Compliant Parallel Micromanipulator for Nanomanipulation,” Proceedings of the 2005 IEEE International Conference on Automation Science and Engineering, Edmonton, Canada, August 1 & 2, 2005

[36] Yangmin Li and Qingsong Xu, “Novel Design of a 3-PUU Spatial Compliant Parallel Micromanipulator for Nanomanipulation,” Proceedings of the IEEE International Conference on Mechatronics & Automation, Niagara Falls, Canada • July 2005

[37] Qingsong Xu and Yangmin Li, “Mechanical Design of Compliant Parallel Micromanipulators for Nano Scale Manipulation,” Proceedings of the 1st IEEE International Conference on Nano/Micro Engineered and Molecular Systems, January 18 - 21, 2006, Zhuhai, China

[38] T. Tanikawa, T. Arai, and T. Masuda, “Development of Micro-Manipulation System with Two-Finger Micro-Hand,” Proc. of the 1996 IEEE/RSJ Int. Conf. on Intelligent Robots and Systems, pp. 850-855, 1996.

[39] T. Tanikawa, et al, ``Design of 3DOF Parallel Mechanism with Thin Plate for Micro Finger Module in Micro Manipulation," Proc. of the 2002 IEEE/RSJ Int. Conf. on Intelligent Robots and Systems, Lausanne, Switzerland, pp. 1778-1783, October 2002.

[40] Yoshihiko KOSEKI, Tamio TANIKAWA, and Kiyoyuki CHINZEI, “MRI-compatible Micromanipulator: Design and Implementation and MRI-compatibility Tests,” The 29th Annual International Conference of the IEEE EMBS, ThC09.4, pp. 465-458, 2007

[41] Kallio P, Lind M, Zhou Q, Koivo HN, “A 3 DOF piezohydraulic parallel micromanipulator,” International Conference on Robotics and Automation Leuven, Belgium, May (1998)

[42] T. FUKUDA and F. ARAI, “Prototyping Design and Automation of Microhano Manipulation System,” Proceedings of the 2000 IEEE International Conference on Robotics & Automation, San Francisco, USA, April 2000

[43] Chonan S, Jiang ZW, Koseki M, “Soft-handling gripper driven by piezoceramic bimorph strips,” Smart Materials and Structures 5:407–414, (1996)

[44] David J. Cappelleri, Mary I. Frecker, Timothy W. Simpson, and Alan Snyder, “Design of a PZT Bimorph Actuator Using a Metamodel-Based Approach,” Trans. of the ASME, Vol. 124, JUNE 2002

[45] Angeles J, Morozov A, Slutski L, Navarro O, Jabre L, “The modular design of a long-reach, 11-axis manipulator,” Proc. 2000 CISM-IFToMM Symposium on Robots and Manipulators, pp. 225–233, Zakopane, Poland, July 3–6, 2000

[46] A. Sokolov, P. Xirouchakis, “Kinematics of a 3-DOF parallel manipulator with an R-P-S joint structure,” Robotica, Cambridge Uni. Press, vol. 23, pp. 207-217, 2005

[47] O. Ibrahim and W. Khalil, “Kinematic and dynamic modelling of the 3-RPS parallel manipulator,” In 12th IFToMM World Congress, Besancon, 2007

[48] J. Gallardo-Alvarado et al., “Kinematics and dynamics of 2(3-RPS) manipulators by means of screw theory and the principle of virtual work,” J. Mech. Mach. Theory (2007), doi:10.1016/j.mechmachtheory .2007.10.009

[49] H. Pendar et al., “Efficient Dynamic Equations of 3-RPS Parallel Mechanism through Lagrange Method,” Proc. IEEE Int. Conf. Robotics, Automation and Mechatronics, Singapore, vol. 2, pp. 1152-1157, 2004

[50] K. Fan et al., “Sensitivity analysis of the 3-PRS parallel kinematic spindle platform of a serial-parallel machine tool,” Int. J. of Machine Tools & Manufacture, 43, pp. 1561–1569, (2003)

[51] Y. Li and Q. Xu, " Kinematic analysis of a 3-PRS parallel manipulator," J. Robotics and Computer-Integrated Manufacturing, vol. 23, pp. 395–408, 2007

[52] A. Ramadan, K. Inoue, T. Arai, T. Takubo, “New Architecture of a Hybrid Two-Fingered Micro-Nano Manipulator Hand: Optimization and Design,” Journal of Advanced Robotics, vol. 22, pp. 235-260, 2008.

[53] A. Ramadan, T. Takubo, Y. Mae, K. Oohara, T. Arai, “Development Process of a Chopstick-Like Hybrid Structure Two-Fingered Micromanipulator Hand for 3D Manipulation of Microscopic Objects,” IEEE Trans. Industrial Electronics, IEEE TIE (Accepted)

[54] Ahmed. A. Ramadan, K. Inoue, T. Arai, T. Takubo, " Design of a Compact 3-DOF Parallel Micro Finger Manipulator," Proc. of Robotics and Mechatronics conference, ROBOMECH2006, Waseda Uni., Tokyo, Japan, 1A1-C35(1-4), May 2006.

[55] Ahmed A. Ramadan, K. Inoue, T. Arai, and T. Takubo, “Design optimization of a compact 3-DOF parallel micro/nano finger manipulator,” in Proc. of the 2006 IEEE/RSJ Int. Conf. on Intelligent Robots and Systems, IROS2006, Beijing, China, pp. 778-783 (2006)

[56] Ahmed. A. Ramadan, K. Inoue, T. Arai, T. Takubo, " New Design of a Compact Two-fingered Micro-hand Parallel Manipulator," Proc. of The 24th Annual conference of the Robotics Society of Japan, RSJ2006, Okayama, Japan, pp. 3L35, September 2006.

[57] Ahmed. A. Ramadan, K. Inoue, T. Arai, T. Takubo, and Tamio Tanikawa, "New Design of a Compact Parallel Micro-Nano Two-Fingered Manipulator Hand," in Proc. of the 2nd IEEE International Conference on Nano/Micro Engineered and Molecular Systems (IEEE-NEMS), Bangkok, Thailand, pp. 515-519 (2007)

[58] Ahmed. A. Ramadan, K. Inoue, T. Arai, and T. Takubo," New Hybrid Two-Fingered Micro-Nano Manipulator Hand: Optimization and Design," in Proc. of the 2007 IEEE International Conference on Mechatronics and Automation (ICMA2007), Harbin, China, pp. 2524-2529, (2007)

[59] A. A. Ramadan, K. Inoue, T. Arai, T. Takubo, and I. Hatta " Micro-Nano Two-Fingered Hybrid Manipulator Hand," Proc. of the 2007 Int. Symposium on Micro-Nano Mechatronics and Human Science, MHS2007, Nagoya, Japan, pp. 32-37 (2007)

[60] Ahmed. A. Ramadan, T. Arai, " Architecture and Synthesis of a Two-Fingered Micro-Nano Hybrid Manipulator," Proc. of The 1st Egypt-Japan International Symposium on Science and Technology 2008, EJISST2008, Waseda Uni., Tokyo, Japan, pp. 127, EJISST-ID 269, June 8-10, 2008, (Abstract + Presentation).

[61] Ahmed. A. Ramadan, K. Inoue, T. Arai, and T. Takubo," Chopstick-like Two-fingered micromanipulator hybrid hand," Accepted to be published in Proc. of the 2008 International Symposium on Flexible Automation (ISFA2008), pp. JL021, Atlanta, Georgia, USA, 23 – 26 June (2008)

[62] Ahmed. A. Ramadan, K. Inoue, T. Arai, and T. Takubo," Synthesis of a chopstick-like Two-fingered micromanipulator based on a novel inverse kinematics solution," Proc. of the 17th CISM-IFToMM Symposium on Robot Design, Dynamics, and Control (RoManSy2008), Waseda Uni., Tokyo, Japan, pp. 273-280, 5 – 9 July (2008)

[63] Ahmed A. Ramadan, T. Arai, T. Takubo, and K. Inoue, " Optimization of a Hybrid Two-Fingered Micro Hand Using Genetic Algorithms," Proc. of the 2008 Int. Symposium on Micro-Nano Mechatronics and Human Science, MHS2008, Nagoya, Japan, pp. 103-107 (2008)

[64] Ahmed. A. Ramadan, T. Arai, T. Takubo, and K. Inoue " An Inverse Kinematics Solution for 3-PRS Parallel Micro Finger Module Based on End Effector Tip Position," Proc. of the 26th Annual conference of the Robotics Society of Japan, RSJ2008, Kobe, Japan, pp. 3L35, September 2008.

[65] Ahmed. A. Ramadan, T. Arai, K. Inoue, and T. Takubo " Solution of Inverse and Forward Kinematics Problems for 3-PRS Parallel Micro Finger," Proc. of the 9th Society of Instrument and Control Engineers (SICE) System Integration Division Annual conference, SI2008, pp. 2C2-3, Gifu, Japan, Dec. 2008.

[66] D.E. Goldberg, "Genetic Algorithms in Search, Optimization, and Machine Learning", Addison-Wesley, Massachusetts, 1989.

[67] I. Rechenberg, "Evolutions strategies", Frommann-Holzboog, Stuttgart, 1973.

[68] H. P. Schwefel, "Evolution and Optimum Seeking", Wiley, New York, 1995.

[69] J.L. Ribeiro, P. C. Treleaven, and C. Alippi, "Genetic-Algorithms Programming Enviroments", IEEE Trans. on Computer, pp. 28-43, 1994.

[70] J. H. Holland, "Adaptation in Natural and Artificial Systems (2^{nd} ed.)", MIT press, Cambridge, MA, 1992.

[71] K.F. Man, K.S. Tang, and S. Kwong, "Genetic Algorithms: Concepts and Applications", IEEE Trans. on Industrial Electronics, pp. 519-532, 1996.

[72] M. Srinivas and L.M. Patnaik, "Genetic Algorithms: A Survey", IEEE Trans. on Computer, pp. 17-26, 1994.

[73] Z. Michalewicz, "Genetic Algorithms + Data Structures = Evolution Programs", AI Series, Springer-Verlag, New York, 1994.

[74] L. J. Fogel, A. J. Owens, and M. J. Walsh, "Artificial Intelligence Through Simulated Evolution", John Wiley, New York, 1966.

[75] C. A. Coello, G. B. Lamont, and D. A. Van Veldhuizen, " Evolutionary Algorithms for Solving Multi-Objective Problems," published by Springer, 2nd edition, 2007.

[76] M. Brameier and W. Banzhaf, "Linear Genetic Programming," published by Springer, 2007

[77] A. Ramadan, et al, "New Genetic-Based Design of a Pi-Like Fuzzy Logic Speed Controller for an Induction Motor," Proc. of the IEEE International Conference on Computational Cybernetics (ICCC 2004), Vienna , Austria, pp. 25-32, Aug. 2004

[78] I. D. Landau and G. Zito, “Digital Control Systems: Design, Identification and Implementation,” published by Springer-Verlag London Limited, 2006.

[79] K. Nakao, et al, “The development of a bioengineered organ germ method,” Nature methods journal, Vol. 4, No. 3, pp. 227-230, 2007.

[80] A. Ramadan, K. Inoue, T. Arai, T. Takubo, and I. Hatta, “Development of a Chopstick-Like Hybrid Structure Two-Fingered Micromanipulator Hand for Cell Manipulation,” Submitted to the 2009 IEEE Int. Conf. ICRA2009, (2009)

List of Publication:

Journal Papers:

[1] A. Ramadan, K. Inoue, T. Arai, T. Takubo, "New Architecture of a Hybrid Two-Fingered Micro-Nano Manipulator Hand: Optimization and Design," *Journal of Advanced Robotics,* **vol.** 22, **pp.** 235-260, 2008.

[2] A. Ramadan, T. Takubo, Y. Mae, K. Oohara, T. Arai, "Development Process of a Chopstick-Like Hybrid Structure Two-Fingered Micromanipulator Hand for 3D Manipulation of Microscopic Objects," *IEEE Trans. Industrial Electronics, IEEE TIE (Accepted)*

International Conference Papers (Reviewed):

[3] Ahmed A. Ramadan, K. Inoue, T. Arai, and T. Takubo, "Design optimization of a compact 3-DOF parallel micro/nano finger manipulator," in *Proc. of the 2006 IEEE/RSJ Int. Conf. on Intelligent Robots and Systems, IROS2006*, Beijing, China, pp. 778-783 (2006)

[4] Ahmed. A. Ramadan, K. Inoue, T. Arai, T. Takubo, and Tamio Tanikawa, "New Design of a Compact Parallel Micro-Nano Two-Fingered Manipulator Hand," in *Proc. of the 2nd IEEE International Conference on Nano/Micro Engineered and Molecular Systems (IEEE-NEMS)*, Bangkok, Thailand, pp. 515-519 (2007)

[5] Ahmed. A. Ramadan, K. Inoue, T. Arai, and T. Takubo," New Hybrid Two-Fingered Micro-Nano Manipulator Hand: Optimization and Design," in *Proc. of the 2007 IEEE International Conference on Mechatronics and Automation (ICMA2007)*, Harbin, China, pp. 2524-2529, (2007)

[6] A. A. Ramadan, K. Inoue, T. Arai, T. Takubo, and I. Hatta " Micro-Nano Two-Fingered Hybrid Manipulator Hand," *Proc. of the 2007 Int. Symposium on Micro-Nano Mechatronics and Human Science, MHS2007*, Nagoya, Japan, pp. 32-37 (2007)

[7] Ahmed. A. Ramadan, K. Inoue, T. Arai, and T. Takubo," Chopstick-like Two-fingered micromanipulator hybrid hand," Accepted to be published in *Proc. of the*

2008 International Symposium on Flexible Automation (ISFA2008), pp. JL021, Atlanta, Georgia, USA, 23 – 26 June (2008)

[8] Ahmed. A. Ramadan, K. Inoue, T. Arai, and T. Takubo," Synthesis of a chopstick-like Two-fingered micromanipulator based on a novel inverse kinematics solution," *Proc. of the 17th CISM-IFToMM Symposium on Robot Design, Dynamics, and Control (RoManSy2008),* Waseda Uni., Tokyo, Japan, pp. 273-280, 5 – 9 July (2008)

[9] Ahmed A. Ramadan, T. Arai, T. Takubo, and K. Inoue, " Optimization of a Hybrid Two-Fingered Micro Hand Using Genetic Algorithms," *Proc. of the 2008 Int. Symposium on Micro-Nano Mechatronics and Human Science, MHS2008*, Nagoya, Japan, pp. 103-107 (2008)

[10] A. Ramadan, K. Inoue, T. Arai, T. Takubo, and I. Hatta, "Development of a Chopstick-Like Hybrid Structure Two-Fingered Micromanipulator Hand for Cell Manipulation," *Submitted to the 2009 IEEE Int. Conf. ICRA2009*, (2009)

Domestic Conferences Papers:

[11] Ahmed. A. Ramadan, K. Inoue, T. Arai, T. Takubo, " Design of a Compact 3-DOF Parallel Micro Finger Manipulator," *Proc. of Robotics and Mechatronics conference, ROBOMECH2006,* Waseda Uni., Tokyo, Japan, 1A1-C35(1-4), May 2006.

[12] Ahmed. A. Ramadan, K. Inoue, T. Arai, T. Takubo, " New Design of a Compact Two-fingered Micro-hand Parallel Manipulator," *Proc. of The 24th Annual conference of the Robotics Society of Japan, RSJ2006,* Okayama, Japan, pp. 3L35, September 2006.

[13] Ahmed. A. Ramadan, T. Arai, " Architecture and Synthesis of a Two-Fingered Micro-Nano Hybrid Manipulator," *Proc. of The 1st Egypt-Japan International Symposium on Science and Technology 2008, EJISST2008,* Waseda Uni., Tokyo, Japan, pp. 127, EJISST-ID 269, June 8-10, 2008, (Abstract + Presentation).

[14] Ahmed. A. Ramadan, T. Arai, T. Takubo, and K. Inoue " New Design of a Compact Two-fingered Micro-hand Parallel Manipulator," *Proc. of The 26th Annual conference of the Robotics Society of Japan, RSJ2008,* Kobe, Japan, pp. 3L35, September 2008.

[15] Ahmed. A. Ramadan, T. Arai, K. Inoue, and T. Takubo " Solution of Inverse and Forward Kinematics Problems for 3-PRS Parallel Micro Finger," Proc. of the 9th

Society of Instrument and Control Engineers (SICE) System Integration Divison Annual conference, SI2008, pp. 2C2-3, Gifu, Japan, Dec. 2008.

Previous publications:

[16] A. A. Ramadan, M. T. Faheem, and A. F. Amer "Design of an Optimal PI-Like Fuzzy Logic Speed Controller of Induction Motor Using Genetic Algorithms", 11th International Conference on Computer Theory and Applications, ICCTA 2001, pp. VI-7 - VI-15, 28 – 30 August 2001 Alex. Egypt.

[17] A. A. Ramadan, M. T. Faheem, and A. F. Amer "Genetic-Based Design of a PI-Like Fuzzy Logic Speed Controller For An Induction Motor", 7th International Conference On Intelligent Engineering Systems, INES 2003, March 4- 6, Assiut-Luxor, Egypt.

[18] A. A. Ramadan, M. T. Faheem, A. F. Amer, and S. A. Sallam "New Genetic-Based Design of a PI-Like Fuzzy Logic Speed Controller For An Induction Motor", International Conference On Computational Cybernetics, ICCC 2004, August 30, Vienna, Austria.

[19] A. F. Amer, A. A. Ramadan, and E. F. Mohamed "Genetic-Based supervisory control of a remote process over an industrial network", 14th International Conference on Computer Theory and Applications, ICCTA 2004, 28 – 30 September 2004 Alex., Egypt.